DANMARKS OG GRØNLANDS GEOLOGISKE UNDERSØGELSE RAPPORT 2012/62

Provenance of sediments in the Faroe-Shetland basin: characterisation of source components in Southeast Greenland

Final report prepared for SINDRI
C46-50-01

Kristine Thrane & Nynke Keulen

GEOLOGICAL SURVEY OF DENMARK AND GREENLAND
DANISH MINISTRY OF CLIMATE, ENERGY AND BUILDING

GEUS

DANMARKS OG GRØNLANDS GEOLOGISKE UNDERSØGELSE RAPPORT 2012/62

Provenance of sediments in the Faroe-Shetland basin: characterisation of source components in Southeast Greenland

Final report prepared for SINDRI
C46-50-01

Kristine Thrane & Nynke Keulen

Released 01.07.2017

GEOLOGICAL SURVEY OF DENMARK AND GREENLAND
DANISH MINISTRY OF CLIMATE, ENERGY AND BUILDING

GEUS

Contents

Abstract

The aim of this Sindri project, C46-50-01, was to broaden our understanding of the timing of pulsing observed between sedimentary and volcanic Palaeogene deposition across the Faroe-Shetland region to better understand the sub-, syn- and early post-basaltic sedimentary succession offshore the Faroe Islands. The project is based on A) a detailed study of the provenance sensitive features of the possible source areas for sediment supply to the Faroe-Shetland basin in Southeast Greenland; and B) exploring the possibilities offered by baddeleyite and zircon for high precision U-Pb dating of the Palaeocene basalts and mafic igneous rocks exposed in the Faroe-Shetland basin.
The two projects are both described in this report.

In project A, geochemical analyses and U-Pb ages from detrital zircons have been carried out for a total of four tillite samples and 19 stream sediment samples collected along the South-East Greenland shore between 62-68°N.

The main conclusions are:

- The age pattern and the geochemical data for samples from Southeast Greenland are markedly different from the drill core samples from the Faroe-Shetland Basin and, therefore, an unlikely source.
- There are several potential source areas for the Faroe-Shetland sediments, e.g. Scotland, Central East Greenland, Svalbard (Scandinavia), which all share a common signature. It is not possible to discriminate the sources based only on U-Pb detrital zircon ages, or geochemical data.
- Central East Greenland is the most likely source when combined with other studies, e.g. pollen studies and flow patterns.
- The Kangerlussuaq sediments show characteristics from both Southeast and Central East Greenland and must, therefore, have been fed from both the north and the south.

In project B, the main aim was to recover baddeleyite crystals from Palaeogene mafic basaltic rocks and tuffs from the lower lava sequence exposed at Sudoroy, to obtain precise crystallization ages from the rocks. Unfortunately, we were not able to find any baddeleyites in any of the samples, because they were too fine grained.

To prove that we are able to recover baddeleyites from mafic samples, three mafic dykes collected in the Skaergaard area were also processed, only one of the dykes had baddeleyite. The grains were analysed and yielded a U-Pb age of 55.87 ± 0.06 Ma. The samples are part of another Sindri project C46-53-02, carried out by Pierpaolo Guarnieri.

Introduction

Palaeogeographic reconstructions of the North Atlantic region at the end of the Mesozoic show that the pre-drift position of the Faroe Islands was located near the Greenlandic coast east of the area between Kangerlussuaq and Kap Gustav Holm in Greenland. During the Cretaceous, a number of basins formed in the North Atlantic region south of the Faroe Islands (e.g. Knott et al. 1993). Sediments in these basins are likely to be partially derived from Greenland. Field studies in the Kangerlussuaq area, where Cretaceous and Early Tertiary sediments outcrop in basins, suggest that Greenland played a role as a sediment supplier during the opening of the Northern Atlantic (Larsen 1996).

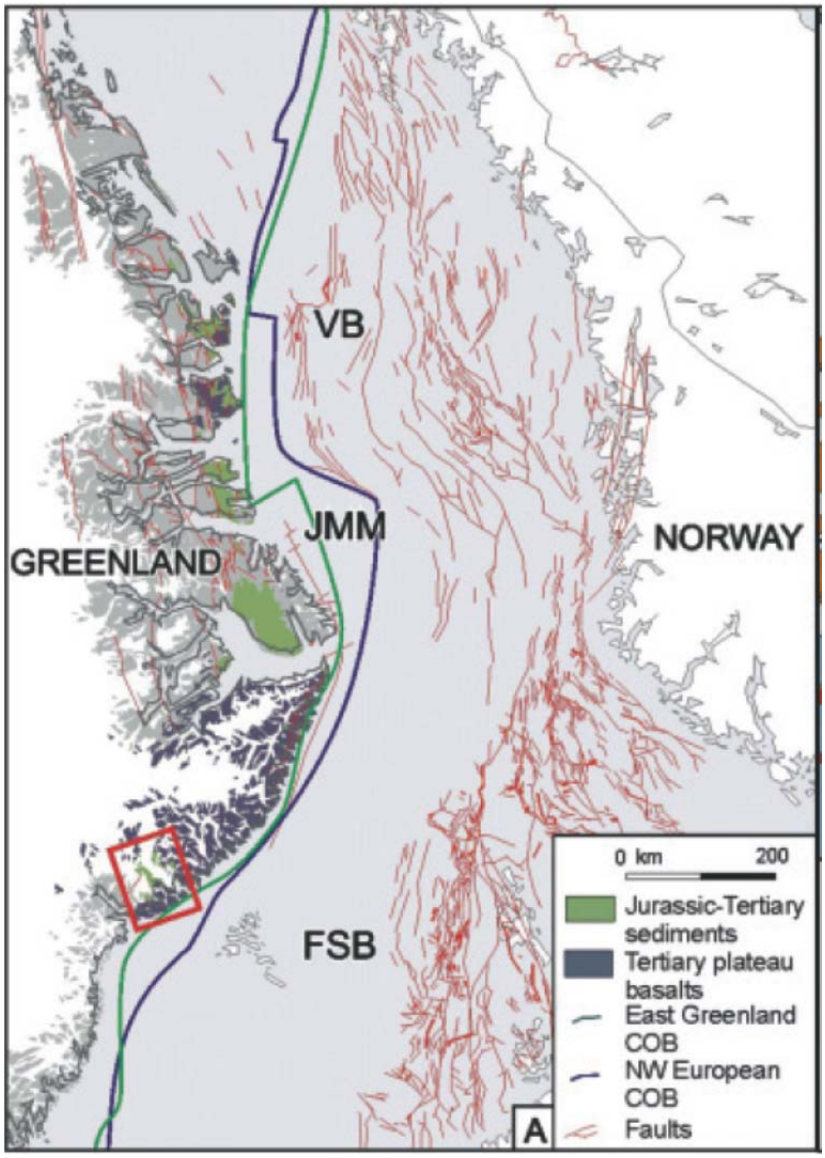

Figure 1. *Tectonic reconstruction of the North Atlantic prior to the onset of seafloor spreading in the Late Palaeocene-Early Eocene. COB: continental ocean boundary; FSB: Faroe-Shetland Basin; JMM: Jan Mayen Microcontinent; VB: Vøring Basin (after Larsen et al. 1996).*

Larsen (1996) suggested that large amounts of sediment bypassed the area that is currently outcropping near Kangerlussuaq and was deposited in basins southeast of that area. A key issue for hydrocarbon exploration in the Faroese region is the understanding of sediment dispersal patterns and depositional systems in the Faroe-Shetland Basin prior to continental breakup in the Late Palaeocene to Early Eocene. Identification of sediment provenance is crucial for this goal. Location of the source areas places important constraints on sediment transport pathways and intrabasinal sand body distribution. Furthermore, the nature of the sediment source has important implications for the porosity and permeability characteristics of the deposited sediments. Identified variations in source might also be used to establish correlation frameworks (at both local and regional scales) and can provide a basis for discrimination of individual sand bodies.

Previous Sindri Projects

This project is a continuation of two former Sindri projects 1) “Linking the Faroese area and Greenland: an innovative, integrated provenance study” (Frei et. al, 2005) and 2) “Provenance of sediments in the Faroese-Shetland basin: Integration of wells in the Faroese sector” in (Frei et al. 2008).

In the “Linking the Faroese area and Greenland: and innovative, integrated provenance study” project samples from three different areas were analysed: from 1) Cretaceous, Palaeocene and Eocene sedimentary successions from the Kangerlussuaq region in East Greenland, 2) Cuttings from five wells of Palaeocene to Eocene sedimentary successions from in the UK sector of the Faroe-Shetland Basin and 3) samples from outcrops on the Orkney Islands. Several different approaches were carried out, such as conventional petrographic and mineral-chemical techniques, CCSEM and U-Pb zircon analyses, TiO_2-distribution of detrital Ti-minerals and chemostratigraphy.

The main conclusion of the project was that the sedimentary successions from the Kangerlussuaq area and the eastern margin of the Faroe-Shetland Basin have differing signatures. These signatures allow distinction between a western, Greenlandic source and an eastern, predominantly UK margin source. The influence from a western source (Greenland) has not been proved in the examined stratigraphic intervals of wells from the UK sector of the Faroe-Shetland Basin. However, the structure of the Faroe-Shetland Basin suggests that the western, Greenlandic source might be much more important for the deeper, central parts of the basin towards the Faroese area.

In the “Provenance of sediments in the Faroese-Shetland basin: Integration of Wells in the Faroese sector” project, U-Pb ages as well as whole rock geochemistry was carried out on sediment samples from the wells 6004/12-1 Svinoy, 6004/16-1z Marjun, 6004/17-1 Marimas and 6005/15-1 Longan from the Faroese sector (Figure 2).

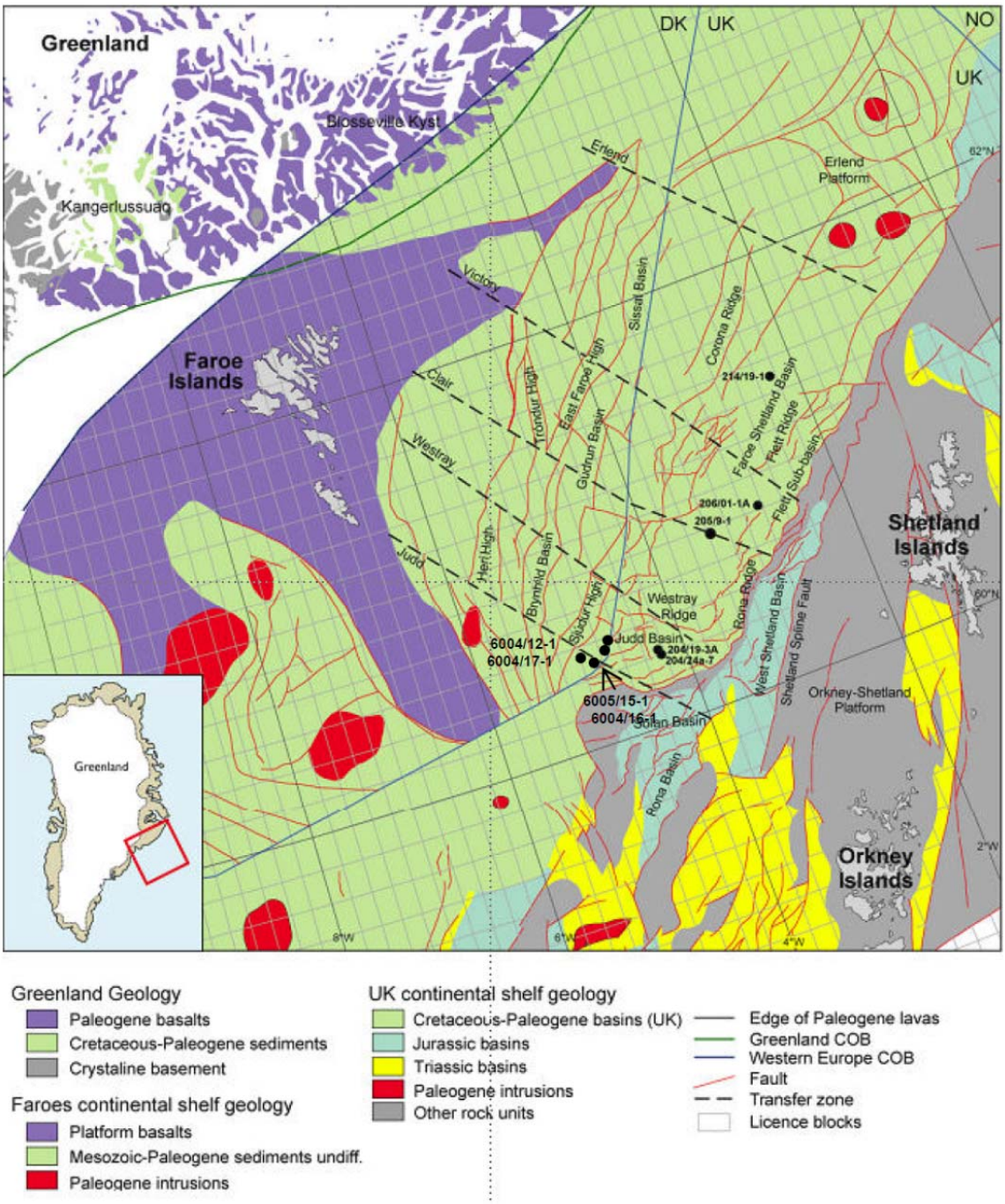

Figure 2. *Location map of East Greenland and the Faroe-Shetland region depicting the geographical position of the areas prior to the onset of seafloor spreading in the Late Palaeocene-Early Eocene. The positions of the Faroese as well as the British wells are shown. After Weibel & Knudsen (2008).*

The main conclusions from the project were as follows:

1) The detrital zircon U-Pb age signatures in all samples from the four wells in the Faroese sector investigated were very similar. The most prominent differences are changes in the relative modal abundances of Archaean to Proterozoic/Palaeozoic zircons as a function of stratigraphic position in the well.
2) The detrital zircon U-Pb age patterns as well as the whole rock geochemistry of the samples from the wells in the Faroese sector are similar to those observed in wells in the UK sector of the Faroese-Shetland basin.
3) The unique Archaean age pattern observed for all samples from wells in the Faroese and the UK sector of the Faroe-Shetland basin suggest that the overwhelming majority of the sediments are sourced from the UK margin, i.e., the Hebridean Foreland and the Scottish Mainland.
4) No evidence could be found for a major role of southern East Greenland as a source of sediments for the Faroe-Shetland basin.

Aim of new project

The aim of this project was to broaden our understanding of the timing of pulsing observed between sedimentary and volcanic Palaeogene deposition across the Faroe-Shetland region to better understand the sub-, syn-, and early post-basaltic and sedimentary succession offshore the Faroe Islands. The project was divided into two individual parts.

A: Provenance of sediments in the Faroe-Shetland basin: Characterisation of source components in Southeast Greenland.

- Identify the provenance signatures (detrital zircon age distributions and heavy mineral signatures) of East Greenland and Southeast Greenland S of Kangerlussuaq by analysing stream sediments.
- Discriminate potential sediment source areas in Greenland
- Integrate all age data in a zircon U-Pb age database for the North Atlantic realm
- Elucidate the effect of large-scale structural grains (tectonic lineaments) and their influence on sediment provenance
- Use the database to qualitatively and quantitatively constrain the source areas for sedimentary input into the Faroe-Shetland basin.

B: Testing baddeleyite and zircon U-Pb age dating as a tool for the establishment of a robust geochronological framework for Palaeocene volcanic rocks in the Palaeocene interval T36 to T50.

- Test whether baddeleyite and zircon are late stage magmatic phases in Palaeogene mafic basaltic rocks and tuffs from the lower lava sequence exposed on Sudoroy as well as cutting samples from interval T36 to T50 in the Faroe-Shetland basin.
- If baddeleyite and zircon are found, to date them by ID-TIMS and LA-SF-ICP-MS using the U-Pb method to obtain highly precise and accurate crystallisation ages.

Database

All U-Pb zircon plots from Frei et al. 2005, Frei et al. 2008 as well as both U-Pb zircon and CCSEM results from this report, are now listed in a GEUS database. Sindri has access to this database and can distribute passwords to whom they wish.
The link to the website is:
http://geusweb01.geus.dk/sindri/home.seam

Publications

This contribution makes available the results originating directly from this Sindri project to the Sindri Group. However, it is our intention that the results should be made available as publications in peer-reviewed journals after the project has been finalised and permission has been granted by the Sindri Group.

Sample preparation and analytical techniques

Introduction to Computer-Controlled Scanning Electron Microscopy (CCSEM)

CCSEM is an analytical tool developed at the Geological Survey of Denmark and Greenland (GEUS). It is a fast and reliable method to determine the chemistry of individual minerals and bulk samples, and it has been used for a wide range of geological or non-geological materials. The chemical analysis is combined with measurements of the two-dimensional size and morphology of every single grain.

Here, the CCSEM technique was applied to 23 stream sediment samples collected from South-East Greenland (Figure 6). Most of the stream sediment samples are derived from Archaean and Proterozoic basement rocks, whereas some dewater Palaeogene and Mesozoic intrusions. The stream sediment samples were investigated to characterise the potential source areas of the sandstones.

To investigate the chemostratigraphy and provenance of the heavy mineral suite of the sediments in South-East Greenland between 62-68°N, the composition of the heavy mineral suite and the composition of garnets in the samples have been analysed. The results of these investigations are discussed here. Appendix A displays the raw data for the composition of the heavy mineral suite and for the garnets. Since most samples are rich in clinopyroxene/clino-amphibole and ortho-pyroxene/ortho-amphibole, an attempt to classify these two groups of minerals more precisely has been undertaken in Appendix B. Appendix C gives further background information on the CCSEM method and the visualisation of the results; this appendix is an addition to the description of the method and visualisation below.

Sample preparation

Samples were washed and sieved to obtain the 45-500 micron fraction. A heavy mineral separate of the sample was collected by putting the sample through bromoform (ρ = 2.9 g/cm^3). If available, approximately 1 g of heavy mineral concentrate was mounted in epoxy resin, using a technique that ensures that almost every grain is completely embedded in the epoxy, without touching any neighbouring grains (e.g. McLimans et al. 1999). The mounts are subsequently polished, and coated with carbon to enhance their conductivity.

CCSEM analysis

CCSEM analysis uses a Philips XL40 SEM equipped with two EDX detectors: a Thermo Nanotrace 30 mm^2 window and a Pioneer Voyager 2.7 10 mm^2 window Si(Li) detector. The tungsten filament of the SEM is operated with an acceleration voltage of 17 kV, a filament current of typically 50–70 µA, and the sample was placed at a distance of 10 mm from the detectors. The Noran System SIX software package automatically collects X-ray spectra, grain size and morphology of all particles and recalculates the data following the Proza ($\phi\rho$Z) data correction and the filtering quantification technique. The technique described

here is an improvement of the method described by Frei *et al.* (2005b) and Bernstein *et al.* (2008). See Keulen *et al.* (2008) for details.

The samples are studied in the back-scattered electron (BSE) contrast mode of the electron microscope. This imaging shows a material contrast in the samples; the individual particles appeared as different shades of grey in their black epoxy matrix (Fig. 3). Grey-level intensity thresholding by the image analysis function integrated in the software creates a binary image of the BSE micrograph and allowed for the separation and selection of individual grains (Fig. 3B). A grid of image frames covering the whole sample area is defined by feeding the end-coordinates of the sample to the computer and by setting the required magnification (typically 30–100x) for the analyses (Fig. 3A). Grids consisted of 15 to 60 frames with approximately 20–35 grains per frame. A guard region between each frame avoids the double measurement of very large particles in the sample and ensured that only grains that lie completely within the image frame are included for analysis and thus recorded the apparent shape of grains.

The binary image created formed the basis for the measurements of the grain chemistry. The software controlled the microscope to scan within the perimeter of each grain to obtain the chemistry of either the whole grain area or from a single point in the centre of the grain mass. A typical spectrum for one particle contained 2000 counts for the highest peak. Spectra with a very low number of counts can be removed to ensure good measurement statistics. Commonly, 800–1200 grains were measured in approximately three to four hours.

CCSEM output files and parameters

The Noran software produces a results table that lists grain shape, grain size and grain chemistry for each individual grain. All spectrum files and image frames, with a typical size of 1024 x 774 pixels are stored after analysis in the database. Spectrum files can be reprocessed to include accidentally omitted elements retrospectively, without the need to physically reanalyse the sample. The chemical data are further reduced using a software package developed at GEUS that is connected to a mineral library database for automatic mineral classification and data storage. Data can be exported from the database in Excel format and pictures of some field outcrops and SEM BSE images of analysed grains can be viewed and saved.

Samples are currently analysed for the following elements:
Na, Mg, Al, Si, P, S, K, Ca, Ti, Cr, Mn, Fe, Ni, Cu, Y, Zr, Nb, Sn and Ce. Oxygen (and other light elements between B and F in the periodic system) is hard to measure precisely. To avoid problems, it is common practise for EDX analyses to assume that all elements are bound to oxygen and to express elements as oxide phases, e.g. Na_2O, MgO, Al_2O_3. For the recalculation, it is assumed that enough oxygen was present in the sample. This can occasionally cause problems in hydrated samples. All EDX measurements are standardless; this means that the total element or oxide concentration in a single measurement is automatically recalculated to 100%.

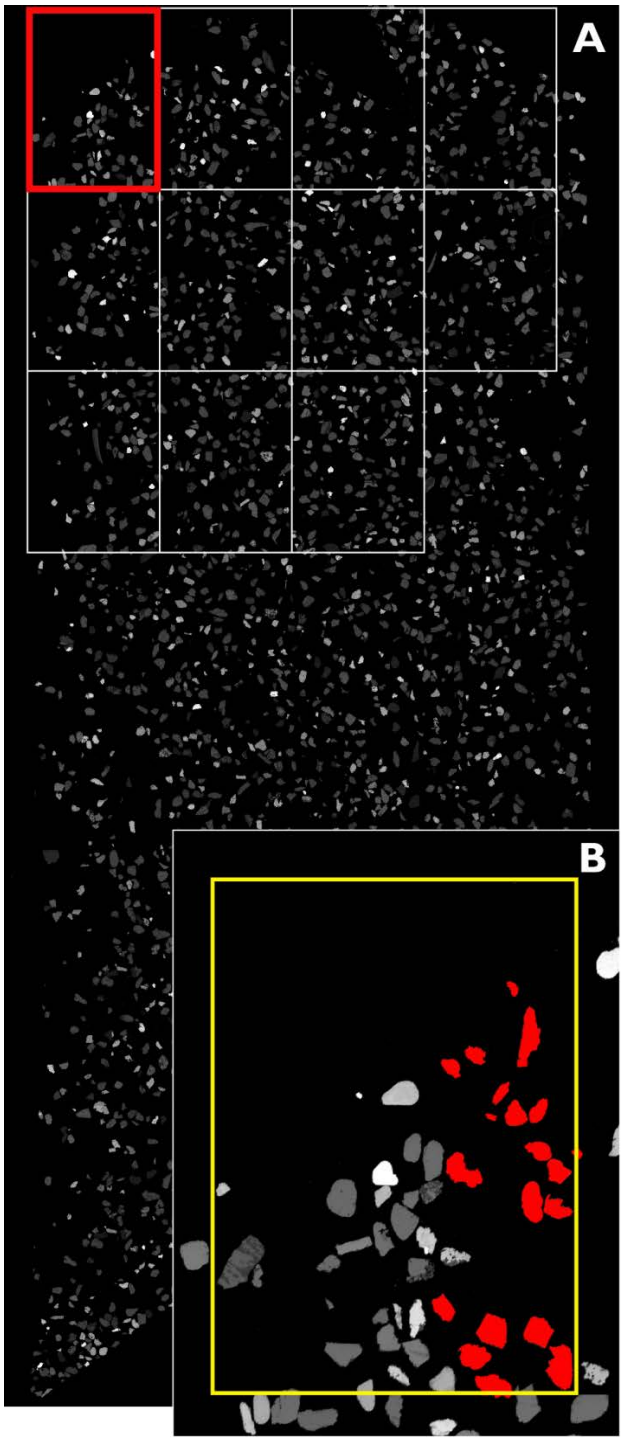

Figure 3. *A: Back-scattered electrons contrast (BSE) micrograph of a CCSEM sample of beach sediment from Jutland, western Denmark, divided into a number of frames in a grid. Part of the grid is outlined in white. Grains of different chemical compositions (different grey values) are embedded in an epoxy resin. Length of the sample is approximately 1.5 cm. B: Enlargement of one of the frames of the grid (indicated in red in A). The guard region (yellow) prevents double or incomplete measurements of grains (see text). The grey-level threshold function selects the grains one after one from the matrix for analyses of chemical composition, grain size and grain shape. Already analysed grains are shown in red; the image represents a snapshot of the CCSEM-procedure.*

The following minerals are currently identified in the database: Ilmenite, leucoxene, rutile, Ti-magnetite, magnetite, chromite, spinel, garnet, sillimanite-kyanite, staurolite, dark mica, white mica, feldspar, quartz, epidote, chlorite, olivine, clino-amphibole/pyroxene, ortho-amphibole/pyroxene, other silicates, corundum, pyrite, monazite, xenotime, phosphates, carbonates, and other minerals (unclassified).

Heavy Mineral Analysis

All the results discussed in this report are solely based on the geochemistry and morphology of the grains in the mounts that were analysed with CCSEM. Only the size fraction 45-500 micrometres has been considered and all results and interpretation are only based on these few grains.

The density of the heavy liquid used is 2.9 g/cm^3, which removes quartz and feldspars, but keeps minerals like hornblende (3-3.4 g/cm^3), dolomite (2.9 g/cm^3), white mica (ca. 2.9 g/cm^3), which are not heavy minerals sensu stricto. In this report, however, all analysed minerals, except quartz and feldspars, will be referred to as heavy minerals. Only a small fraction, one or a few percent for most sediments, of the grains remains after heavy liquid treatment. For brevity, we will refer to the analysed mounts as “the sample” and not as “the heavy mineral s.l. suite of the sample”. Terms like “abundant” or “rare” should thus be read in perspective, since they reflect the composition of the heavy mineral suite only, unless stated differently.

Limitation to the mineral classification based on CCSEM

Care should be taken when interpreting the CCSEM results on heavy minerals. The mineral classification is purely based on chemical composition of the measured grains. There are no further petrologic investigations involved in the classification. The distinction between ilmenite, leucoxene and rutile for example occurs on the measurements of the TiO_2 wt.% only. The boundaries in the CCSEM classification scheme for Ti-minerals lie at:
Magnetite < 21 wt.% TiO_2 <Ti-Magnetite < 46 wt.% TiO_2 <Ilmenite< 70 wt.% TiO_2 < Leucoxene < 87.5 wt.% TiO_2 < Rutile. For the same reason, sillimanite, andalusite and kyanite cannot be distinguished, they have the same chemical composition and are grouped as one mineral.

This can have major implications for the provenance and metamorphic history of the samples, as grains interpreted as leucoxene based on their TiO_2 grade can in fact be ilmenite or rutile grains and areas with abundant kyanite have very different history from areas where sillimanite is abundant.

Additionally, grains might have (micro-) inclusions, which composition will be included in the chemistry of the host grain. Grains can incidentally be non-liberated, which leads to a mixed chemistry of the two compositions. For a full interpretation of the data, additional petrography is needed.

The amount of water in the crystal lattice cannot be determined with EDX (and thus not with CCSEM) analyses for two reasons: 1) it is not possible to measure light elements, like O, precisely and very light elements, like H, cannot be measured at all. Thus, it cannot be determined whether water is present in the crystal structure. 2) The EDX software au-

tomatically recalculates the obtained concentrations to 100%, since analyses cannot be quantified absolutely (standard-less analysis). Therefore, it is not possible to observe that certain elements were missing in the analysis. As a result it is not possible to distinguish between pyroxenes and hornblendes. There is a large compositional overlap between the two minerals, if the water in hornblende crystal lattice is not taken into account. Therefore, the mineral classification scheme lists both minerals together: clino-amphibole/pyroxene and ortho-amphibole/pyroxene, or clino-pyrobole and ortho-pyrobole for short. For the same reasons, no distinction can be made between magnetite and hematite (and even goethite or siderite) or between corundum and bauxite.

There is a minor compositional overlap between hornblende/Al-rich clino-pyroxene, epidote and garnet. Therefore, there remains a small possibility that some of the garnets are in fact hornblende, or some of the garnets are classified as epidote or pyroxene/amphibole. The analysis for garnet only includes Al-garnets. Garnets that are very rich in Fe, like e.g. andradite, are classified as clino-pyrobole or ortho-pyrobole.

Garnet classification

For the aluminous garnets in the metamorphic and igneous rocks a classification based on 7 groups defining rock types and metamorphic conditions has been used (Keulen & Heijboer 2011; Figure 4). Garnets in group 1 include kimberlitic garnets and other garnets that experienced ultra-high pressure metamorphism. They are mainly derived from rock types with a mafic to ultramafic composition. Garnets in group 2 are mainly felsic granulites. “Felsic” includes all source rock with a pelitic, semipelitic, metasedimentary, granitic and granodioritic composition. Group 3 comprises mainly felsic amphibolite facies rocks; these are the lower temperature equivalents of group 2. The transition between these two groups is artificially put at XMg = 25, which corresponds roughly to a temperature of ca. 700-750 ºC. Group 4 consists of a) garnet amphibolites, generally formed at lower pressure conditions, or b) felsic amphibolite facies rocks that either have a more Ca-rich or more intermediate composition, like Ca-rich semipelites, or c) felsic rocks that underwent eclogite facies metamorphism, or d) charnockitic rocks. Group 5 includes intermediate and mafic amphibolites, and intermediate and mafic eclogites that were formed under relatively low temperature. Group 6 comprises most garnet amphibolites, mafic granulites and higher temperature mafic eclogites. Garnets derived from calc-silicates and anorthositic rocks plot in group 7. See Appendix C for further discussion.

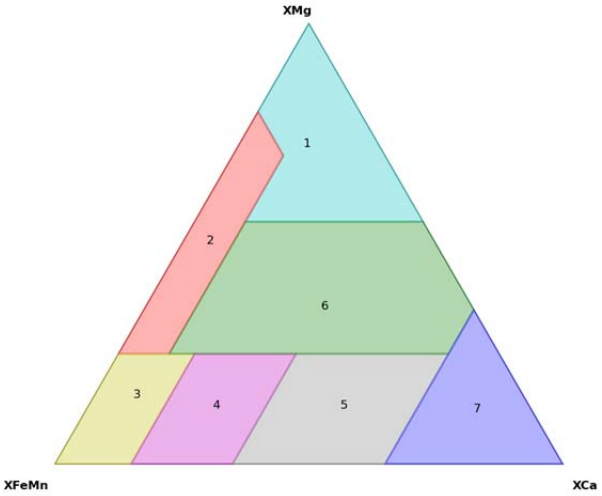

Figure 4. *Ternary diagram showing the seven classes of garnets, as used in this report. The three corners of the diagram show the aluminous garnets' end member compositions: XMg (pyrope), XFeMn (almandine & spessartine), XCa (grossular).*

Zircon provenance by LA-SF-ICPMS

Constraining sediment provenance through detrital zircon U-Pb age dating is now a well-established technique (Fedo et al. 2003 and references within). An important breakthrough has been the realisation of high throughput micro-beam technologies, such as ion probe or laser ablation based mass spectrometry, which enables acquisition of larger sample sets thereby reducing sampling biases (Williams & Claesson 1987, Jackson et al. 2004). Laser Ablation Inductively Coupled Plasma Mass Spectrometry (LA-ICP-MS) is particularly promising as it combines low cost and high speed with suitable accuracy and precision (Frei et al. 2006).

Attempts to characterize the diversity and complexity of sediment source regions using zircon age spectra requires assumptions regarding zircon distribution in the source regions as well as efficiency of transport and preservation. In granitoid terrains that represent the most common prospective source regions in the North Atlantic region, we presume that zircons reflecting the dominant igneous and metamorphic events are widely available and that they will be transported and preserved with comparable efficiencies. As such, we assume that zircon age spectra derived from young sediments will be indicative of the simplicity or diversity of source regions. Well-defined unimodal age spectra will indicate restricted and/or locally derived sediment whereas broad, complex multimodal age spectra are more likely to reflect large and/or distally-derived source regions. The likelihood of successfully identifying an individual age component in a sample is a function of its relative abundance in the zircon population and the number of zircons analysed. The more zircon grains that are analysed in any given sample, the more likely that all present age components will be successfully identified. This relationship can be described as:

$$P = (1-f)^n \quad (1)$$

where P is the probability for finding a single component in the population, f is the relative abundance of any given component in the population and n is the number of dated grains (Dodson et al. 1988). However, 117 grains have to be dated for a 95% confidence level in which all present components are identified in a worst-case population. We have been aiming for 120 grains or more when possible, but some samples, especially the cuttings samples yielded considerably fewer grains.

Methods

Zircons from all the large samples (the stream sediment samples), were separated using the Wilfley table. The cutting samples were too small for this procedure. Instead, the samples were sieved and passed through heavy liquids as for the CCSEM samples described below. The zircons were handpicked and mounted in epoxy and polished to expose a central cross section of each grain. Pictures were taken of the different samples such that the individual grains can be located and identified. Prior to loading the mount into the instrument, it is cleaned with ethanol to remove surface Pb contamination.

All U-Pb age determinations reported in this study were done at GEUS in Copenhagen, Denmark. The analyses were done in situ using a ThermoScientific Element2 Sector Field Inductively Coupled Plasma Mass Spectrometer (SF-ICP-MS) coupled to a New Wave Research®/Merchantek® UP213 laser ablation unit that is equipped with a frequency quintupled ND-YAG laser (wavelength of 213 nm).

Samples and standards were mounted in a low-volume ablation cell specially developed for U-Pb-dating (Horstwood et al. 2003). The laser ablation microprobe uses a focused laser to ablate a small amount of a sample contained in an air-tight cell. The ablated material is transferred to the mass-spectrometer in a carrier gas (Argon mixed with Helium) via Tygon® tubing for analysis.

All data were acquired using a 30 µm diameter single spot and an ablation time of 30 s. The result is ablation crater depths of approximately 15-20 µm, and ablated masses of approximately 65 ng. The laser was operated at a repetition rate of 10 Hz and a nominal energy output of 45 %, corresponding to a laser fluency of 3.5 J/cm^2. The total acquisition time for each analysis is 75 s with the first 30 s used to determine the gas blank, followed by 30 s of ablation and 15 s of washout time. The instrument is tuned to give stable signals for the ^{206}Pb and ^{238}U peaks, low background count rates (typically around 150 counts per second for ^{207}Pb) and low oxide production rates (^{238}U^{16}O/^{238}U generally below 1 %). ^{202}Hg, ^{204}(Pb + Hg), ^{206}Pb, ^{207}Pb, ^{208}Pb, ^{232}Th, ^{235}U and ^{238}U intensities were determined through peak jumping using electrostatic scanning in low resolution mode and with the magnet resting at ^{202}Hg. All data were acquired on four peaks per sample with a sampling and settling time of 1 ms for each isotope. Mass ^{202}Hg was measured to monitor the ^{204}Hg interference on ^{204}Pb where the ^{202}Hg/^{204}Hg = 4.36. If necessary, common Pb corrections were done using the interference and background corrected ^{204}Pb signal in combination with a model Pb composition (Stacey & Kramers 1975). The laser induced elemental fractionation was corrected by the intercept method (Sylvester & Ghaderi 1997; Kosler & Sylvester 2003) and the instrumental mass-bias on measured isotopic ratios was corrected through standard sample bracketing using the GJ-1 zircon (Jackson et al. 2004). Samples were analysed in sequences where an initial six standards are followed by ten samples, then three stand-

ards, followed by ten samples, three standards, and so on. The Plesovice zircon standard (Aftalion et al. 1989) has been used as an external reproducibility check, and yield short-term precisions (2σ RSD) of 1.5 %, 1.8 % and 1.1 % for the $^{206}Pb/^{238}U$, $^{207}Pb/^{235}U$ and $^{207}Pb/^{206}Pb$ ratios, respectively (Frei & Gerdes 2009).

The raw data is corrected for instrumental mass bias and laser-induced U-Pb fractionation through normalisation to the GJ-1 zircon using our in-house software ZIRCHRON. Data evaluation and presentation is done in Excel spread sheets and take advantage of IsoplotEx v. 3.0 (Ludwig 1999) and AgeDisplay (Sircombe 2004). All the results are stored in the zircon database accessible through the secure Sindri Web Site.

Discordance

Zircon ideally incorporates U and Th but not their decay products, isotopes of Pb, into its crystal structure. Zircon that remains closed with respect to U-Th-Pb will plot along a so called concordia curve as a function of their age. The concordia curve is characterised by increasing $^{206}Pb/^{238}U$, $^{207}Pb/^{235}U$ and $^{207}Pb/^{206}Pb$ ratios with increasing age (Fig. 5). The zircon may, however, be displaced from the concordia curve through either incorporation of common Pb, through Pb-loss or mixing of different age domains. Common Pb contamination will increase the measured $^{207}Pb/^{206}Pb$ ratio, and is the easiest cause to identify, as it is associated with elevated ^{204}Pb (Fig. 5). Common Pb contamination is normally confined to polishing surfaces, mineral inclusions or fractures. In this study, a large fraction of the zircons were metamict and very fractured, consequently, the results yield a high percentage of discordant ages.

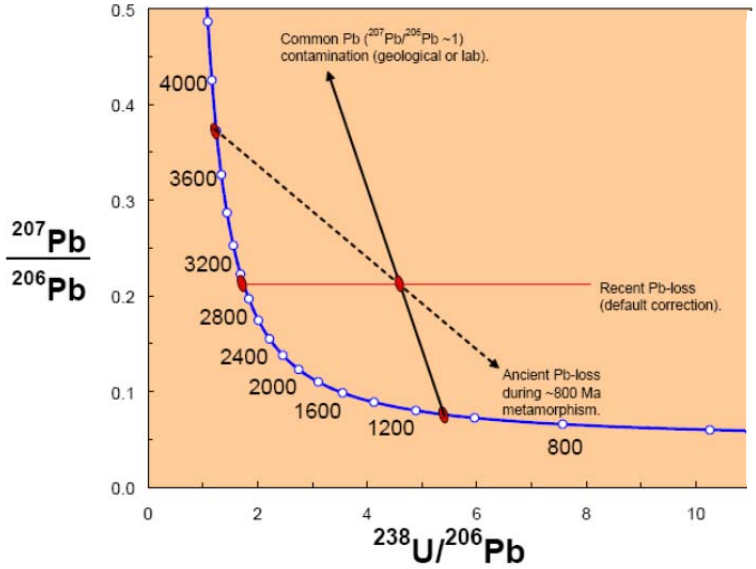

Figure 5. *The Tera-Wasserburg concordia diagram illustrates three possible causes of zircon discordance, namely common Pb contamination, mixing of age domains (or ancient Pb-loss) and recent Pb-loss. A single discordant U-Pb zircon analysis is not readily interpreted as the Pb-loss history cannot be constrained through discordia trends.*

Ancient Pb-loss has the same effect on the zircon as do mixed ages, and consequently will yield younger ages than the true age. Recent Pb-loss has no effect on the $^{207}Pb/^{206}Pb$ age and is assumed for all discordant data. Although assuming recent Pb-loss can be incorrect, the $^{207}Pb/^{206}Pb$ age is a minimum age, which may sometimes be useful. The causes of discordance are several, and may vary infinitely as functions of relative proportions in

mixed ages, and provide little or no useful additional information in a provenance study. We, therefore, use an arbitrarily chosen filter criteria, where all data that is between 90-110% concordant are plotted together with a dark grey colour in the histograms whereas all data more than 10% discordant are plotted with a light grey colour. The two patterns mostly follow each other, but when they do not, we only refer to the concordant ages.

TIMS analyses of Baddeleyites

The U-Pb age determinations of baddeleyite are analysed using Isotope-Dilution Thermal Ionisation Mass Spectrometry (ID-TIMS) at the University of Toronto. This is necessary as the typical grain sizes are smaller than 30 µm and they are also extremely thin. ID-TIMS analyses also offer an order of magnitude better precision, than the LA-ICPMS, which is important especially when the ages are very young e.g. Palaeocene in this case.

Project A: Provenance of sediments in the Faroe-Shetland basin: Characterisation of source components in Southeast Greenland.

Plate reconstructions of the North Atlantic region indicate the former proximity of East Greenland to the Faroe Island region. Consequently, as hydrocarbon exploration pushes further westward in the Faroe-Shetland Basin, there are increasing questions as to the role that Greenland has played as a source of sediment to the basin. Studies by GEUS and CASP on the Cretaceous–Early Palaeogene sedimentary succession in Kangerlussuaq, East Greenland, have indicated that a major sediment input point may have existed in the Kangerlussuaq Basin in the earliest Palaeocene (Larsen et al. 2005, Nøhr-Hansen et al. 2006).

The SINDRI project ”Linking the Faroese area and Greenland: an innovative, integrated provenance study” (2005) conclusively demonstrated that the sedimentary sources from the eastern (i.e. UK margin) and western (i.e. Kangerlussuaq, East Greenland) marginal areas have distinctive provenance sensitive signatures with respect to detrital U-Pb zircon age distributions and heavy mineral characteristics (Frei and Knudsen 2008, Morton et al. 2009, Frei et al. 2005,) that can be employed to distinguish between these two different sources. The detrital zircon age distributions and the bulk rock geochemistry of the sedimentary successions drilled in the Faroese sector have been investigated in the SINDRI project No. 46-32-01 “Provenance of sediments in the Faroe-Shetland basin” (Frei and Knudsen 2008). However, the full potential of this extensive database for the reconstruction of the sediment supply history to the Faroe-Shetland basin is only realised if the provenance sensitive signatures (especially on detrital zircon U-Pb age distributions and heavy mineral signatures) in possible source areas are sufficiently well constrained.

Determination of the provenance sensitive signatures is especially difficult for the East Greenlandic source, where the major part of the potential source area is covered by the Inland Ice and is not amenable to sampling. In this project we constrain the provenance signatures of the potential sediment source areas south of Kangerlussuaq by analysing 4 tillite samples and 19 stream sediment samples. These data will significantly contribute to our understanding of the provenance characteristics of the southeast Greenland source and may give new information on provenance changes across major structural lineaments identified in the area (Karson and Brooks 1999). It will, therefore make a significant contribution to a more sophisticated and coherent framework for the interpretation of the sediment supply history to the Faroe-Shetland basin and the correlation of sediment units across the basin based on sedimentary provenance characteristics. Furthermore, the intention was to incorporate all of the detrital zircon U-Pb age distribution data obtained in this study into a database together with data from previous SINDRI funded work.

Samples

We processed 4 tillite samples and 19 stream sediment samples from streams that drain basement rocks in South-East Greenland between 62-68°N (Table 1). A stream sediment sample is a volume of recently deposited sediment from a minor stream with a local catchment area. Sand in stream sediment samples is related to the local bedrock geology in an area, while reworking of glacial material and the change in composition of the sand due to sedimentary processes only plays a minor role (Kalsbeek et al., 1974). Thus, as long as streams do not directly drain moraine deposits, their sediments are a good way to describe the local geology. Samples are referred to in the text by their GGU-number. See Figure 6 for a map with sample localities.

GGU#	lab#	Latitude	Longitude
483291	2001289	67.76983	-32.71700
483292	489292	67.76983	-32.71700
483297	483297	66.98917	-34.01183
483298	483298	66.98917	-34.01183
552661	2004724	66.93505	-34.00037
552670	2004725	66.66594	-34.23270
550895	2004718	66.50599	-38.05720
552653	2004727	66.32974	-35.45693
550686	2004716	66.18732	-37.90037
550886	2004717	66.08301	-36.38179
550903	2004719	66.03695	-37.36369
552564	2004721	65.69694	-38.68417
552530	2004720	65.66334	-37.42408
552620	2004723	65.63042	-39.57883
552708	2004726	65.58403	-36.93141
550662	2004715	65.09523	-40.00115
552607	2004722	64.89316	-41.08442
550645	2004714	64.33511	-40.92412
550120	2004674	63.75409	-41.27476
550052	2004673	63.39660	-41.54573
550148	2004675	63.08039	-41.77446
550272	2004676	62.86389	-42.48464
550512	2004678	62.41740	-42.34688

Table 1. *Overview of samples collected for analysis.*

The geological map that forms the basis for the Figure 6, and others is modified by T.F.D. Nielsen (2010) after the three original 1:500 000 scale maps produced by the Geological Survey of Greenland (now Geological Survey of Denmark and Greenland, GEUS): Skjoldungen (Escher 1990), Kangerlussuaq (Myers, Dawes & Nielsen 1988) and Sydgrønland (2nd edition, Garde 2007). Selected topographic names are shown in Figure 7.

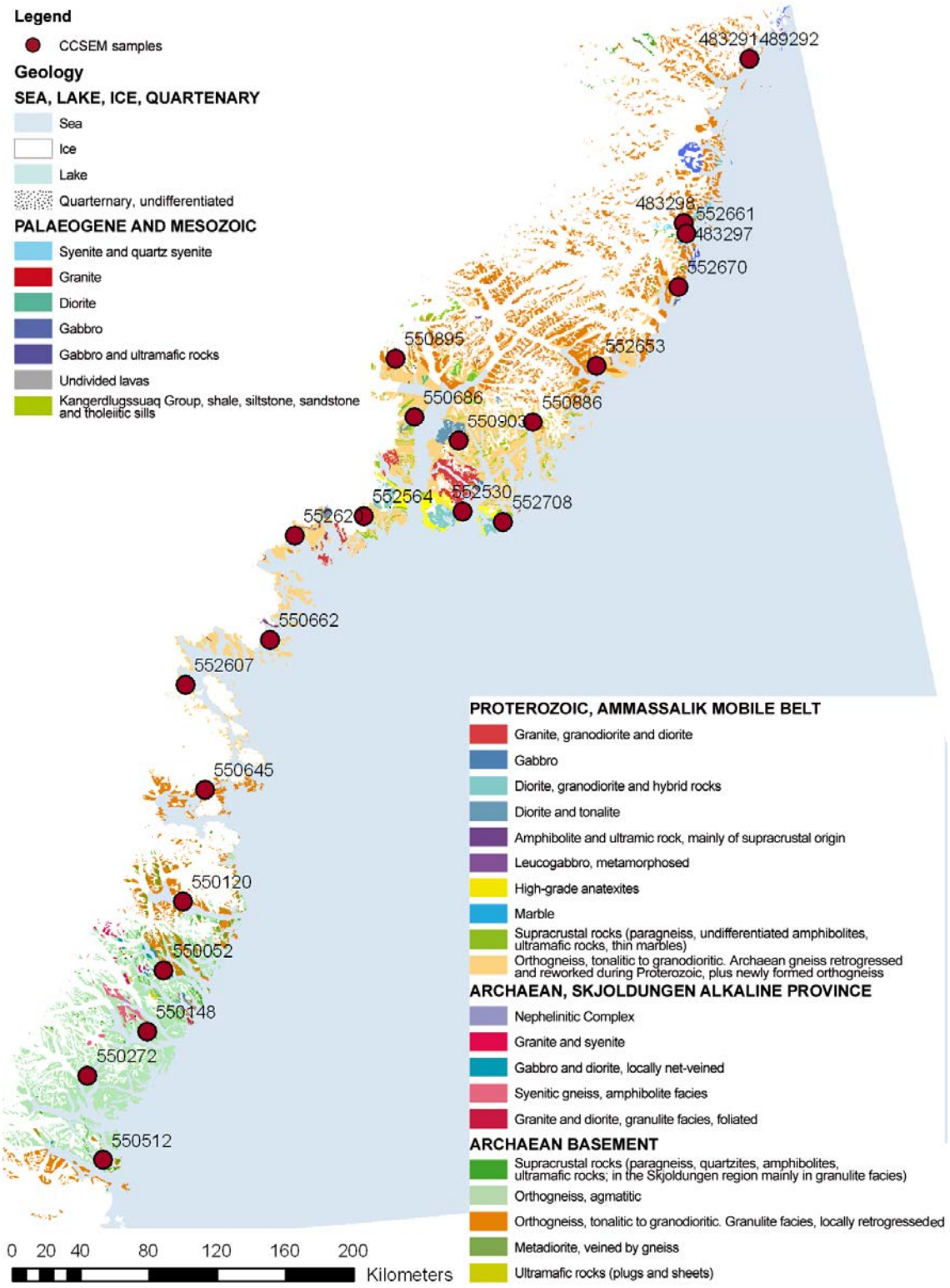

Figure 6. *Overview of all sample localities.*

Figure 7. *Selected place names for South-East Greenland between 68° and 62°N.*

CCSEM Results

Results for the stream sediment samples will be described from north to south along the coast. For sample localities and the geological legend, the reader is referred to Figure 6. First the results for the modal heavy mineral suites will be discussed. Additional information can be found in Appendix A. Since clino-pyroxene/clino-amphibole is the main heavy mineral in the region, an attempt to further classify these minerals is given, the results are displayed in Appendix B. Finally, the results for the garnet composition and their rock-type and metamorphic association are discussed. Details on the garnet measurements are shown in Appendix C.

The sample 483291 and 483292 were collected between Kap Edvard Holm and the Nordre Parallelgletscher (Kong Christian IX Land), where tonalitic and granodioritic-granitic orthogneiss, amphibolite and ultramafic rocks are the main outcropping units (Figure 6). The area is reported to be mainly in granulite facies (Myers et al. 1988). The samples have garnet as their major heavy mineral (Figure 5). Clino-pyroxene/clino-amphibole, biotite and ortho-pyroxene/ortho-amphibole are common. Less abundant are sillimanite-kyanite, muscovite, epidote and ilmenite-Ti-magnetite (Figure A2, A9). The clino-pyroxene/clino-amphibole in these samples has an augite composition. Muscovite, sillimanite/kyanite and garnet suggest that some more aluminous rocks are present in the area, which could be a more felsic-aluminous component in the gneiss or metamorphosed sediments. The assemblage partially exists of metamorphic minerals of granulite facies or upper amphibolite facies grade, while retrograde minerals (e.g. epidote) were observed as well.

Peak metamorphic conditions and a more felsic rock composition are confirmed by the composition of the garnets (Figure 9). They consist of a mixture of group 2 and group 3 garnets (red and yellow field; see also Figure A8). These groups represent garnets from felsic rock at high to intermediate metamorphic grade.

Sample 483297, 483298, and 552661 were collected in the Skrækkensbugt area and sample 552670 from Kap Gustav Holm. 483297, 483298, and 552670 were collected from the tonalitic and granodioritic-granitic orthogneiss, which represents the major rock unit in the area. Sample 552661 was collected in the vicinity of the contact between this orthogneiss and Palaeogene syenite and quartz-syenite. The four samples show a very similar heavy mineral suite: clino-pyroxene/clino-amphibole, ortho-pyroxene/ortho-amphibole, Ti-magnetite (Figure A9) and biotite are the most common minerals. Figure A2 and A3 show that iron-oxide (probably magnetite) is found abundantly as well. Sample 552661 was very rich in feldspars, even after heavy liquid separation (Fig. A3). The four samples have hornblende (of edenite-hastingite composition) and augite or diopside-augite as clino-pyroxene/clino-amphibole minerals. The ortho-pyroxene/ortho-amphibole in samples 483297 and 483298 might possibly be pigneonite (Figure B2). The observed minerals are stable over a wide range of temperature conditions, up to lower granulite facies. Some retrograde minerals like epidote were observed, especially in sample 552670.

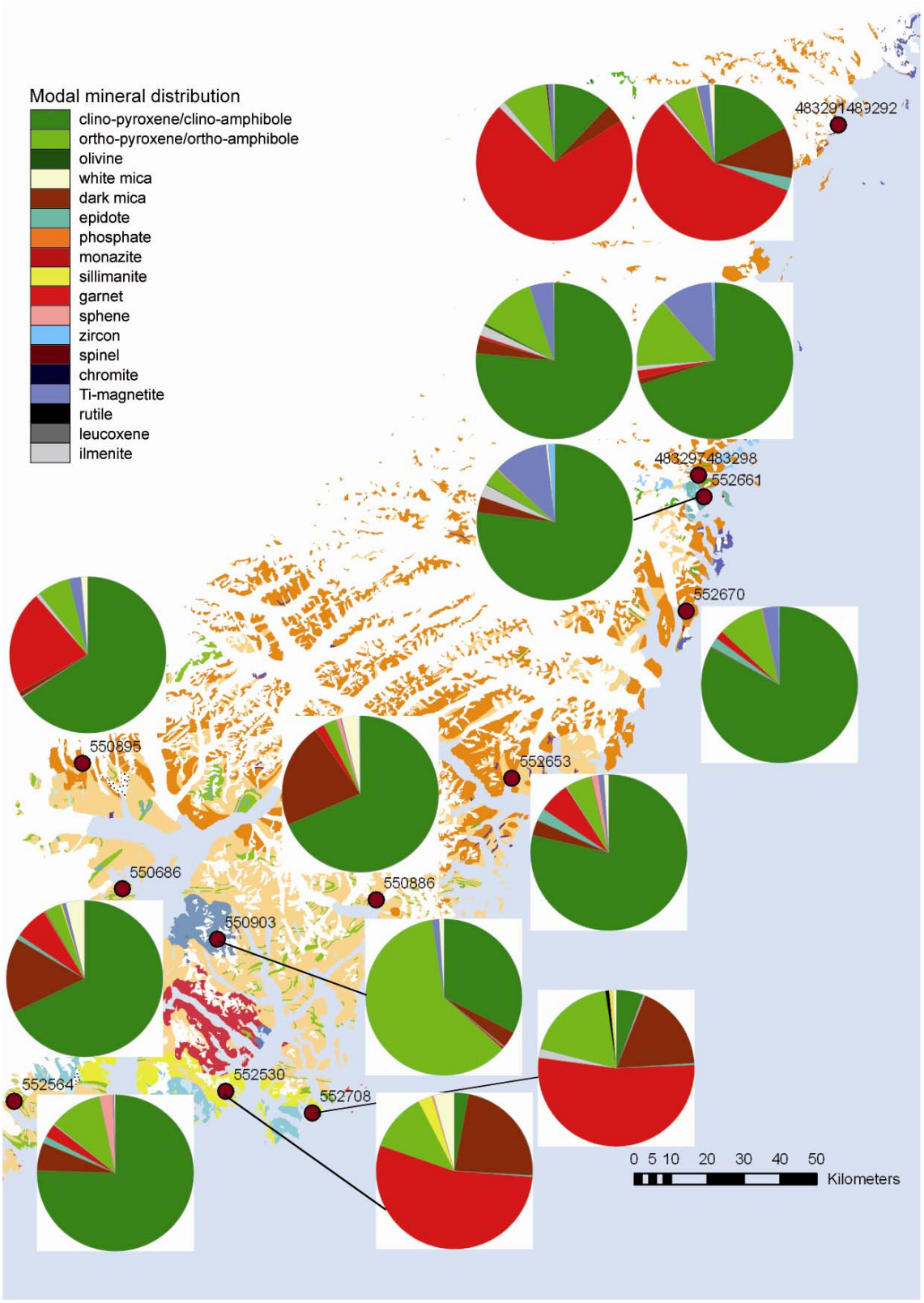

Figure 8. *Modal heavy mineral distributions in pie-diagrams for the samples collected between 65°30' and 68°N. Geological legend in Figure 6.*

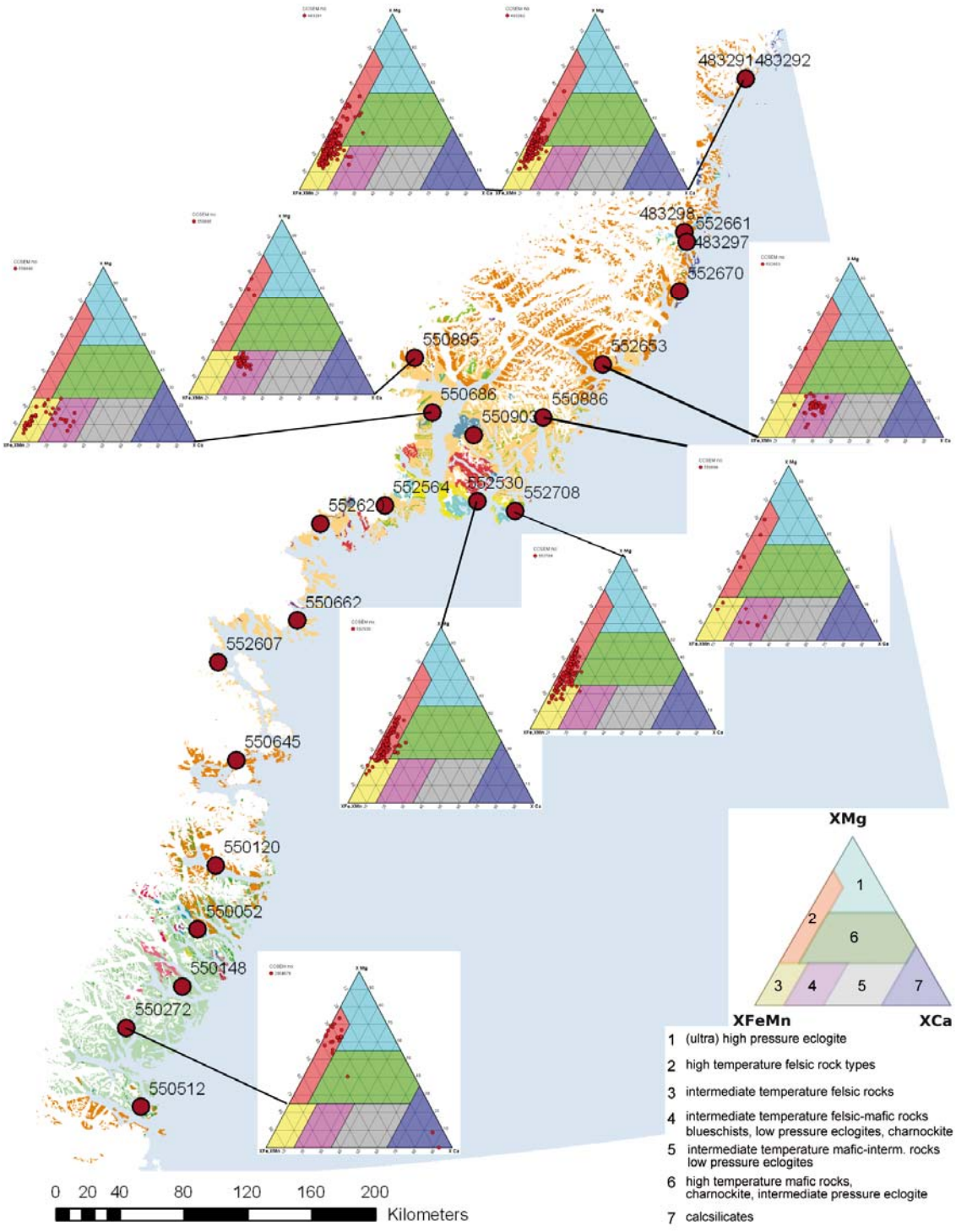

Figure 9. *Garnet composition in ternary-diagrams for the samples collected between 62° and 68°N. Only samples with more than ten garnets are shown. Geological legend in Figure 6.*

Sample 552653, 550895, 550686 and 550886 represent the basement west of Nigertuluk, on Niflheim, west of the Sermilik fjord, and north of the Sermiligaaq fjord, respectively. The major lithology in these areas is an Archaean tonalitic to granodioritic orthogneiss, which is retrogressed from granulite facies and reworked during the Proterozoic (Myers, Dawes & Nielsen 1988). In this orthogneiss, supracrustal rocks (including paragneiss, quartzites, amphibolites, and ultramafic rocks) were observed. The first sample (552653) has a heavy mineral suite that is similar to the previous four, but the latter three yield more garnet, dark mica and white mica than the previous (Figure 5). Some sillimanite-kyanite was observed in sample 550686, indicating that the sample has a more felsic component. Investigations of the heavy mineral suite's clino-pyroxene/clino-amphibole minerals yield a strong presence of hornblende (mainly hastingite, some of more kærsutite and edenite compositions) and some augite-diopside (Figure B2 and B3). The rocks have a typical amphibolite facies mineral paragenesis with hornblende and biotite.

All four samples yielded abundant garnet (Figure 9) that mainly plot in garnet group 4. This group represents garnets derived from intermediate to mafic composition rocks that were metamorphosed at intermediate temperature conditions. Sample 550686 additionally has garnet that was derived from a more felsic rock. These observations fit well with an assumed amphibolite facies metamorphism and a more felsic component in the drainage area of sample 550686.

Sample 550903 is derived from the large body of diorite and tonalite east of the fjord Sermilik north of Ikasarvitak. The body is one of the post-tectonic, Palaeoproterozoic intrusive bodies in the area (Chadwick et al. 1989). The intrusion is layered and includes anorthosite and more ultramafic layers, apart from the diorite and tonalite. Figure 8 show that ortho-pyroxene/ortho-amphibolite is the most common mineral in this stream sediment sample. Furthermore, clino-pyroxene/clino-amphibole occurs abundantly as well. Many feldspar grains remained after heavy liquid treatment (see Figure A4) these feldspars are Ca-rich plagioclase minerals. The ortho-pyroxene/ortho-amphibolite is probably pigeonite (see Figure B3). This fits with fieldwork observations from the area (2010): ortho-pyroxene has abundantly been observed in the area, while ortho-amphiboles were not observed (J. Kolb, pers. comm. 2011).

Two samples, 552708 and 552530, are derived from the Ammassalik Intrusive Complex East of Kulusuk and East of Tasiilaq, respectively. The intrusive complex consists of undeformed diorite, granodiorite and hybrid rocks. The instrusion was emplaced into a package of supracrustal rocks dominated by sedimentary protolits, within which it caused widespread anatexis. The anatexites were described as garnet-gneiss envelope, consisting of graphitic semi-pelitic and psammitic metasediments intercalated with grey gneisses. Restitic sillimanite has been observed in the metasedimentary rocks (Friend & Nutman 1989). The intrusive rocks are both acidic and mafic, consisting of ortho-pyroxene + biotite ± hornblende and quartz + plagioclase. This composition is reflected in the heavy mineral suite (Figure 5). The two samples yield abundant garnet, biotite and some sillimanite/kyanite. Ortho-pyroxene/ortho-amphibole is more abundant than clino-pyroxene/clino-amphibole. Figure B3 shows some pigeonite in sample 552708. The heavy mineral suite suggests that peak metamorphic conditions might have been up to granulite facies, as has been suggested before by Friend & Nutman (1989) who reported granulite facies rocks in the area, with a large amphibolite facies overprint.

The garnet distribution for these two samples is clearly supportive of the felsic composition, e.g. metasedimentary or granitic-derived rock composition, for the garnets' parent rock (Figure 5). Most of the garnets in sample 552730 plot in garnet group 2 (felsic rock composition, high grade metamorphic temperature conditions), while sample 552708 also has a small component in garnet group 3 (felsic rock composition, intermediate temperatures of metamorphism) (Figure A9).

The tonalitic to granodioritic orthogneiss between Kap Tycho Brahe and Jens Munk Ø in the Køge Bugt and near the Graah Øer are represented by the stream sediment samples 552564, 552620, 550662, and 552607. This orthogneiss consists of tonalitic to granodioritic, retrogressed Archaean brown gneiss, reworked (during the Early Proterozoic) Archaean grey gneisses and in places newly, formed Early Proterozoic orthogneisses occur (Escher 1990). The heavy mineral suite consists of mainly clino-pyroxene/clino-amphibole, and ortho-pyroxene/ortho-amphibole, biotite, epidote, sphene and garnet also have been observed (Figure 7). None of the samples had enough garnets to give a qualified estimation of the rock composition or temperature of metamorphism. Figure B4 and B5 show that hastigite hornblende, locally with a more edenite-hornblende composition is the common clino-pyroxene/clino-amphibole. In most samples these hornblendes cover a whole range of compositions (Figure B4 and B5). Hornblende, biotite and epidote are typical for rocks with peak metamorphism at amphibolite conditions.

Samples 550645 and 550120 are collected from the tonalitic to granodioritic gneiss at Umiviik and North of Bernstorff Isfjord. Escher (1990) describes the orthogneiss in this area as grey gneiss, tonalitic to granodioritic, amphibolite facies, in places retrogressed from granulite facies. The heavy mineral suite is dominated by clino-pyroxene/clino-amphibole; the samples show epidote and biotite, and some sphene, garnet, muscovite, and ortho-pyroxene/ortho-amphibole (Figure 10). Figure B5 shows that the clino-pyroxene/clino-amphibole minerals in these two samples mainly are hastingite hornblende with a little augite in the samples. In sample 5504645, the hornblende composition ranges so broadly that some of the minerals are of tremolite composition. Hastingite hornblende and tremolite are typical minerals for amphibolite facies gneiss or amphibolites included in them. The presence of a small quantity of augite hints at slightly higher temperatures. If these minerals are not derived from intrusive bodies, peak metamorphic conditions might have at upper amphibolite-lower granulite conditions. Epidote and possibly biotite might have formed during retrogression of the gneiss.

The agmatitic orthogneiss is represented by the stream sediment samples 550052, 550148 and 550512. Kolb et al. (in press) refer to these orthogneisses as orthopyroxene-bearing granitic (charnockitic) gneiss. The observed heavy mineral suite consists of similar portions of clino-pyroxene/clino-amphibole and ortho-pyroxene/ortho-amphibole, a large fraction of Ti-magnetite (Figure A10), some biotite, ilmenite, and some minor amounts of garnet, muscovite and epidote (Figure 10). Figure B5 and B6 show that the clino-pyroxene/clino-amphibole and ortho-pyroxene/ortho-amphibole are pigeonite and augite, while Figure A6 and A7 show that the samples yield abundant iron-oxide, probably magnetite as well.

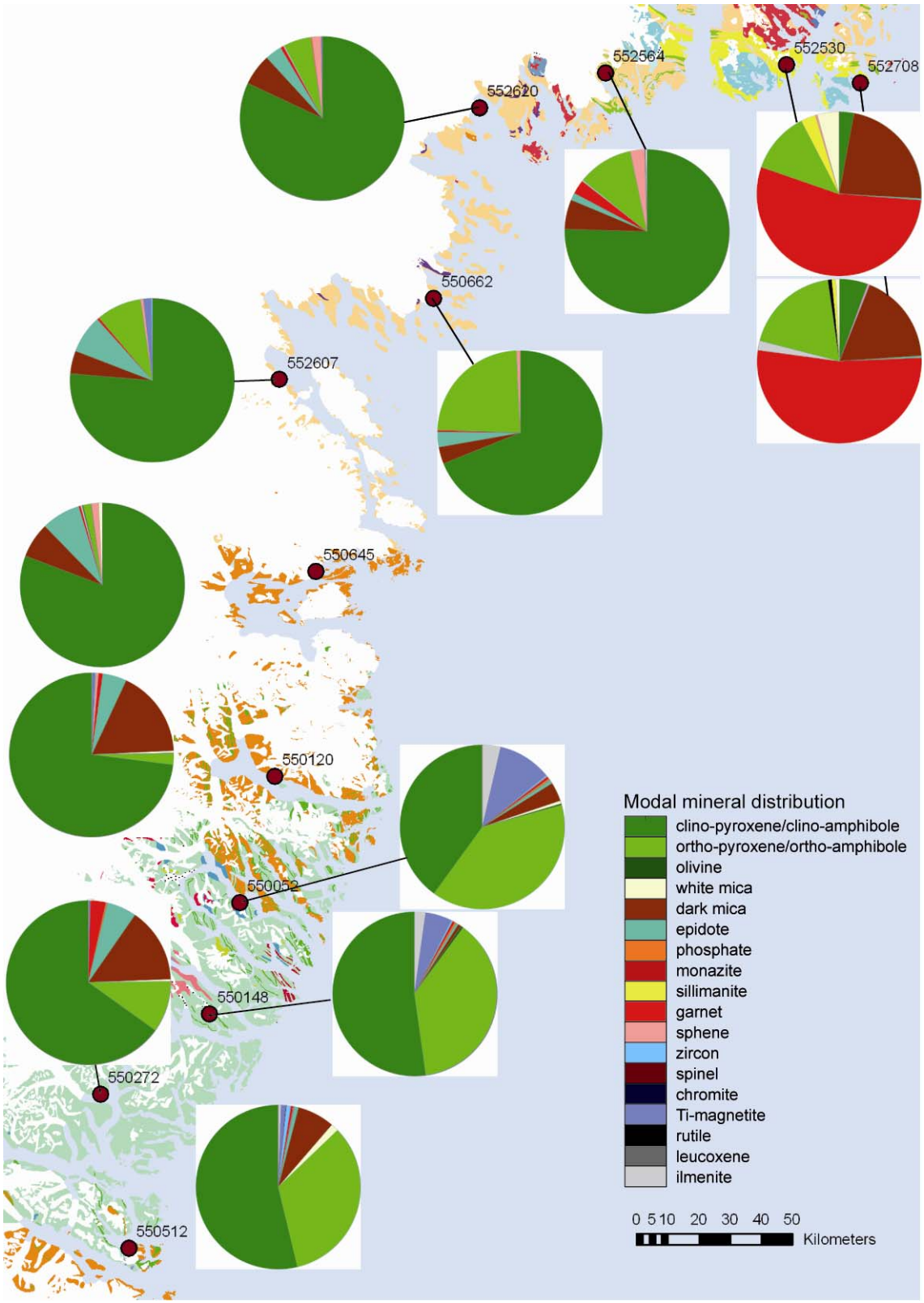

Figure 10. *Modal heavy mineral distributions in pie-diagrams for the samples collected between 65°30' and 62°N. Geological legend in Figure 6.*

These observations concur with Kolb et al. (in press), who describe the gneiss as orthopyroxene, clinopyroxene, magnetite, quartz, feldspar, biotite and pyrite-bearing. This mineral paragenesis indicates that peak-metamorphic conditions were at granulite facies conditions. Sample 550512 shows less ortho-pyroxene, magnetite, and Ti-magnetite, and more hornblende and biotite. This indicates either that peak metamorphic temperatures in the southern part of the agmatitic gneisses were lower, or that retrogression was more pervasive.

Sample 550272 is also collected from a stream dewatering the agmatitic orthogneiss, like the three samples discussed above. Its mineral assemblage resembles the sample from North of Bernstorff Isfjord (550120) with mainly clino-pyroxene/clino-amphibole and common ortho-pyroxene/ortho-amphibole, biotite, epidote and garnet. Figure B6 shows that the clino-pyroxene/clino-amphibole mainly consists of hastingite-edenite hornblende, and some augite. Retrogression from granulite facies to amphibolite facies seems to be more pervasive here than in the other three samples from the agmatitic gneiss (550052, 550148 and 550512). Alternatively, more supracrustal-derived lenses or bands (like mafic granulites/amphibolites or metasedimentary-derived rocks) could be present in the drainage area of these samples, which would also explain the higher amount of biotite, muscovite and garnet in these rocks.

The garnet in this sample shows that at least part of the stream sediment was derived from a felsic rock type that has been metamorphosed under high-temperature conditions. Some garnets are derived from a calc-silicate rock (Figure A9).

U-Pb results

Four tillite samples and 19 stream sediment samples were selected for zircon U-Pb analyses. Two of the samples (552661 and 550903) had no zircons. Results will be described from north to south just as for the CCSEM data. Sample localities are seen in Figure 6 and Table 1. Further details on the sample location and composition can also be found in the section on the CCSEM results.

The results are depicted in probability density distribution plots, using an arbitrarily chosen filter criteria, where all data between that are 90-110% concordant are plotted together with a dark grey colour in the histograms, whereas all data more than 10% discordant are plotted with a light grey colour. The two patterns mostly follow each other, but when they do not, we only refer to the concordant ages.

Sample 483291 and 483292 are tillite samples, collected between Kap Edvard Holm and the Nordre Parallelgletscher (Kong Christian IX Land). The samples were small and not many zircons were retrieved from these samples. The concordant fraction yielded ages between 3000 and 2500 Ma with the main peak at approximately 2700 and 2770 Ma, respectively (Figure 11 and 12).

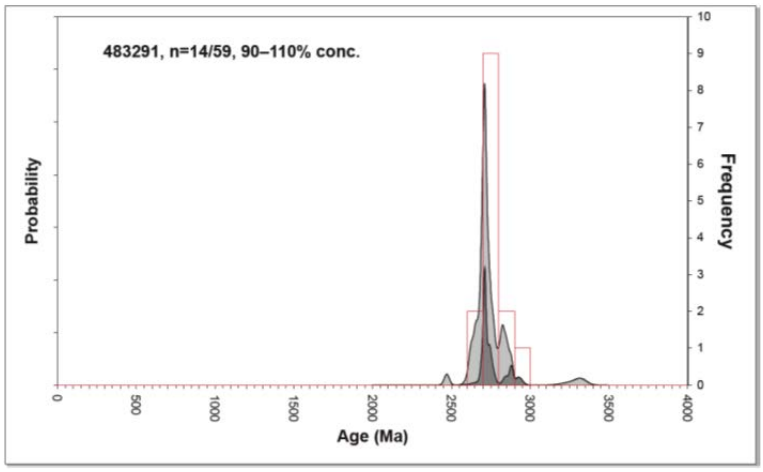

Figure 11. *Probability density distribution for sample 483291.*

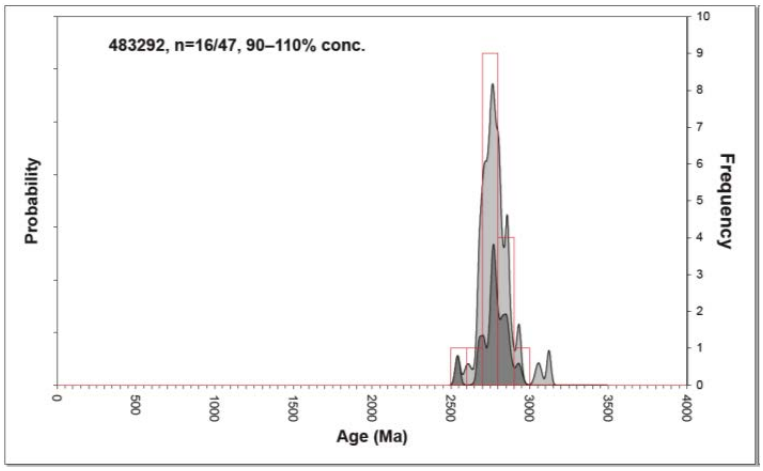

Figure 12. *Probability density distribution for sample 483292.*

Sample 483297 and 483298 are tillite samples collected in the Skrækkensbugt area. These samples were also small, but where sample 483297 contained a relatively large amount of zircons, 483298 only had 10 grains. Sample 483297 yielded ages between 3100 and 2600 Ma with a prominent peak at 2700 Ma. Sample 483298 also had the main peak at 2700 Ma, despite much fewer analyses (Figure 13 and 14).

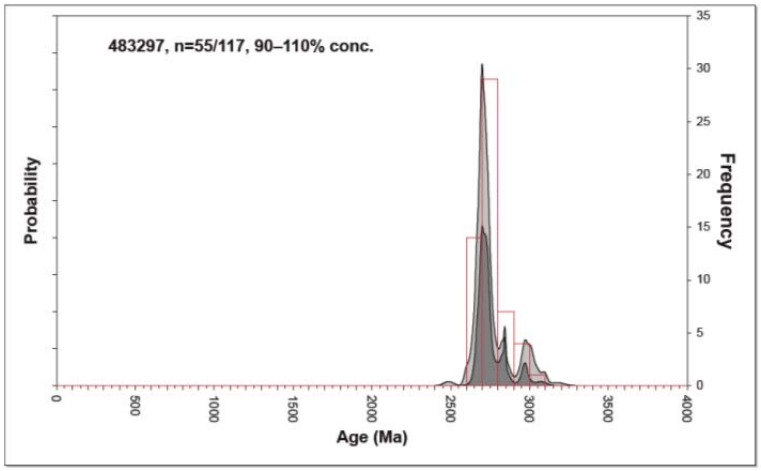

Figure 13. *Probability density distribution for sample 483297.*

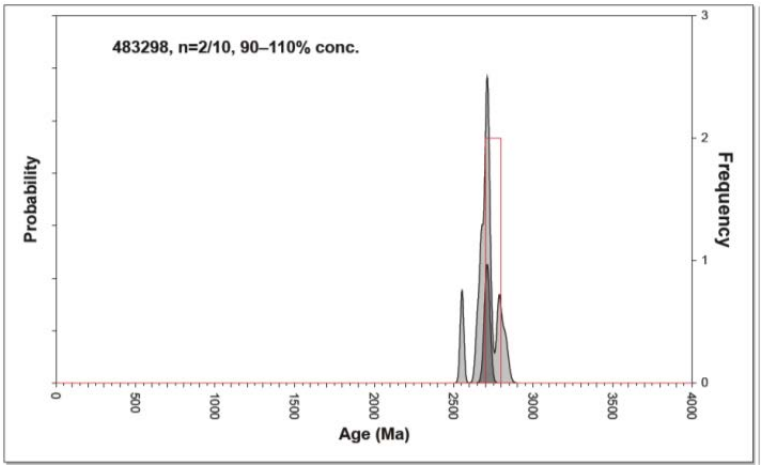

Figure 14. *Probability density distribution for sample 483298.*

The remaining samples described are stream sediment samples. Sample 552670 was collected at Kap Gustav Holm and sample 552653 was collected further south, at Kap Japetus Stenstrup. Both samples are dominated by one very large peak at 2750 Ma, but where sample 552670 has some smaller and older peaks at 2900 and 2850 Ma, then the detrital zircon pattern from 552653 yields one large unimodal population (Figure 15 and 16).

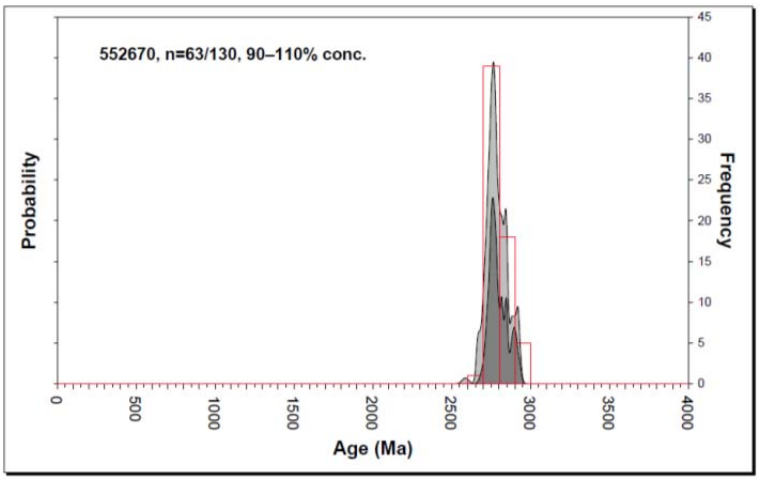

Figure 15. *Probability density distribution for sample 552670.*

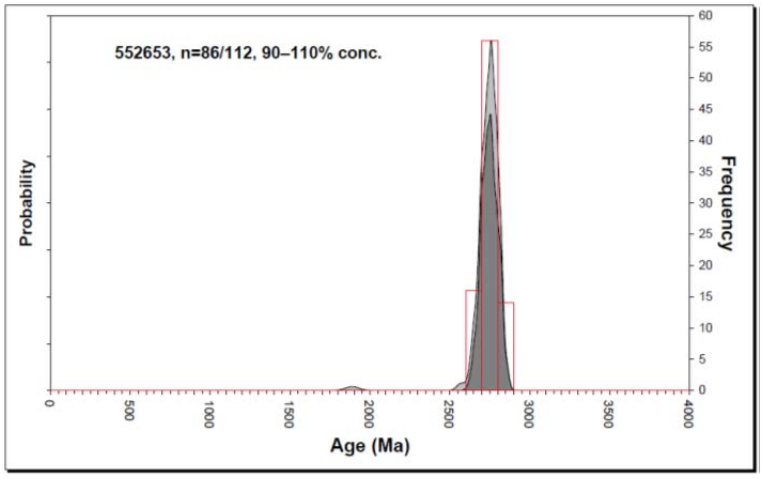

Figure 16. *Probability density distribution for sample 552653.*

Sample 550895 is from the Niflheim area. The zircon population shows the same age range as the previous samples ranging from approximately 3000 to 2500 Ma. The detrital zircon pattern yields the largest peak at c. 2775 with a smaller one at 2700 Ma.

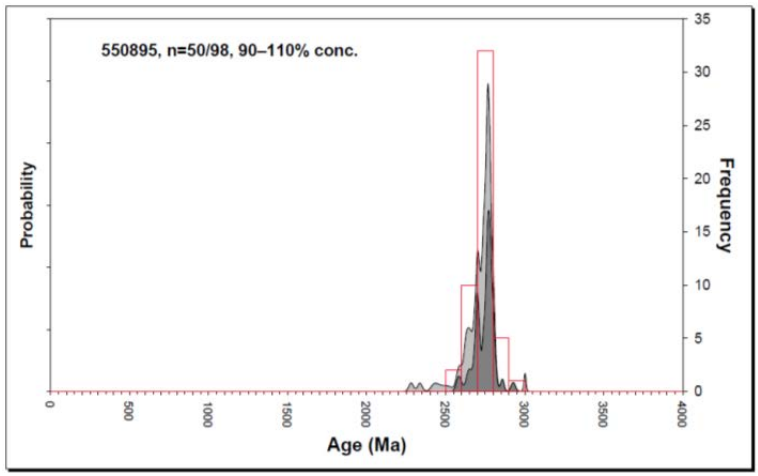

Figure 17. *Probability density distribution for sample 550895.*

Sample 550886 is collected along the coast, north of the Sermiligaaq fjord. This sample yields a much larger range of ages than seen in the previous samples. The bulk of the zircon ages fall between 3200 and 2450 Ma. This is the only sample in the northern part of the area that yields ages above 3000 Ma. This age range is characterized by many different peaks of similar sizes; however, the three most dominating ages are from 3100-3000 Ma and around 2800 Ma and 2700 Ma. In addition, the sample also has a small zircon population of 1850 Ma ages, which is not seen in the previous samples (Figure 18).

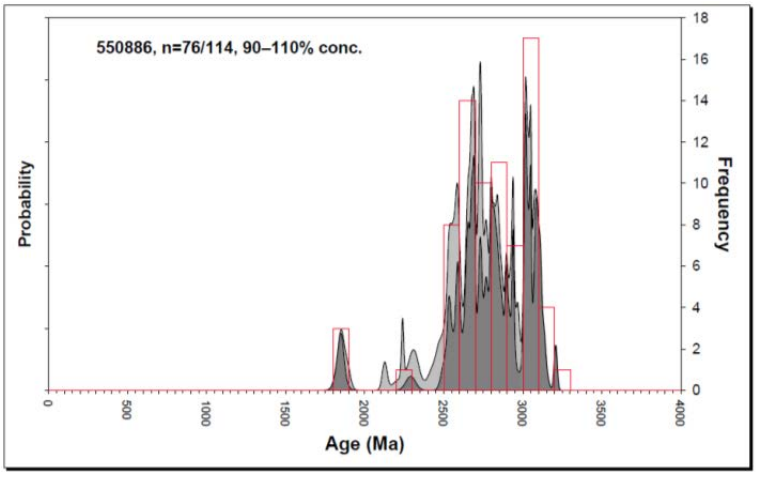

Figure 18. *Probability density distribution for sample 550886.*

Sample 550686 from the north-western part of Sermilik Fjord is dominated by a large peak at 2820 Ma and by a smaller, but still significant peak at 2975 Ma. The zircon pattern yields a tail of ages from 2820 and down to 2100 Ma (Figure 19).

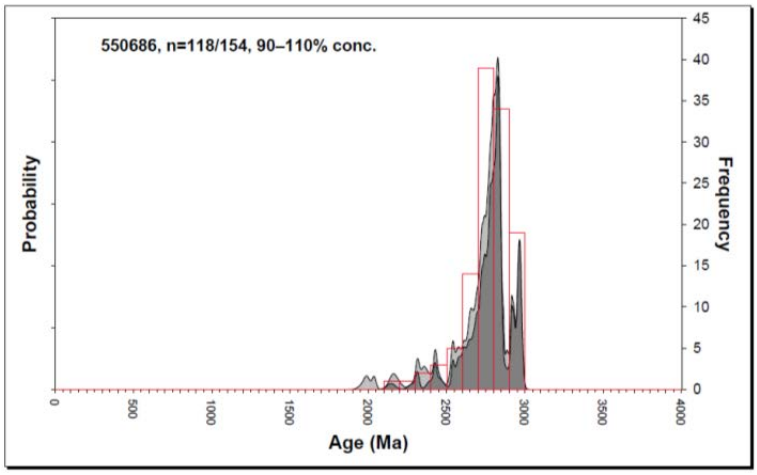

Figure 19. *Probability density distribution for sample 550686.*

Sample 552708 and 552530 are both from the Ammassalik Intrusive Complex area. These samples are in contrast to the former dominated by Palaeoproterozoic peaks, and they only have minor occurrences of Archaean grains. The main peak in sample 552708 is at 1900 Ma and in sample 552530 it is at 1950 Ma. The age range spans from 3000 to 1850 Ma (Figure 20 and 21).

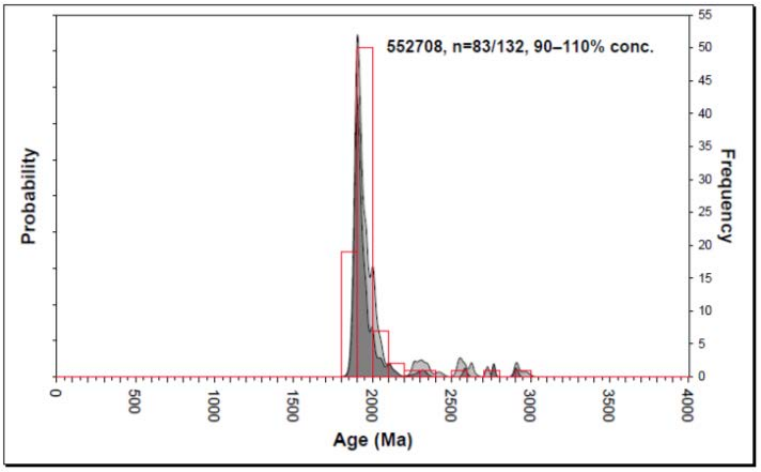

Figure 20. *Probability density distribution for sample 552708.*

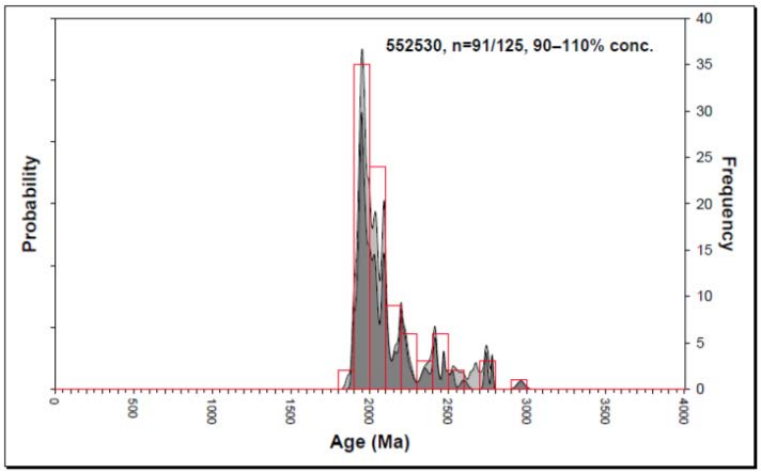

Figure 21. *Probability density distribution for sample 552530.*

Sample 552564 is collected west of Kap Tycho Brahe, in the close vicinity to a proposed suture zone. The zircon pattern is very different from any other samples and yield ages which have not previously been recognized in the area. The ages range from 2850 to 1850, with the most dominating peak around 2500 Ma and a couple of smaller peaks at 2650 and 2600 Ma (Figure 22).

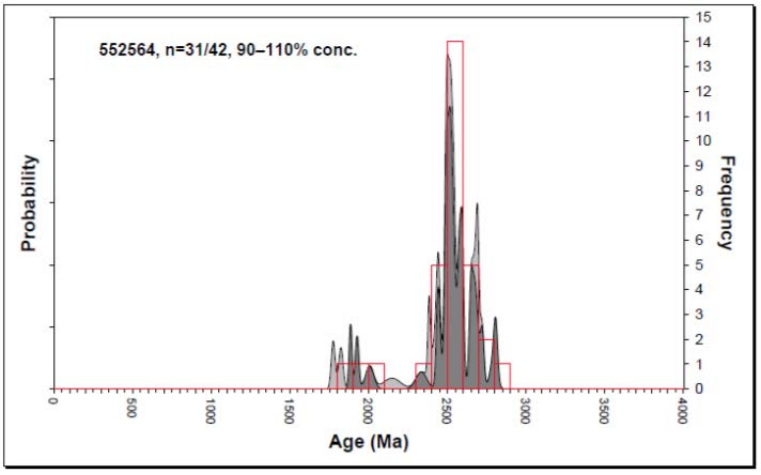

Figure 22. *Probability density distribution for sample 552564.*

Sample 552620 is collected near Ikertivaq. The zircon pattern is dominated by ages from 2900 to 2600 Ma with the most prominent peak at 2700 Ma. A small Palaeoproterozoic peak at 1900-1800 Ma is also present (Figure 23).

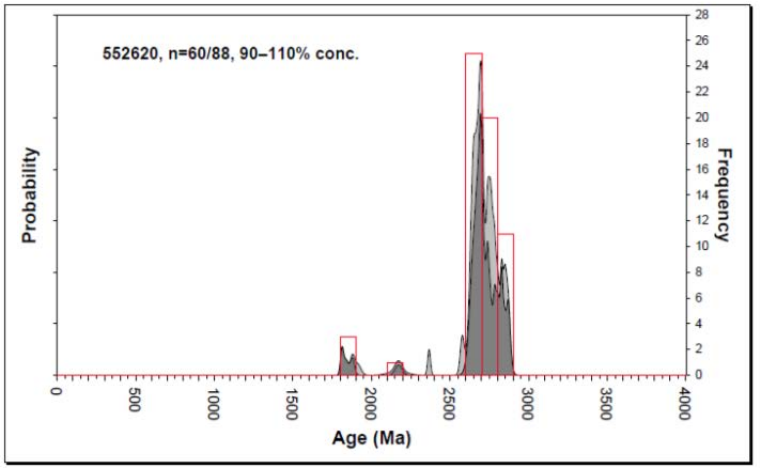

Figure 23. *Probability density distribution for sample 552620.*

Sample 550662 is collected in the area of Graah Øer. From this point and southwards we enter an area with prominent amount of Meso- and even Palaeoarchaean zircon grains. The ages in this sample range from 3300 to 2550 Ma and in addition there is a minor occurrence of zircons with age of 3750 Ma (Figure 24).

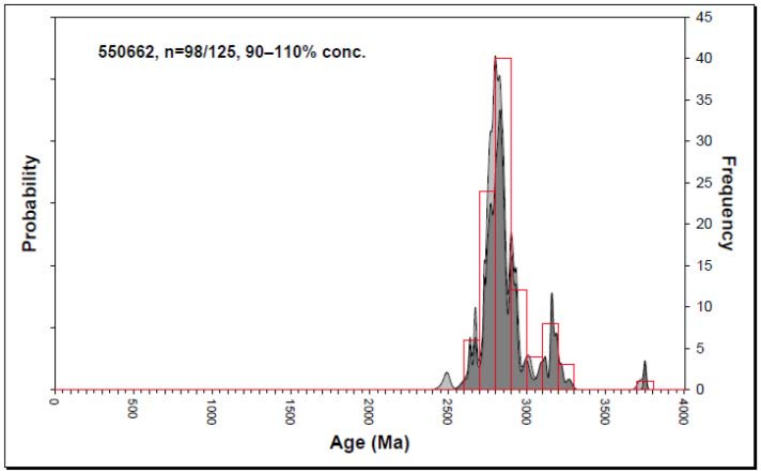

Figure 24. *Probability density distribution for sample 550662.*

Sample 552607 is collected in the Køge Bugt region. The ages range from 3200 to 2550 Ma, with the dominating peak at 2900 Ma (Figure 25).

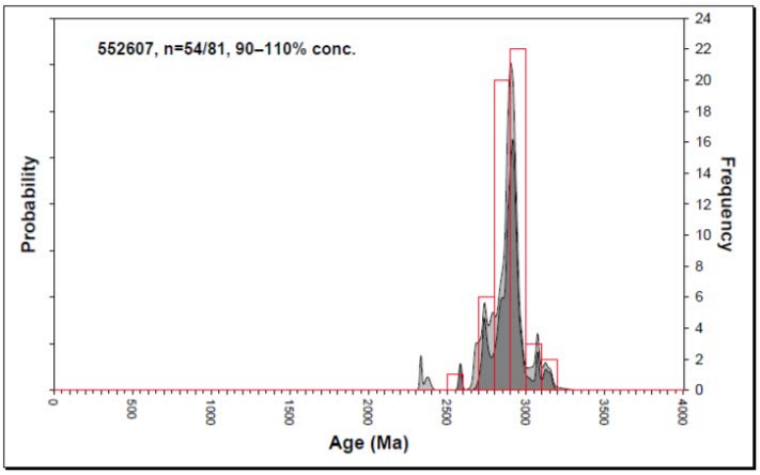

Figure 25. *Probability density distribution for sample 552607.*

Sample 550645 is collected at Umiivik. The detrital age pattern spans a large range of ages from 3200 to 1800 Ma. The pattern is dominated by two almost equally large peaks at 2820 and 2750 Ma. In addition there is pronounced peaks around both 3150 and 1900 Ma, just as ages between 3000 and 2850 occurs in high number. This is the only sample in the southern part of the region in where Palaeoproterozoic zircons are found (Figure 26).

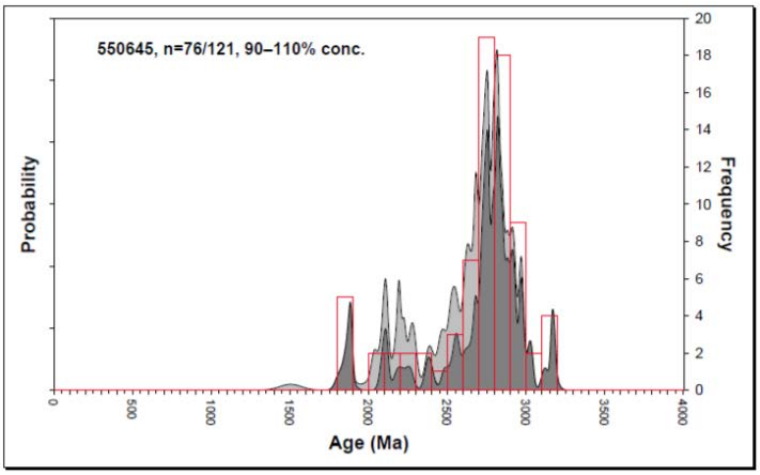

Figure 26. *Probability density distribution for sample 550645.*

Sample 550120 is from the northern coast of Bernstorff Isfjord. The bulk of the ages are between 3150 and 2700 Ma, while the full spectrum range from 3250 to 2550 Ma. There are several peaks, the most dominant once are between 3050-2950, around 2850 and between 2775 and 2700 Ma (Figure 27).

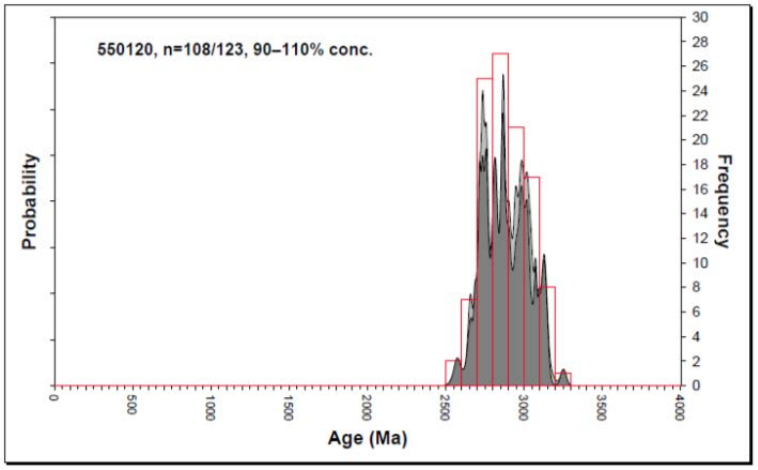

Figure 27. *Probability density distribution for sample 550120.*

Sample 550052, 550148, 550272 are from the agmatitic orthogneiss area in Skjoldungen, Kong Dan Halvø and by Heimdal glacier, respectively (Figure 28, 29 and 30). The detrital zircon pattern from these three samples has similar characteristics. They are all dominated

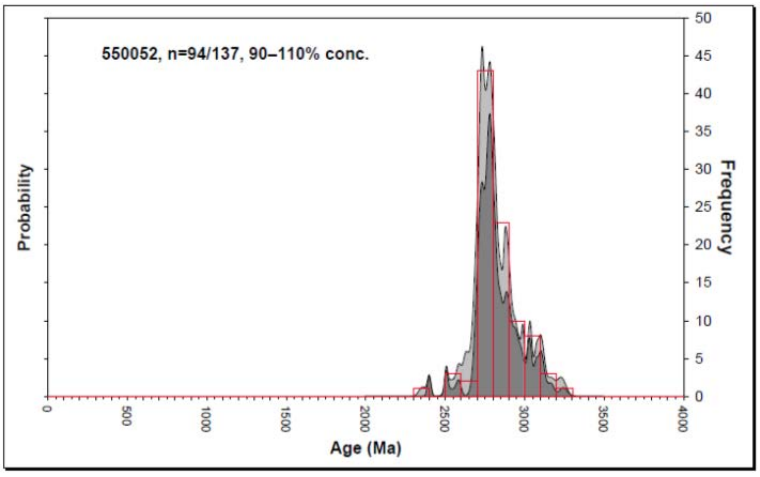

Figure 28. *Probability density distribution for sample 550052.*

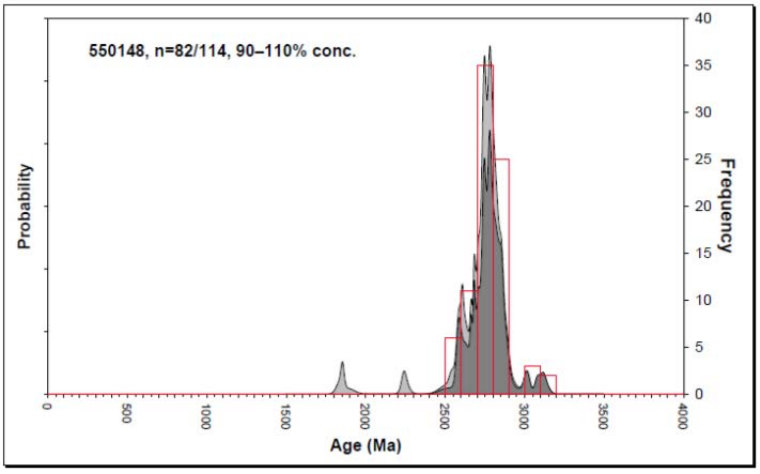

Figure 29. *Probability density distribution for sample 550148.*

by a large peak between 2800 and 2700 Ma, in some of the plots it is a broad peak in others a very narrow one. In all three samples there are few younger ages and the youngest are around 25 -2400Ma. All samples also contain older populations of zircons, but to varying extent. In sample 550552 there is a significant amount of older grains with the oldest being around 3300 Ma. Sample 550148 only have a minor amount of older grains with the oldest being 3150 Ma. Sample 550272 has the largest range of old ages with the oldest being 3650 Ma.

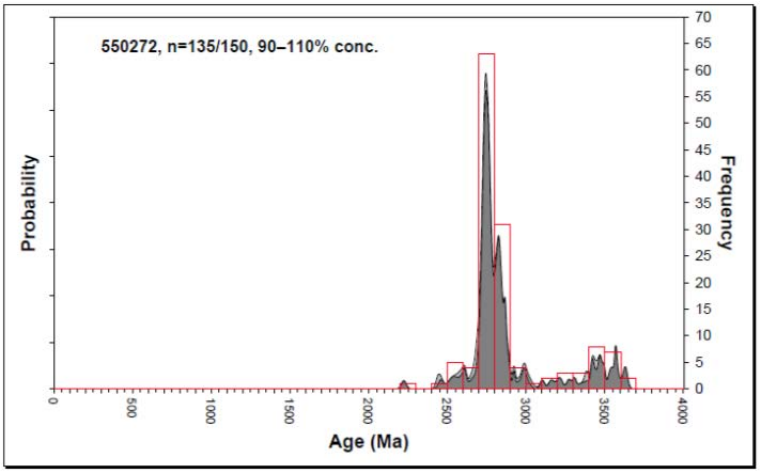

Figure 30. *Probability density distribution for sample 550272.*

Sample 550512 is collected north of Mogens Heinesen Fjord. The sample is similar to the samples in the previous group, as it is dominated by a large peak between 2800 and 2700 Ma, with minor younger grains, but the difference is that it has almost no zircons older than 2950 Ma (Figure 31).

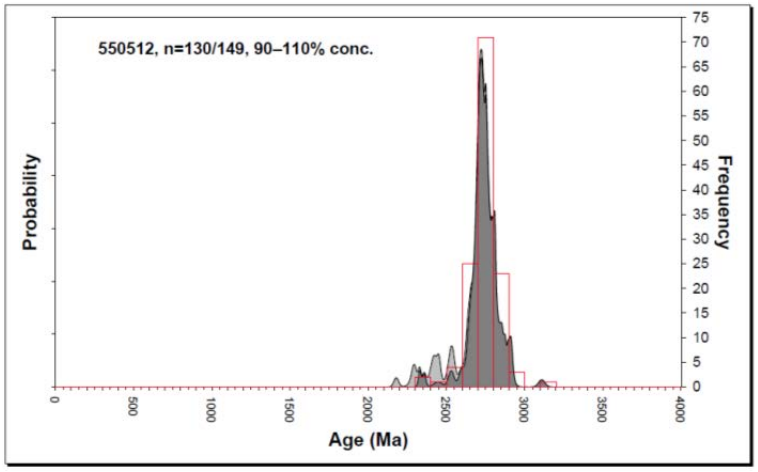

Figure 31. *Probability density distribution for sample 550512.*

Discussion

Provenance characteristics of the Eastern Greenlandic basement between 62° and 68° N.

CCSEM

On the basis of the CCSEM analyses the orthogneiss in the area between 62° and 68° N can be divided into five different zones (Figure 32). Within these zones six analysed stream sediment samples can be grouped as special inclusions, covering two intrusive complexes and two areas rich in supracrustal rocks. The orthogneisses comprise, from North till South:

Orthogneiss A: The heavy mineral assemblage of this orthogneiss was interpreted as ortho-pyroxene, clino-pyroxene, Ti-magnetite and magnetite-bearing. This mineral assemblage suggests that peak metamorphic temperatures were up to granulite facies conditions. Other characteristic minerals for this orthogneiss, e.g. for provenance purposes, are biotite, ilmenite and hornblende. Epidote was observed locally, which is resulting from retrograde reactions in the orthogneiss.

The high metamorphic conditions are confirmed by the presence of felsic Al-rich rocks in the northern part of the study area (marked with 1 in Figure 32). Here, garnet is the major part of the heavy mineral suite and those indicate a felsic rock composition, and metamorphic peak conditions at high-temperatures. Augite, biotite, ilmenite, Ti-magnetite and minor sillimanite-kyanite are further defining the heavy mineral suite.

Orthogneiss B: The heavy mineral suite of the orthogneiss B has been interpreted as amphibolite facies, with hornblende, clino-pyroxene, biotite and garnet. Muscovite, sphene and Ti-magnetite form minor but distinctive contributions. The exact boundary between orthogneiss A and B is not known everywhere, in Figure 32; we followed the boundary indicated by Myers et al. (1988) and Escher (1990). Sample 550895 and 552653 are collected more or less on the boundary between the granulite facies rocks and the amphibolite facies rocks, but are dominated by the amphibolite facies gneiss. Thus some of the clinopyroxene in these samples are richer in Na than usual augite is (ca. 4 wt%), which does indicates a composition between omphacite and augite. Omphacite is indicative for high-pressure during metamorphism. Nutman & Friend (1989) describe “eclogitic” cores in dykes (their quotation marks) with sodic clinopyroxene. They interpret these “eclogitic” cores as indicative for an early high pressure deformation phase. Thus the “eclogitic” cores could not be confirmed during fieldwork in 2010.

In this area, a large post-tectonic, Palaeoproterozoic intrusive body of diorite and tonalite has been sampled, which is a major source for the orthopyroxene.

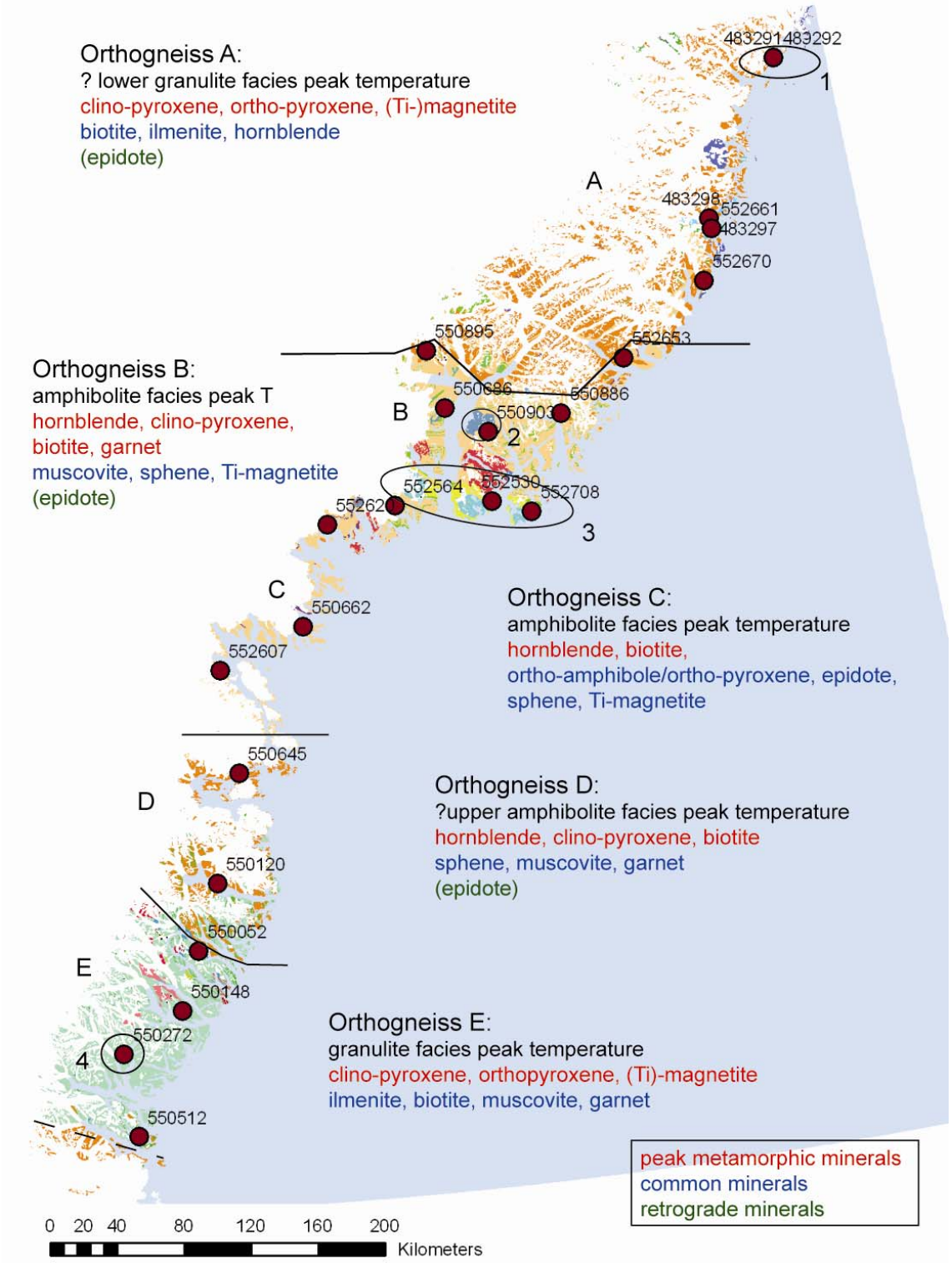

Figure 32. *Overview map for the results of the CCSEM samples collected between 68° and 62°N. Five different zones with orthogneiss and four special areas have been defined by their mineralogy. Geological legend in Figure 6.*

Orthogneiss C has also been interpreted as an amphibolite facies orthogneiss. However, its mineral assemblage is slightly different from orthogneiss B. Here hornblende and biotite, ortho-amphibole/ortho-pyroxene, epidote, biotite, Ti-magnetite and sphene are the major contributors to the heavy mineral suite. The hornblende in these samples is rather rich in aluminium and mainly of a hastingite composition. The amount of aluminium in hornblende increases with increasing pressure (Ernst & Liu 1998). Thus, here as well as in orthogneiss B, slightly higher pressures during metamorphism might have occurred.

Between orthogneiss B and orthogneiss C the Ammassalik Complex intrusive rocks and high-grade anatexites occur. These anatexites are garnet-bearing graphitic semi-pelitic and psammitic metasediments that were metamorphosed at high temperatures. Apart from garnet, sillimanite-kyanite, ortho-pyroxene, biotite, and muscovite were found in these rocks, resulting from contact metamorphism. So even though the surrounding orthogneisses might not have reached metamorphic conditions higher than amphibolite facies, higher temperatures seemed to have occurred related to the large intrusions in the Ammassalik area. Friend & Nutman (1989) describe the presence of these sediments to be related to an unconformity, and mention that these play a major role in thrusting and folding of the area.

Chadwick et al. (1989) describe that the area covered by orthogneiss B and C and their intrusive rocks form the Proterozoic mobile belt of Ammassalik. They suggest that the boundary between orthogneiss B and orthogneiss C indicates the transition between an area of reworking, retrogression (from granulite to amphibolite facies) of gneisses and of acid and basic intrusive rocks to the north and reworked amphibolite facies gneiss to the south. This reworking however, is not obvious from the obtained heavy mineral suites.

Orthogneiss D has been indicated as retrogressed from granulite facies according to Escher (1990). Chadwick et al (1989), however, describe the gneiss as amphibolite facies. The heavy mineral suite does not give much evidence for granulite facies relict minerals. Hornblende, clino-pyroxene and biotite define the peak metamorphic assemblage, which is typical for amphibolite facies conditions. Other minerals in the heavy mineral suite include epidote and small amounts of sphene, muscovite, and garnet. Thus, it is important to emphasise that we only have 2 samples from this area.

Orthogneiss E has a high temperature mineral assemblage including orthopyroxene, clinopyroxene, magnetite and Ti-magnetite, which indicate that temperatures might have been up to granulite facies conditions. Other common minerals are ilmenite, biotite, muscovite and garnet. The assemblage is distinctive by its high amount of ortho-pyroxene. Escher (1990) indicated granulite facies for the northern half of the area covered by orthogneiss E and amphibolite facies for the southern half. A temperature gradient in the gneisses might exist from north to south, visible in the decreasing amount of orthopyroxene, magnetite and Ti-magnetite. Kolb et al. (in press) on the other hand, interpretate the whole area as granulite facies rocks.

In sample 550272, the minerals yield a more intense retrogression from granulite facies to amphibolite facies than in the other three samples from the orthogneiss E. Its mineral assemblage resembles orthogneiss D. No difference between this area and the surrounding orthogneiss has been indicated on the map (Escher 1990).

U-Pb data

The age pattern changes from north to south commensurate with ages of the basement rocks, with an overall dominate age range from 2900-2700 Ma. Some samples contain older ages, a single sample yield ages up to 3700 Ma, and several samples have significant amounts of 3200-3000 Ma ages. Other samples contain younger Archaean ages down to 2500 Ma. Most samples do not contain Proterozoic zircons except the two samples collected in the Palaeoproterozoic Ammassalik Intrusive Complex area which yield age patterns dominated by 1950-1900 Ma zircons, in good agreement with the intrusion age.

Even though the age patterns of the different samples are relatively similar, there are still differences, which make it possible to divide the basement of Southeast Greenland into various zones. Most of the time the zones correspond to the ones made based on the CCSEM analyses.

Orthogneiss A: Represent the area shown in Figure 32, thus, from the U-Pb analyses it is clear that sample 550895 and 552653 belong to this section and not orthogneiss B. These seven most northern orthogneisses all yield a very similar age pattern, dominated by ages between 2800 and 2700 Ma. In most of these samples, the total age range goes from 2900 to 2600 Ma. None of the samples have any concordant Proterozoic ages, and only one sample yield few ages around 3100-3000 Ma.

Orthogneiss B and C: The area is a much more complex area than the previous. Whereas the area north of here is dominated by Archaean granulite facies orthogneisses, this area is dominated by Archaean amphibolite facies orthogneisses, which have undergone strong deformation and probably subduction during the Palaeoproterozoic. Palaeoproterozoic intrusions are numerous. Therefore, the detrital age pattern is very subjective to where the sample is taken and consequently the age patterns vary a lot. In general, the patterns are still dominated by Archaean ages, but several of the samples have input of Palaeoproterozoic ages between 2000 to 1850 Ma. In most samples, these Palaeoproterozoic peaks are small, but two samples collected within the Ammassalik Intrusive Complex is, not surprisingly, dominated by the Palaeoproterozoic ages. Apart from the Palaeoproterozoic ages this area is also characterised by having several samples with a significant amount of older Archaean ages between 3250 to 3000 Ma, which is not seen to the north. One sample, 552564, is differently than the rest. The main peak is around 2500 Ma, which is an uncommon age in this region. The sample is taken near a potentially large shear zone, which has not been studied in any detail.

Orthogneiss D: This area is only represented by two samples. The age pattern of these two samples is not distinctly different from the age patterns of the previous area B and C and they could be included in the same group, on the basis of the zircon data.

Orthogneiss E: Covers the area of main Skjoldungen region (Figure 32). All the samples from this area are very similar and the age patterns in all the samples are dominated by 2800 to 2700 Ma ages. The age patterns are very similar to the pattern of orthogneiss A in the very northern part of the area, as basically all the Palaeoproterozoic ages is lacking here. The difference is that in this area, there are still occurrences of older Archaean grains in some of the samples, with ages up to 3250 Ma. The exception is sample 550272, which has ages ranging all the way up to 3650 Ma, with a small but distinct population between 3600 and 3400 Ma.

Comparison of the Faroe-Shetland Basin with the Kangerlussuaq region and other source regions

CCSEM

In “Linking the Faroese area and Greenland: an innovative, integrated provenance study” (2005), a number of provenance techniques were discussed. Here, we will shortly summarize the results from 2005 and compare them with the new CCSEM data.

Morton et al. (2005) discuss conventional petrographic and mineral-chemical techniques applied to sandstones from the Faroe-Shetland basin and the Kangerlussuaq area. They apply three mineral ratios to classify the sandstones from the Kangerlussuaq area and Faroese basin: Rutile:zircon (RuZi), apatite:tourmaline (ATi) and garnet:zircon (GZi) ratios. CCSEM analyses do not analyse for tourmaline, thus the ATi could not be applied to our samples. Our studies usually did not yield enough zircons and nearly no rutile, thus calculations were not made. Qualitatively we can state that zircon is more abundant than rutile for the whole area between 62° and 68° N on the Greenlandic coast, such that low RuZi ratios are expected. Garnet was abundant in some samples, especially those of a more metasedimentary nature. For these samples a high GZi ratio is expected, as was described for the Faroese well data (Morton et al. 2005).

Morton et al. (2005) and Frei et al. (2005a) use a different garnet classification than we did, but the results can easily be compared. Morton et al. (2005) divide their garnets into three groups A; low Ca, high Mg, group B: low Mg, variable Ca and Fe, and group C: high Mg and high Ca. Group A is subdivided into Ai: X_{Mg}>30% and Aii: XMg= 20-30%. The latter grouping is comparable to our group 2 garnets (felsic rock composition, high metamorphic temperature) and group 3 garnets (felsic rock composition, intermediate metamorphic temperature), respectively. Samples with an X_{Mg} of up to 50% have been described for the Kangerlussuaq basin, but are uncommon for other source areas to the Faroese basin e.g. the Orkney-Shetland Platform and the Lewisian or Moine/Dalradian (Morton et al. 2005; Frei et al. 2005a). These high X_{Mg} values are typical for granulite facies felsic rocks. We show here (Figures 8, A8, A9) that these high metamorphic grade rocks occur in the basement between 62° and 68° N; around 68° and immediately north of 62° N (Figure 32). However, high grade metamorphic rocks have also been found and described in Eastern and Northeast Greenland, where the Precambrian basement has been metamorphosed to amphibolite and granulite facies (Gilotti et al. 2002). In addition, the wide-spread Proterozoic Krummedal sequence rocks are typically garnet-bearing.

Frei et al. (2005a) used the TiO_2 distribution of the Ti-mineral fraction to describe the maturity of the sediment in the sandstone of the Kangerlussuaq Basin. Appendix A10 and A11 show the measurements for TiO_2 distribution in the analysed stream sediment samples. Deer et al. (1992) indicate that primary ilmenite has a TiO_2 concentration of 48-52.6 wt%, which is slightly lower than its stoichiometric value. Ti-magnetite is an igneous mineral that can form in a range of rock types substituting magnetite. Magnetite is also common in metamorphic rocks that recrystallized at high temperatures. Rutile is common in igneous rocks, mainly plutonic ones, and a common assessor in metamorphic rocks at intermediate to high temperatures and pressures (Deer et al. 1992). Ilmenite can leach iron in weathering and

alteration processes, which leads to a relative increase in TiO_2 concentration (Grey & Reid 1975). Due to this leaching process ilmenite can change into leucoxene or even rutile.

In the samples at this study, no leucoxene or rutile was measured, but Ti-magnetite and ilmenite were observed. This indicates that the stream sediment samples were derived from nearby sources and did not experience alteration. This is also confirmed by the high concentration of clino-amphibole/clino-pyroxene, ortho-amphibole/ortho-pyroxene and feldspar in the samples, minerals that are most prone to weathering processes. The sandstone samples from Kangerlussuaq show a bimodal distribution with a peak for Ti-magnetite, which is stable with respect to the leaching of iron, and one for leucoxene and rutile that was probably derived from leucoxene. Thus, from a point of view of the Ti-minerals, the samples from Kangerlussuaq might have been derived from a basement with supracrustal rocks with similar properties as the current Greenlandic coast between 62° and 68° N, where both ilmenite and Ti-magnetite occur. Before deposition or consolidation, the precursors to the Kangerlussuaq sandstones were subject to iron-leaching that matured the ilmenite in the sediment.

U-Pb zircons

The overall age pattern for Southeast and East Greenland is markedly different from that of the samples from the drill core in the Faroese sector making it unlikely that this part of Greenland was the source for this segment of the Faroe-Shetland basin.

The wells of the Faroese sector are very close to some of the wells in the UK sector of the Faroe-Shetland Basin (Figure 2), whereas others are up to 100 km away. Frei et al. (2005) and Frei and Knudsen (2008) analysed zircons from samples from wells in both sectors, and despite the distance, the age patterns from all the wells are very similar. The average age patterns for the wells in the two sectors are shown in Figure 33. They both contain a large Archaean peak around 2800-2700 Ma and only very few ages above 3000 Ma. In addition, they both have a significant broad range of Palaeo-, Meso- and even early Neoproterozoic ages, ranging approximately from 1900 to 900 Ma, and, lastly, they have a peak around 500-400 Ma.

Frei et al. (2005) also analysed zircons from the Cretaceous, Palaeocene and Eocene sedimentary successions from the Kangerlussuaq region to evaluate whether this sediment could be the source for the Faro-Shetland basin. Frei and Knudsen (2008) reported the average Kangerlussuaq signature as shown in Figure 34, such that, this pattern does not represent the true result as only analyses carried out by LA-SF-ICP-MS is used in the plot. All the Late Cretaceous to Late Palaeocene samples, containing abundant Palaeo- to Mesoproterozoic zircons, were originally analysed by the old LA-Q-ICP-MS method and could therefore not be included in the plot. Consequently the Palaeo- to Mesoproterozoic ages are underrepresented in the Kangerlussuaq signature and the correct signature would be very similar to the pattern from the Faroe-Shetland Basin sediments.

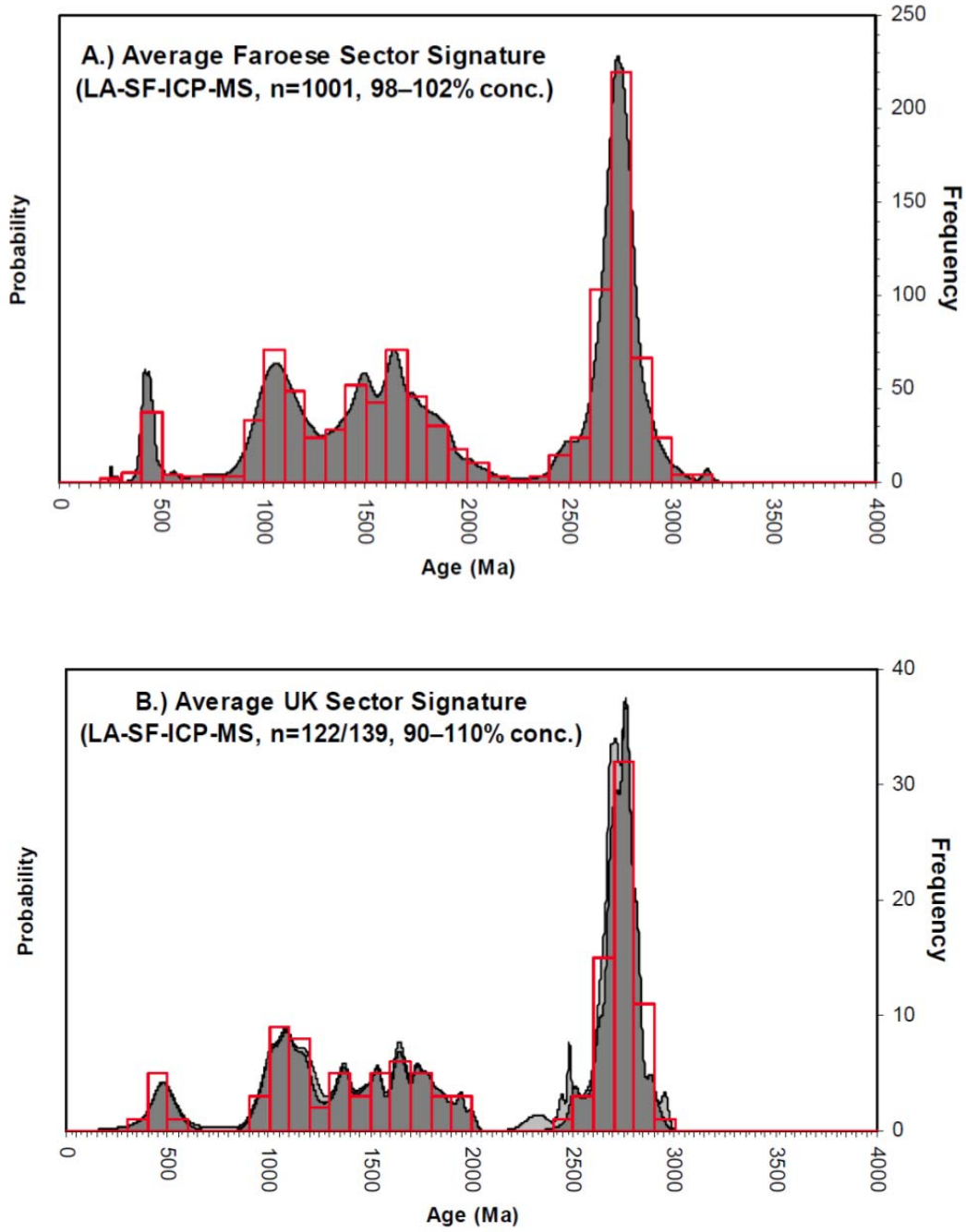

Figure 33. *Average detrital zircon age pattern of wells in A) the Faroese sector of the Faroe-Shetland basin, and B) the UK sector of the Faroe-Shetland basin. After Frei & Knudsen (2008).*

However, there is one important difference; the Kangerlussuaq sediments have a significant zircon population of 3250 to 3000 Ma grains. This population does not occur in the Faroe-Shetland Basin. Instead, this age population has been documented in this study to exist in Southeast Greenland, both in the Skjoldungen area and in the Tasiilaq region.

The large Palaeo- to Neoproterozoic age population, as well as the Caledonian peak present in the Kangerlussuaq Signature, does not occur in Southeast Greenland, but instead these ages are present to the north in Central Greenland in large and widespread

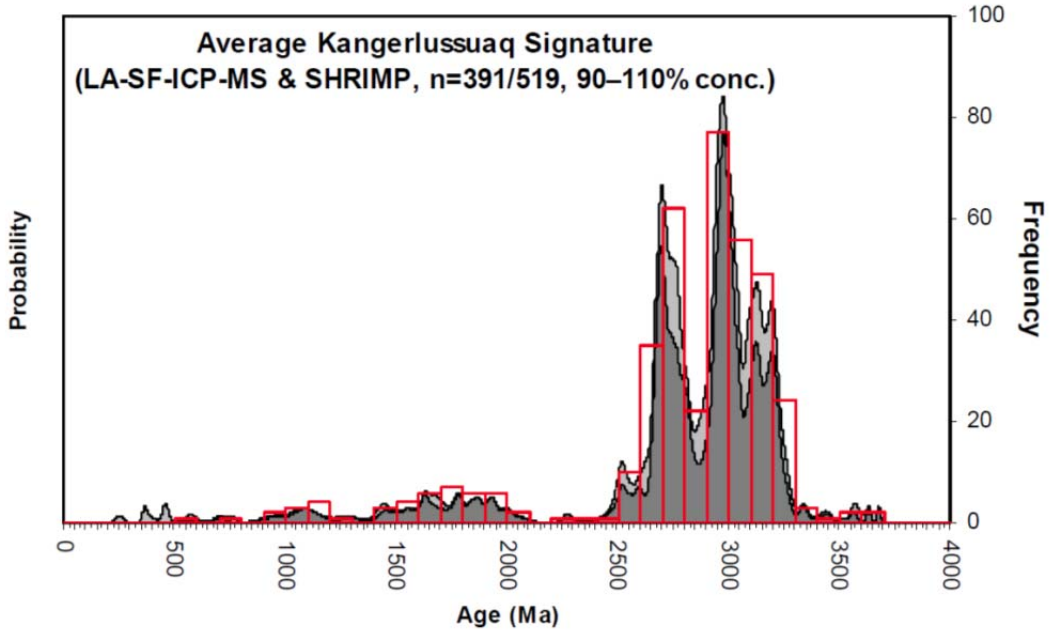

Figure 34. *Average detrital zircon age pattern of the Kangerlussuaq basin, East Greenland, displayed in a combined relative probability/histogram plot. According to Frei and Knudsen the modal proportion of the Palaeo- and Mesoproterozoic zircon population is underestimated in this plot. After Frei & Knudsen (2008).*

Neoproterozoic basins e.g. the Smallefjord group, the Krummedal Supracrustals and the Eleonora Supergroup.

We, therefore, suggest that the sediments in the Kangerlussuaq region must have been sourced both from the north, given the range of Palaeoproterozoic to Neoproterozoic zircons, and from the south where we have several occurrences of 3250 to 3000 Ma zircons.

Due to the large amount of zircons older than 3000 Ma in the Kangerlussuaq region, this area cannot be the source for the Faro-Shetland Basin.

Dirk and Knudsen (2008) refers to the Kangerlussuaq Signature as the East Greenland Signature, and discard an East Greenland source for the Faro-Shetland Basin on this basis. But the Kangerlussuaq region is only one minor part of East Greenland. Moving northwards, to Central East Greenland, the signature changes and zircons older than 3000 Ma are not present. The detrital zircon pattern for this area matches well with the Faro-Shetland Basin (Cawood et al. 2007, Kalsbeek et al. 2000, Rehnström et al. 2010). Due to the large area covered by thick Palaeogene flood basalts, just north of Kangerlussuaq, it is not possible to determine where the signature changes from the Kangerlussuaq Signature to the Central East Greenland Signature, nor is any alternative pathways visible.

Central East Greenland is not the only place with this very characteristic age pattern. The same pattern is found in northern Scotland, parts of Scandinavia and Siberia. These regions have shared a common history and, therefore, have the same detrital age pattern (Watt & Thrane 2001).

Most of the mentioned areas are made up of Archaean cratons of similar age, and large packages of sediment were deposited between ca. 1000 and 950 Ma. The sediments were dominated by zircons populations of Palaeoproterozoic to Mesoproterozoic ages. The Grenville orogenic belt of the Laurentian margin is the most likely source for the majority of the detritus. The sediment was transported to the north along the Laurentian and the East Greenlandic margin where it was deposited. After deposition, metamorphism, anatexis and granite emplacement occurred during the amalgamation and break up of Rodinia around 950-870 Ma and again during the Caledonian Orogeny around 450-430 Ma.

In the previous Sindri-project, Frei and Knudsen (2008) suggested that the sediment of the Faroese sector was sourced from the UK margin. But given the similar history and signature of the areas described above, it is not possible to discriminate the different sources on the basis of zircon data alone.

Summary and Conclusions of Project A

In previous SINDRI-studies, it has been suggested that the sediment of the Faroe-Shetland Basin was sourced from the UK margin, since the detrital zircon age patterns from the Faroe-Shetland Basin did not match with sediment samples from the Kangerlussuaq region, East Greenland.

However, the authors of this study do not see that as the only solution. There are several other potential source areas, than the UK margin with similar detrital age patterns, e.g. Central East Greenland, Svalbard, (Scandinavia) and Siberia, which all share a similar history and hence a similar age pattern signature, it is not possible to discriminate the different sources on the basis of zircon data.

Frei and co-workers use samples from the Kangerlussuaq area as a proxy for the Greenlandic source in the Faroe region, but the Greenlandic source for the Faroese sediments cannot be defined based on the properties of the Kangerlussuaq area only.

A source in Central East Greenland, where suitable-aged source rocks are known to occur, would be more compatible with other studies pointing to an East Greenlandic source, such as heavy mineral analyses, pollen records and sediment transport directions (Larsen et al. 2005; Jolley and Morton 2007).

Project B: Testing baddeleyite and zircon U-Pb age dating as a tool for the establishment of a robust geochronological framework for Palaeocene volcanic rocks in the Palaeocene interval T36 to T50

A detailed understanding of the timing of the interaction between volcanic extrusive and intrusive sills and sediments in the Palaeocene interval T36 to T50 in the Faroe-Shetland basin hinges critically on a sound geochronological framework for the extrusion and intrusion ages of the volcanic rocks in this interval. The geochronological data available for extrusive volcanics in the North Atlantic region are isolated ages for basalts and tuffs exposed in East Greenland, the Faroe Islands and the UK margin (e.g. Hamilton et al. 1998; Tegner et al. 1998; Tegner and Duncan 1999; Chambers and Pringle 2001; Waagstein et al. 2002; Chambers et al. 2005; Storey et al. 2007) and recovered from the Lopra-1 (Waagstein et al. 2002; Storey et al. 2007) and ODP (leg 152; Sinton and Duncan 1998; holes 917 and 918; Werner et al. 1998) as well as DSDP (leg 81; Sinton and Duncan 1998) wells. For the Faroe-Shetland basin, the only existing data is that from Waagstein et al. (2002) and Storey et al. (2007). No radiometric data currently exists for the extrusive volcanics and intrusive sills present in wells in the Faroe and UK sector of the Faroe-Shetland basin. This predicament is compounded by the fact that the basalts examined in the Faroe-Shetland basin are characterised by low potassium contents (e.g. Hald and Waagstein 1984; Hald and Waagstein 1991) and are pervasively metamorphosed at zeolite to prehnite-pumpellyite facies (Waagstein et al. 2002; Glassley 2006). As a result, the $^{40}Ar/^{39}Ar$ data are difficult to interpret and have been controversially discussed (Jolley et al. 2002; Aubry et al. 2003; Srivastava 2003, Thomas 2003; Wei 2003; Jolley et al. 2003a; Jolley et al. 2003b). The difficulties related to any interpretation of $^{40}Ar/^{39}Ar$ data for basalts from the North Atlantic Igneous Province was recently demonstrated by Sherlock et al. (2009). Therefore, there is an obvious need for more robust geochronological data for the extrusive volcanic rocks present in the Faroe-Shetland basin. A possible remedy for the dilemma of obtaining high-precision geochronological data from metamorphosed and/or hydrothermally altered mafic extrusive rocks with low potassium contents is U-Pb age dating of baddeleyite and zircon. Conventional wisdom excludes baddeleyite and zircon as primary magmatic phases in mafic and ultramafic extrusive rocks. However, there is an increasing body of evidence that baddeleyite indeed occurs as a late stage, primary magmatic phase even in extrusive volcanic rocks with low Zr-contents and that it can be successfully used to date the extrusive crystallisation ages (e.g. Heaman and LeCheminant 1993; Söderlund et al. 2005; Upton et al. 2005, Holm et al. 2006). Zircon is indeed a ubiquitous phase in acidic volcanic tuff layers (e.g. Schmitz and Bowring 2001) and is frequently observed in mafic to intermediate tuffs.

This study was a pilot study that explored the possibilities for the utilisation of baddeleyite and zircon as a highly robust and precise geochronological tool for dating mafic extrusive volcanics and intrusive sills from the lower basalt series exposed on Sudoroy. Samples from the lower lava series were chosen because they represent the closest analogues to the offshore lavas in the Faroe-Shetland basin (Ellis et al. 2002). The results had the poten-

tial to make a major contribution towards the establishment of a solid geochronological framework for the crystallisation of volcanic rocks in the Faroe-Shetland basin.

Samples

The lower basalt series occurs on Suduroy, Mykines, Gáshólmur, Tindhólmur and Vágar. The dip of the flows on Sudoroy is NNE, NE and ENE. The lower basalt series is built up of lava flows 10-30 m thick, with thin layers of subordinate inter-basaltic sediments. Thinner lava flows do occur, however, and a few flows as thick as 50-70 m can be seen. The rock is very uniform in character; it is a compact, hard, bluish basalt, which only exceptionally contains phenocrysts. The total thickness of the series is almost 900 m (Rasmussen & Noe-Nygaard, 1970).

All the basalts from the lower basalt sequence are very fine grained. The four most course-grained samples we could find in the GEUS archives were chosen for further analyses (Table 2). Unfortunately, there was no baddeleyite or zircon in any of the samples. Since there was no baddeleyite in these samples there was no reason to attempt with other more fine-grained samples.

Sample nr.	Location	Rock type
RW2006.09.08-08	Hov-Túgvan, central Suduroy	Massive basalt
1981.02.27-1	Oyrnavik,Lopra	Massive basalt
1981.02.24-2	Sumba	Massive basalt
1981.03.01-5	Siglifelli	Massive basalt
RW2006.09.08-09	Hov-Túgvan, central Suduroy	Tuff
RW2006.09.08-07	Hov-Túgvan, central Suduroy	Tuff

Table 2. *Four basalt and two tuff samples from the lower lava sequence exposed on Sudoroy. The samples are from GEUS' archives and were collected by Regin Waagstein, who is a senior researcher at GEUS and has worked many years on the Faroe Islands. Waagstein has collected many samples of basalts and the tuff layers from the lower lava sequence exposed at Sudoroy.*

The inter-basaltic sediments in the lower basalt series are essentially limited to tuffaceous and clayey sediments, shales, basaltic sandstone sediments and basaltic conglomerates. The tuff beds vary greatly in colour. They are usually brownish or reddish, but occasionally bright red. They can also be yellowish, green or grey-black in colour. The thickness usually varies from less than 1 m to 2-3 meters, but greater thicknesses are however not uncommon (Rasmussen & Noe-Nygaard, 1970).

Two tuff samples from exposed tuff layers with in the lower basalt were processed for zircons, but neither of these samples contained any zircons.

Five tuff samples from cutting material from the Faroese sector were also processed for zircons. The cutting samples are from the interval T36 to T50, covering from 2224 to 3117 meters depths. The samples are from well 6001/12-1, 6004/16-1, 6004/17-1 and 6005/15-1 (Table 3). These samples were very small, less than 40 grams, but we managed to retrieve some zircons from all five samples.

Sample nr.	Well	Depth (m)	Geology
230507-25	6004/16-1	2224	Lamba Fm.
230507-26	6004/16-1	2221	Lamba Fm.
240507-12	6004/17-1	2650	Lamba Fm.
240507-61	6005/15-1	2760	Lamba Fm.
240507-82	6004/12-1	3117	Lamba Fm.

Table 3. *Cutting samples of tuff layers from wells in the Faroese sector. The samples are from interval T36 to T50. For location of the wells can be seen in Figure 2.*

Due to the failed attempt to find baddeleyite in the lower basalt sequence, we chose to try to extract baddeleyites from mafic dykes collected in the Skaergaard area related to Sindri Project C46-53-02 carried out by Pierpaolo Guarnieri (Guarnieri et al. 2012).

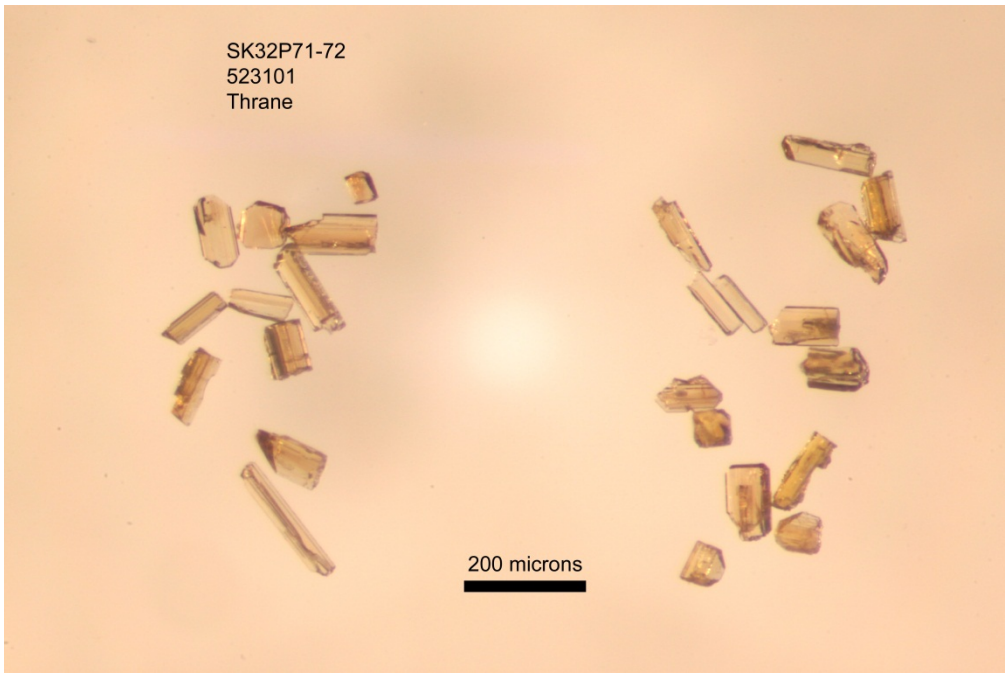

Figure 35. *Two fractions of baddeleyite crystals from sample 523101.*

Three samples were processed: Sample 523101 belongs to the Miki Fjord Macrodyke while sample #523102 belongs to the Vandfaldsdalen Macrodyke. The two layered dykes, up to 500-m wide, are NNE-SSW oriented and related to the breakup of the continental crust with composition and age similar to the Skaergaard Layered Gabbro. Sample #516051 belongs

to a E-W oriented dyke system cross-cutting old structures and dykes. This late dyke swarm could be considered post-breakup since it cuts through the flexure-related structures that are coeval with the breakup.

Only one sample, 523101, contained baddeleyite (Figure 35).

Results

Unfortunately Project B did not turn out as we had originally hoped. We did not retrieve any baddeleyites or zircons from the basalt samples or the onshore tuff layers within the lower basalt series. But we did retrieve zircons from the cutting samples of the tuff horizons as described below. Baddeleyite was retrieved from one mafic dyke from the Skaergaard area.

Tuff samples from cuttings

The detrital zircon patterns, for the five tuff/cutting samples are surprisingly similar (Figure 36). They are all dominated by a prominent Archaean peak around 2850-2700 Ma, thus the sample highest in the sequence also has a dominant 2700-2600 Ma peak. In addition, all samples have a minor content of Palaeo- to Mesoproterozoic ages. A couple of the samples also have Caledonian age zircons. Most samples contain zircon ages between 3000-2800, while only a very limited amount of grains are older than 3000 Ma.

Overall the patterns are very similar to the general pattern of the sediments in the Faroe-Shetland Basin.

Figure 36 (next page). *Average detrital zircon age pattern of the cutting samples of tuff layers from wells in the Faroese sector (see table 3). The samples are from T36 to T50, covering from 2224 to 3117 meters depths.*

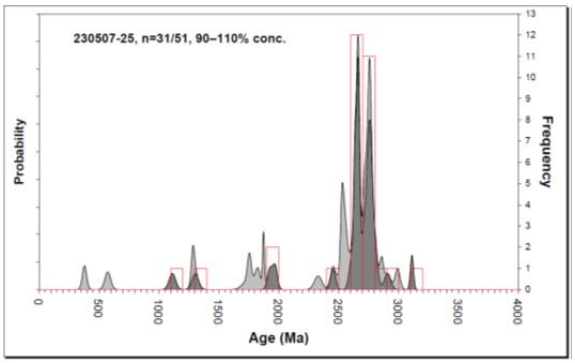
230507-25, n=31/51, 90–110% conc.
Probability
Frequency
Age (Ma)

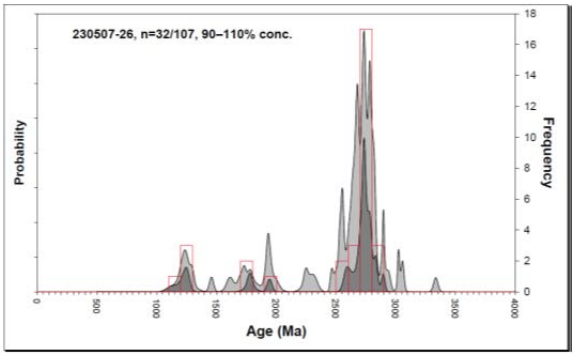
230507-26, n=32/107, 90–110% conc.
Probability
Frequency
Age (Ma)

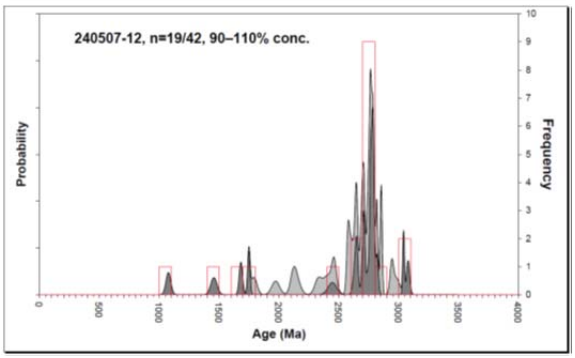
240507-12, n=19/42, 90–110% conc.
Probability
Frequency
Age (Ma)

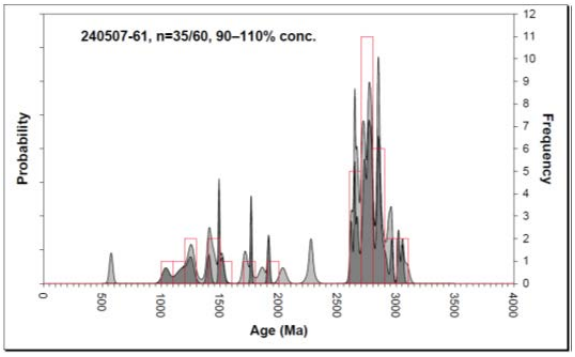
240507-61, n=35/60, 90–110% conc.
Probability
Frequency
Age (Ma)

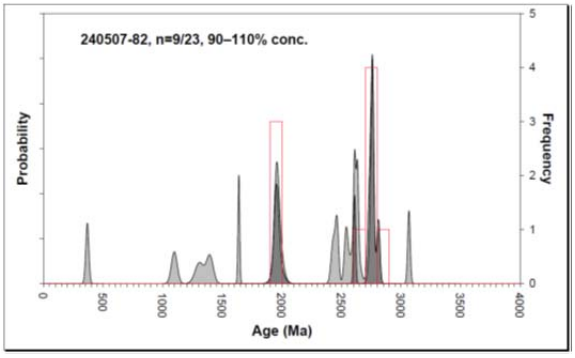
240507-82, n=9/23, 90–110% conc.
Probability
Frequency
Age (Ma)

Kangerlussuaq

Dating these intrusive events is important to define the relationship between the Macrodyke complex and the Skaergaard intrusion, both related to the breakup history at 55 Ma and the initiation of the post-breakup tectonics that is supposed to be younger (Late Eocene) and responsible for uplift and inversion of the Kangerlussuaq Basin.

Two fractions of baddeleyite were picked and analysed using ID-TIMS at the University of Toronto. The result yielded a weighted mean $^{206}Pb/^{238}U$ age of 55.87±0.06 Ma (MSWD = 0.43).

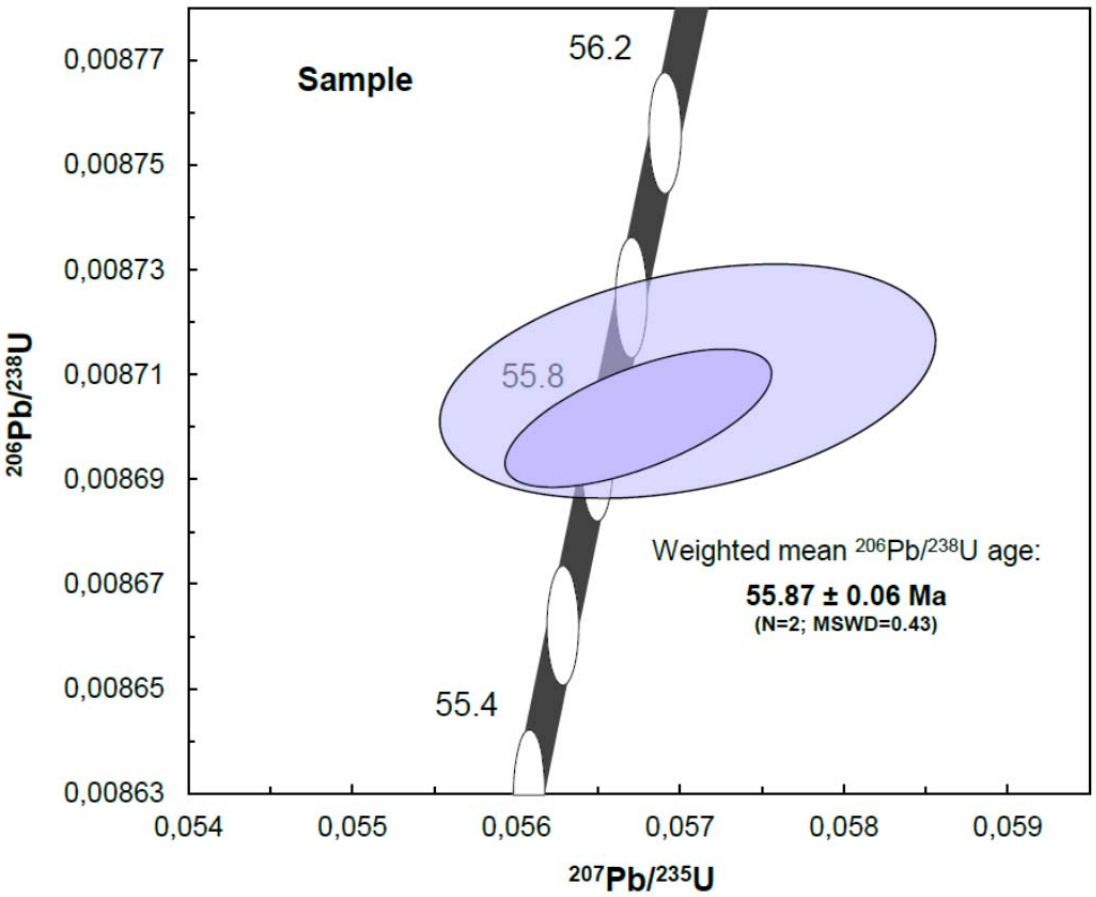

Figure 37. *Weighed mean U-Pb age obtained from the two fractions of baddeleyite*

Summary and Conclusions of Project B

It was not possible to retrieve any baddeleyites or zircons from the basalt samples or the onshore tuff layers within the lower basalt series, and therefore a reliable and precise crystallization age of the lower basalts is still lacking. Instead we analysed zircons from the cutting samples of the tuff horizons as described below, and we also obtained an age of a mafic dyke from the Skaergaard area.

Tuff samples from cuttings

The tuff samples from the cuttings contained zircons, but some of the samples had very few. Consequently, the age distribution diagrams, especially the one from the lowest sample in the sequence, are very scarce. The overall conclusion is that the tuff samples are dominated by Archaean grains from 2850 to 2700 Ma. In addition, all samples have a minor content of Palaeo- to Mesoproterozoic ages. A couple of the samples also have Caledonian age zircons. Most samples contain zircon ages between 3000-2800, while only a very limited amount of grains are older than 3000 Ma.

This general pattern is very similar to the pattern of the sediments in the Faroe-Shetland Basin, and it is therefore most likely that the tuffs were sourced from the local sediment of the Faroe-Shetland Basin.

Kangerlussuaq

The U-Pb age of the mafic dyke is a very important result that establishes chronological relationship between the gabbro intrusions close to or related to the continental breakup: Macrodykes at 55.87 Ma followed by the Skaergaard Gabbro at 55.4 Ma that in turn, is thought to be expression of the breakup.

The macrodykes cut through the Sødalen Fault, previously documented, and show en-echelon geometry. This structural relationship and the direction of extension combined with strike-slip evidences documented along the fault, suggest a mechanism of oblique rifting in Selandian-Thanetian, until the intrusion of the macrodykes at 55.87 Ma that correspond to the Paleocene/Eocene boundary. This mechanism is coherent with the paleostress reconstructed from analysis of fault-slip data (Guarnieri et al. 2012).

Oblique rifting arises when the bulk extension direction is not perpendicular to the boundaries of a deforming zone. In extensional environments, the geometry and kinematics of fault patterns often suggest that extension is not perpendicular to the boundaries of the deforming domain (Tron and Brun 1991; McClay and White 1995; Corti 2008).

Possible Future Plans

Projects which could potentially discriminate between Greenlandic and Scottish sources:

- U-Pb analyses of rutile and monazite.
- Pb-Pb analyses of feldspars.

Other related projects:

- Detrital zircon U-Pb age study of samples from well 6104/21-1 (Brugdan), which is located closer to Greenland, than the studied ones.
- Detrital zircon U-Pb age study of samples from below the basalts, taken during IODP operation.
- Detrital zircon U-Pb age study of the samples from Jurassic sediments in drill cores.
- Update database to include all published detrital zircon data from the area.

Acknowledgements

The work presented in this volume was funded by SINDRI and GEUS and the samples were collected by GEUS. Peter Riisager, GEUS, is thanked for constructing the database. Sandra Kamo, University of Toronto, for carrying out the U-Pb analyses of the baddeleyite. Mojagan Alaei, Fiorella Aguilera, Michael Nielsen and Jørgen Kystol (GEUS) are all thanked for help with the lab work, with everything from preparing the samples to carrying out part of the analyses. Regin Waagstein is thanked for help with the samples and insight into the Faroe geology.

References

Aftalion, M., Bowes, D.R. & Vrana, S. 1989: Early Carboniferous U-Pb zircon ages for garnetiferous perpotassic granulites, Blansky les massif, Czechoslovakia. Neues Jahrbuch für Mineralogie, Monatshefte **4**, 145-152.

Aubry, M-P., Swisher, C.C. & Berggren, W.A. 2003: Comment on “Paleogene time scale miscalibration: Evidence from the dating of the North Atlantic igneous province”. Geology **31**, 468.

Bernstein, S., Frei, D., McLimans, R.K., Knudsen, C. & Vasudev, V.N. 2008: Application of CCSEM to heavy mineral deposits: source of high-Ti ilmenite sand deposits of South Kerala beaches, SW India. Journal of Geochemical Exploration **96**, 25–42.

Cawood, P., Nemchin, A.A., Strachan, R., Prave, T. & Krabbendam, M. 2007: Sedimentary basin and detrital zircons record along East Laurentia and Baltica during assembly and breakup of Rodinia. Journal of the Geological Society, London, **164**, 257-275.

Chadwick, B., Dawes, P.R., Escher, J.C., Friend, C.R.L., Hall, R.P. Kalsbeek, F., Nielsen, T.F.D., Nutman, A.P., Soper, N.J. & Vasudev, V.N. 1989: The Proterozoic mobile belt in the Ammassalik region, South-East Greenland (Ammassalik mobile belt): an introduction and re-appraisal. In: Kalsbeek, F.: Geology of the Ammassalik region, South-East Greenland. Rapport Grønlands Geologiske Undersøgelse **146**, 5-12.

Chambers, L.M. & Pringle, M.S. 2001: Age and duration at the Isle of Mull Tertiary igneous centre, Scotland, and confirmation of the existence of subchrons during Anomaly 26r. Earth and Planetary Science Letters **193**, 333-345.

Chambers, L.M., Pringle, M.S. & Parrish, R.R. 2005: Rapid formation of the Small Isles Tertiary centre constrained by precise $^{40}Ar/^{39}Ar$ and U-Pb ages. Lithos **79**, 367-384.

D’Alessio, A., Bramanti, E., Piperno, M. Naccarato, G. Vergamini, P. & Fornaciari, G. 2005: An 8500-year-old bladder stone from Uzzo cave (Trapani): Fourier transform-infrared spectroscopy. Archaeomotry **47**, 127–136.

Deer W.A., Howie, R.A., & Zussman, J. 1992: An introduction to the Rock Forming Minerals, 2nd Edition. Longman Scientific & Technical, 696p.

Dodson, M.H., Compton, W., Williams, I.S., Wilson, J.F. 1988: A search for ancient detrital zircons in Zimbabwean sediments. Journal of the Geological Society of London **145**, 977–983.

Ernst, W.G. & Liu, J. 1998: Experimental phase-equilibrium study of Al- and Ti-contents of calcic amphibole in MORB—A semiquantitative thermobarometer. American Mineralogist, **83**, 952–969.

Escher, J.C. 1990: Geological map of Greenland, 1:500 000, Skjoldungen, Sheet 14. Copenhagen: Grønlands Geologiske Undersøgelse.

Ferry, J.M. & Spear F.S. 1978: Experimental Calibration of the Partitioning of Fe and Mg Between Dark mica and Garnet. Contrib. Mineral. Petrol. **66**, pp. 113 – 117.

Fedo, C.M., Sircombe, K.N., Rainbird, R.H. 2003: Detrital zircon analysis of the sedimentary record. In: Hanchar, J.M., Hoskin, P.W.O. (Eds.), Zircon. Reviews in Mineralogy and Geochemistry **53**, 277-303.

Frei, D., Frei, M. Klünder, M.H., Rasmussen, T. & Knudsen, C. 2005a: Heavy mineral characteristics of Cretaceous-Eocene sandstones in the Kangerlussuaq Basin, East Greenland – results from CCSEM. In: Frei, D., Frei, M. & Knudsen, C. (eds.): Linking the Faroese area and Greenland: an innovative, integrated provenance study. Geological Survey of Denmark and Greenland report **2005/54**, 77-92.

Frei D., Hollis J.A., Gerdes A., Harlov D., Karlsson C., Vasquez P., Franz G., Johansson L., & Knudsen C. 2006: Advanced in-situ trace element and geochronological microanalysis of geomaterials by laser ablation techniques. Geological Survey of Denmark and Greenland Bulletin **10**, 25-28.

Frei, D. & Knudsen, C. 2008: Understanding sedimentary provenance in the Faroe-Shetland basin: constraints from detrital zircon geochronology. Geological Survey of Denmark and Greenland report **2008/21**, 11-33.

Frei, D., Rasmussen, T., Knudsen, C., Larsen, M., Whitham, A. & Morton, A. 2005b: Linking the Faroese area and Greenland: new methods and techniques used in an innovative, integrated provenance study. Fróðskaparrit **43**, 96–108.

Frei, D. & Gerdes, A. 2009: Precise and accurate in-situ zircon U-Pb dating with high sample throughput by automated La-SF-ICP-MS. Chemical Geology **261**, 261-270.

Friedrichs, K.H. 1987: Electron microscopic analyses of dust from the lungs and the lymph nodes of talc-mine employees. American Industry Hygiene Association Journal **48**, 626–633.

Friend, C.R.L. & Nutman, A.P. 1989: The geology and structural setting of the Proterozoic Ammassalik Intrusive Complex, East Greenland. In: Kalsbeek, F.: Geology of the Ammassalik region, South-East Greenland. Rapport Grønlands Geologiske Undersøgelse **146**, 41-45.

Garde, A.A., 2007: Geological map of Greenland, 1:500 000, Sydgrønland, Sheet 1. Copenhagen: Geological Survey of Denmark and Greenland.

Gilotti, J.A., Jones, K.A. & Elvevold, S. 2002: Caledonian metamorphic patterns in Greenland *in* Higgins, A.K., Gilotti, J.A. & Smith, M.P. eds., The Greenland Caledonides: Evolution of the Northeast Margin of Laurentia: Geological Society of America Memoir 202, p. 201-225.

Glassley, W.E. 2006: Mineralogical and thermodynamic constraints on Paleogene paleotemperature conditions during low-grade metamorphism of basaltic lavas recovered from the Lopra-1/1a deep hole, Faroe Islands. Geological Survey of Denmark and Greenland Bulletin **9**, 109-118.

Grey, I.E., & Reid, A.F. 1975: The structure of pseudorutile and its role in the natural alteration of ilmenite. American Mineralogist **60**, 898-906.

Grütter, H.S., Gurney, J.J., Menzies, A.H. & Winter, F. 2004: An updated classification scheme for mantle-derived garnet, for use by diamond explorers. Lithos **77**, 841– 857.

Guarnieri, P., Hopper, J.R. & Anderson, M.S. 2012: Timing of deformation and structural styles along Fracture Zone/Transfer Zone in East Greenland and Faroes area: impact on plate tectonics, implications for inversion structures and basin architecture. Geological Survey of Denmark and Greenland report **2012, in press.**

Hamilton, M.A., Pearson, D.G., Thompson, R.N., Kelley, S.P. & Emeleus, C.H. 1998: Rapid eruption of Skye lavas inferred from precise U-Pb and Ar-Ar dating of the Rum and Cuillin plutonic complexes. Nature **394**, 260-263.

Hald, N. & Waagstein, R. 1984: Lithology and chemistry of a 2-km sequence of Lower Tertiary tholeiitic lavas drilled on Sudoroy, Faroe Islands (Lopra-1). *In* Berthelsen, O., Noe-Nygaard, A. and Rasmussen, J. (eds) *The Deep Drilling Project 1980-1981 in the Faeroe Islands*, 15-38. Tórshavn: Føroya Frodskaparfelag.

Hald, N. & Waagstein, R. 1991: The dykes and sills of the Early Tertiary Faeroe Island basalt plateau. Transactions of the Royal Society of Edinburgh **82**, 373-388.

Heaman, L. & LeCheminat A.N. 1993: Paragenesis and U-Pb systematics of baddeleyite (ZrO2). Chemical Geology **110**, 95-126.

Heasman I. & Watt, J. 1979: Particulate pollution case studies which illustrate uses of individual particle analysis by scanning electron microscopy. Environmental Geochemistry and Health **11**, 157–162.

Hensen, J.B. & Green, D.H. 1972: Experimental Study of the Stability of Cordierite and Garnet in Pelitic Compositions at High Pressures and Temperatures.II. Compositions without Excess Alumino-Silicate. Contr. Mineral. and Petrol. **35**, 331-354.

Holm, P.M., Heaman, L. & Pedersen, L.E. 2006: Baddeleyite and zircon U-Pb ages from the Kærven area, Kangerlussuaq. Implications for the timing of Paleogene continental breakup in the North Atlantic. Lithos **92**, 238-250.

Horstwood, M., Foster, G.L., Parrish, R.R. & Nobel, S.R. 2003: Common-Pb corrected in situ U-Pb accessory mineral geochronology by LA-MC-ICP-MS. Journal of Analytical Atomic Spectrometry **18**, 837-846.

Huggins, F.E., Kosmack, D.A., Huffman, G.P. & Lee, R.J. 1980: Coal mineralogy by SEM analysis. Scanning Electron Microscopy **1**, 531–540.

Huffman, G.P. et al. 1994: Investigation of ash by microscopic and spectroscopic techniques. In: Williamson, J. & Wigley, F. (eds): Proceedings of the Engineering Foundation Conference (June 20–25, 1993, Solihull, Birmingham, UK), The impact of ash deposition on coal fired plants, 409–423. London: Taylor & Francis.

Hutchison, M.T. 2005: Diamondiferous kimberlites from the Garnet Lake area, West Greenland: exploration, methologies and petrochemistry. In: Secher, K & Nielsen, M.N. (eds.): Workshop on Greenland's diamond potential. Geological Survey of Denmark and Greenland Geological Report **2005/68**, 33–42.

Jackson, S., Pearson, N.J., Griffin, W.L. & Belousova, E.A. 2004: The application of laser ablation – inductively coupled plasma – mass spectrometry to in situ U-Pb zircon geochronology. Chemical Geology **211**, 47-69.

Jolley, D.W., Clarke, B. & Kelley, S.P. 2002: Paleogene time scale miscalibration: Evidence from the dating of the North Atlantic igneous province. Geology **30**, 7-10.

Jolley, D.W., Clarke, B. & Kelley, S.P. 2003a: Reply to comment on "Paleogene time scale miscalibration: Evidence from the dating of the North Atlantic igneous province" by Aubry et al. and Wei. Geology **31**, 469.

Jolley, D.W., Clarke, B. & Kelley, S.P. 2003b: Reply to comment on "Paleogene time scale miscalibration: Evidence from the dating of the North Atlantic igneous province" by Thomas and Srivastava. Geology **31**, 471.

Jolley, D.W. & Morton, A.C. 2007: Understanding basin sedimentary provenance: evidence from allied phytogeographic and heavy mineral analysis of the Palaeocene of the NE Atlantic. Journal of Geological Society, London **164**, 553-563.

Kalsbeek, F. Ghisler, M. & Thomsen, B. 1974: Sand analysis as a method of estimating bedrock compositiions in Greenland, illustrated by fluvial sands from the Fiskenæsset region. Grønlands Geologiske Undersøgelse Bulletin **111**, 32pp.

Kalsbeek, F., Thrane, K., Nutman, A.P. & Jepsen, H.F. 2000: Late Mesoproterozoic metasedimentary and granitic rocks in the King Oscar Fjord region, east Greenland Caledonides fold belt: evidence for Grenville orogenesis. Journal of the Geological Society, London, **157**, 1215-1225.

Karson, J.A. and Brooks, C.K. 1999: Structural and magmatic segmentation of the Tertiary East Greenland volcanic rifted margin. In. Mac Niocaill, C & Ryan, P.D. (eds) Continental Tectonics. Geological Society, London, Special Publications **164**, 313-338.

Keulen, N., Frei, D., Bernstein, S., Hutchison, M.T., Knudsen C., & Jensen L. 2008: Fully automated analysis of grain chemistry, size and morphology by CCSEM: examples

from cement production and diamond exploration. Reviews of the Survey's Activities 2007, Geological Survey of Denmark and Greenland **15**, 93-96.

Keulen, N. & Heijboer, T. 2011: The provenance of garnet: semi-automatic plotting and classification of garnet compositions. Geophysical Research Abstracts, **13**, EGU2011-4716-1.

Knott, S.D., Burchell, M.T., Jolley, E.J. & Fraser, A.J. 1993: Mesozoic to Cenozoic plate reconstructions of the North Atlantic and hydrocarbon plays of the Atlantic margins. In: Parker, J.R.: Petroleum Geology of Northwest Europe: Proceedings of the 4th Conference. Petroleum Geology '86 Ltd. The Geological Society, London, 953-974.

Knudsen, C., Frei, D., Rasmussen, T., Rasmussen, E. S. & McLimans, R. 2005: New methods in provenance studies based on heavy minerals: an example from Miocene sands in Jylland, Denmark. Geological Survey of Denmark and Greenland Bulletin **7**, 29–32.

Kolb, J., Thrane, K. & Bagas, L., accepted: Tectonic and magmatic evolution of high-grade Neo- to Mesoarchaean rock in South-East Greenland. Gondwana Research, in press.

Kosler, J. & Sylvester, P.J. 2003: Present trends and the future of zircon in geochronology: Laser ablation ICP-MS. In: Hanchar, J.M, Hoskin, P.W.O. (Eds.), Zircon. Reviews in Mineralogy and Geochemistry **53**, Mineralogical Society of America, Washington, DC, 243-275.

Kretz, R. 1959: Chemical study of garnet, dark mica, and hornblende from gneisses of southwestern Quebec, with emphasis on distribution of elements in coexstingminerals. The Journal of Geology **67(**4) 371-402.

Krogh, R.E. 2000: The garnet–clinopyroxene Fe^{2+}–Mg geothermometer: an updated calibration. J. metamorphic Geol., **18**, 211–219.

Larsen, M. 1996: Sedimentology and Basin Evolution of the Cretaceous-Early Tertiary Knagerlussuaq Basin, southern East Greenland. Denmark and Greenlands Geological Survey Report **1996/35**, 24pp.

Larsen, M., Nøhr-Hansen, H., Whitham, A.G. & Kelly, S.R.A. 2005: Stratigraphy of the pre-basaltic sedimentary succession of the Kangerlussuaq Basin. Volcanic basins of the North Atlantic. Denmark and Greenlands Geological Survey Report **2005/62**, 141pp.

Larsen, L.M. & Whitham, A.G. 2005: Evidence for a major sediment input point into the Faroe-Shetland Basin from the Kangerlussuaq region of southern East Greenland. In: Doré, A. & Vining, B. (Eds.) Petroleum Geology: North-West Europe and global perspective. Proceedings of the 6th petroleum geology conference. Geological Society, London **2**, 913-922.

Lee, R.J. & Kelly, J.F. 1980: Overview of SEM-based automated image analysis. Scanning Electron Microscopy **1**, 303.

Lin, M.C. & Barnes, R.G. 1984: Møssbauer spectroscopy and scanning electron microscopy study of iron-graphimetry. Journal of Applied Physics **55**, 2294–2296.

Ludwig, K.R., 1999: Isoplot/Ex version 2.00 – A geochronological toolkit for Microsoft Excel. Berkeley Geochronology Center, Special Publication No. 2

McLimans, R. K., Rogers, W. T., Korneliussen, A., Garson, M, & Arenberg, E., 1999: Norwegian eclogite; an ore of titanium; Miner. Deposits: Processes, Proc. Fifth Bien. SGA Mtg, IAGOD symp – 1999; **2**, 1125-1127; Stanley, C.J., ed.; A. A. Balkema, pub., Rotterdam, Netherlands.

Morton, A.C., Ellis, D., Fanning, M., Jolley, D.W. and Whitham, A. G. 2009: Heavy mineral constraints on Paleocene sand transport in the Faroe-Shetland basin. Faroe Islands Exploration Conference 2009.

Morton, A.C. & Hallsworth, C.R., 1999: Processes controlling the composition of heavy mineral assemblages in sandstones. Sedimentary Geology **124**, 3–29.

Morton, A.C., Hallsworth, C.R. & Whitham, A.G. 2005: Heavy mineral provenance of Paleocene-Eocene sandstones in the Faroe-Shetland Basin – results from conventrional petrographical and mineral-chemical techniques. In: Frei, D., Frei, M. & Knudsen, C. (eds.): Linking the Faroese area and Greenland: an innovative, integrated provenance study. Geological Survey of Denmark and Greenland report **2005/54**, 17-49.

Myers, J.C., Dawes, P.R. & Nielsen, T.F.D. 1988: Geological map of Greenland, 1:500 000, Kangerdlugsuaq, Sheet 13. Copenhagen: Grønlands Geologiske Undersøgelse.

Nutman, A.P. & Friend, C.R.L. 1989: Reconaissane P,T, studies of Proterozoic crustal evolution of the Ammasalik area, East Greenland. In: Kalsbeek, F.: Geology of the Ammassalik region, South-East Greenland. Rapport Grønlands Geologiske Undersøgelse **146**, 41-45.

Nøhr-Hansen, H., Larsen, M., Kelly, S.R.A. & Whitham, A.G. 2006: Biostratigraphy zonation (palynology and macrofossil) for the Upper Cretaceous – Lower Palaeogene based on the sedimentary succession in the Kangerlussuaq, southern East Greenland. Phase 1 report for the Sindri Group, March 2006, Danmarks og Grønlands Geologiske Undersøgelse Rapport **2006/23**.

O'Neill, H.S.C & Wood B.J. 1997: An Experimental Study of Fe-Mg partitioning Between Garnet and Olivine and Its Calibration as a Geothermometer. Contrib. Mineral. Petrol **70**, 59-70.

Pirrie, D., Butcher, A.R., Power, M.R., Gottlieb, P. & Miller, G.L. 2004: Rapid quantitative mineral and phase analysis using automated scanning electron microscopy (QemSCAN); potential applications in forensic geoscience. In: Kenneth, P. & Croft, D.J.: Forensic geoscience; principles, techniques and applications.Geological Society, London, Special Publications **232**, 123–136.

Ramberg, H. 1952: Chemical bonds and the distribution of cations in silicates. The Journal of Geology, **60**(4) 331-355.

Rasmussen, J. & Noe-Nygaard, A. 1970: Geology of the Faeroe Islands. Geological Survey of Denmark I. Series No. 25. Copenhagen.

Rehnström, E.F., Thrane, K., Kokfelt, T.F. & Frei, D. 2010: Age distribution of detrital zircon grainsin sandstones and stream sediments from East Greenland north of 70°N. Geological Survey of Denmark and Greenland report **2010/130**, 1-138.

Scherstén, A., Sønderholm, M. & Steenfelt, A. 2007: Provenance of West Greenland Cretaceous and Paleocene sandstones and stream sediment samples based on U-Pb dating of detrital zircon: data and results. Geological Survey of Denmark and Greenland report **2007/21**, 1-121.

Schmitz, M.D. & Bowring, S.A. 2001: U-Pb zircon and titanite systematics of the Fish Canyon Tuff: an assessment of high-precision U-Pb geochronology and its application to young volcanic rocks. Geochimica et Cosmochimica Acta **65**, 2571-2587.

Schwoeble, A.J., Dalley, A.M., Henderson, B.C. & Casuccio, G.S. 1988: Computer-Controlled SEM and microimaging of fine particles. Journal of Metals **40**, 11–14.

Sen, S.K. & Bhattacharaya, A. 1984: Anorthopyroxene-garnet thermometerand its application to the Madras charnockites. Contrib Mineral Petrol **88,** 64-71.

Sherlock, S.C., Halton, A.M., Kelly, S.P. & Jolly, D.M. 2009: Why is basalt dating so difficult? A brief overview of ^{40}Ar-^{39}Ar dating system focussed on the North Atlantic Igneous Province. Faroe Islands Exploration Conference 2009, Abstract Volume.

Sinton, C.W. & Duncan, R.A. 1998: ^{40}Ar-^{39}Ar ages of lavas from the Southeast Greenland Margin, ODP Leg 152 and the Rockall Plateau, DSDP Leg 81. *In* Saunders, A.D.,

Larsen, H.C., Wise, W. (eds) *Proceedings of the Ocean Drilling Programme, Scientific Results* **152**, 387-402.

Sircombe, K.N. 2004: AgeDisplay: an Excel workbook to evaluate and display univariant geochronological data using binned frequency histograms and probability density distributions. Computer and Geosciences **30**, 21-31.

Stacey J.S. & Kramers J.D. 1975: Approximation of terrestrial lead isotope evolution by a 2-stage model. Earth and Planetary science letters **26**, 207-221.

Steffen, S., Otto, M., Niewoehner, L., Barth, M., Brozek-Mucha, Z., Biegstraaten, J. & Horvath, R. 2007: Chemometric classification of gunshot residues based on energy dispersive X-ray microanalysis and inductively coupled plasma analysis with mass-spectrometric detection. Spectrochimica Acta **B62**, 1028–1036.

Storey, M., Duncan, R.A. & Tegner, C. 2007: Timing and duration of volcanism in the North Atlantic Igneous Province: Implications for geodynamics and links to the Iceland hotspot. Chemical Geology **241**, 264-281.

Srivastava, S.K. 2003:Comment on “Paleogene time scale miscalibration: Evidence from the dating of the North Atlantic igneous province”. Geology **31**, 470.

Sylvester, P.J. & Ghaderi, M. 1997: Trace element analysis of scheelite by excimer laser ablation inductively coupled plasma mass spectrometry (ELA-ICP-MS) using a synthetic glass standard. Chemical Geology **141**, 49-65.

Söderlund, U., Isachsen, C.E., Bylund, G., Heaman, L., Patchett, P.J., Vervoort, J.D. & Andersen, U.B. 2005: U-Pb baddeleyite ages and Hf, Nd isotope chemistry constraining repeated mafic magmatism in the Fennoscandian shield from 1.6 to 0.9 Ga. Contributions to Mineralogy and Petrology **150**, 174-194.

Tegner, C., Duncan, R.A., Bernstein, S., Brooks, C., Bird, D.K. & Storey, M. 1998: Ar40-Ar39 geochronology of Tertiary mafic intrusions along the East Greenland rifted margin: relation to flood basalts and the Iceland hotspot track. Earth and Planetary Science Letters **156**, 75-88.

Tegner, C. & Duncan, R.A. 1999: Ar40-Ar39 chronology for the volcanic history of the Southeast Greenland rifted margin. *In* Larsen, H.C., Duncan, R.A., Allan, J.F. and Brooks, K. (eds) *Proceedings of the Ocean Drilling Programme, Scientific Results* **163**, 53-62.

Thomas, E. 2003: Comment on “Paleogene time scale miscalibration: Evidence from the dating of the North Atlantic igneous province”. Geology **31**, 470.

Upton, B.G.J., Rämö, O.T., Heaman, L., Blichert-Toft, J., Kalsbeek, F., Barry, T.L. & Jepsen, H.F. 2005: The Mesoproterozoic Zig-Zag Dal basalts and associated intrusions of eastern North Greenland: mantle plume-lithosphere interaction. Contributions to Mineralogy and Petrology **149**, 40-56.

Waagstein, R., Guise, P. & Rex, D. 2002: K/Ar and 39Ar/40Ar whole-rock dating of zeolite facies metamorphosed flood basalts: the upper Paleocene basalts of the Faroe Islands, NE Atlantic. *In* Jolley, D.W. & Bell, B.R. (eds) The North Atlantic Igneous Province: Stratigraphy, Tectonic, Volcanic and Magmatic processes. Geological Society, London, Special Publications **197**, 219–252.

Watt, G.R. & Thrane, K. 2001: Early Neoproterozoic events in East Greenland. Precambrian Research **110**, 165-184.

Wei, W. 2003: Comment on “Paleogene time scale miscalibration: Evidence from the dating of the North Atlantic igneous province”. Geology **31**, 467.

Weibel, R. & Knudsen, C. 2008: Provenance of sediments in the Faros-Shetland Basin: constrains from whole-rock geochemistry. Geological Survey of Denmark and Greenland report **2008/21**, 35-70.

Werner, R., van den Boogard, P., Lacasse, C. & Schmicke, H.U. 1998: Chemical composition, age, and sources of volcanoclastic sediments from sites 917 and 918. *In* Saunders, A.D., Larsen, H.C., Wise, W. (eds) *Proceedings of the Ocean Drilling Programme, Scientific Results* **152**, 93-113.

Williams, I.S. & Claesson, S. 1987: 1987: Isotopic evidence for the Precambrian provenance and Caledonian metamorphism of high grade paragneisses from the Seve Nappes, Scandinavian Caledonides: II. Ion microprobe zircon U-Th-Pb. Contribution to Mineralogy and Petrology **97**, 205-217.

Yin, C. & Johnson, D.L. 1984: An individual particle analysis and budget study of Onondaga Lake sediments. Limnology & Oceanography **29**, 193–1201.

Appendix A: Modal mineral distributions, Garnet compositions, and Titanium concentrations in Titanium minerals

This appendix shows the modal mineral distribution, as obtained with CCSEM, and the modal heavy mineral composition as used in this. In the modal heavy mineral diagrams in the report the data for quartz, feldspar, carbonate, iron oxides (magnetite), pyrite, chlorite and other (i.e., unspecified) silicates have been removed. See the Method description section for a discussion of this procedure.

Thereafter, the results of the garnet composition measurements, as obtained with CCSEM, are shown and their classification into seven different groups as used in this report. The results in the triangular diagrams and in the circular diagrams show the same results in two different ways. See the Appendix C for a discussion of this procedure. Samples with less than 10 garnets were discarded for interpretation.

The last two Figures show the relative frequency of titanium concentrations for the titanium minerals Ti-magnetite, ilmenite, leucoxene and rutile.

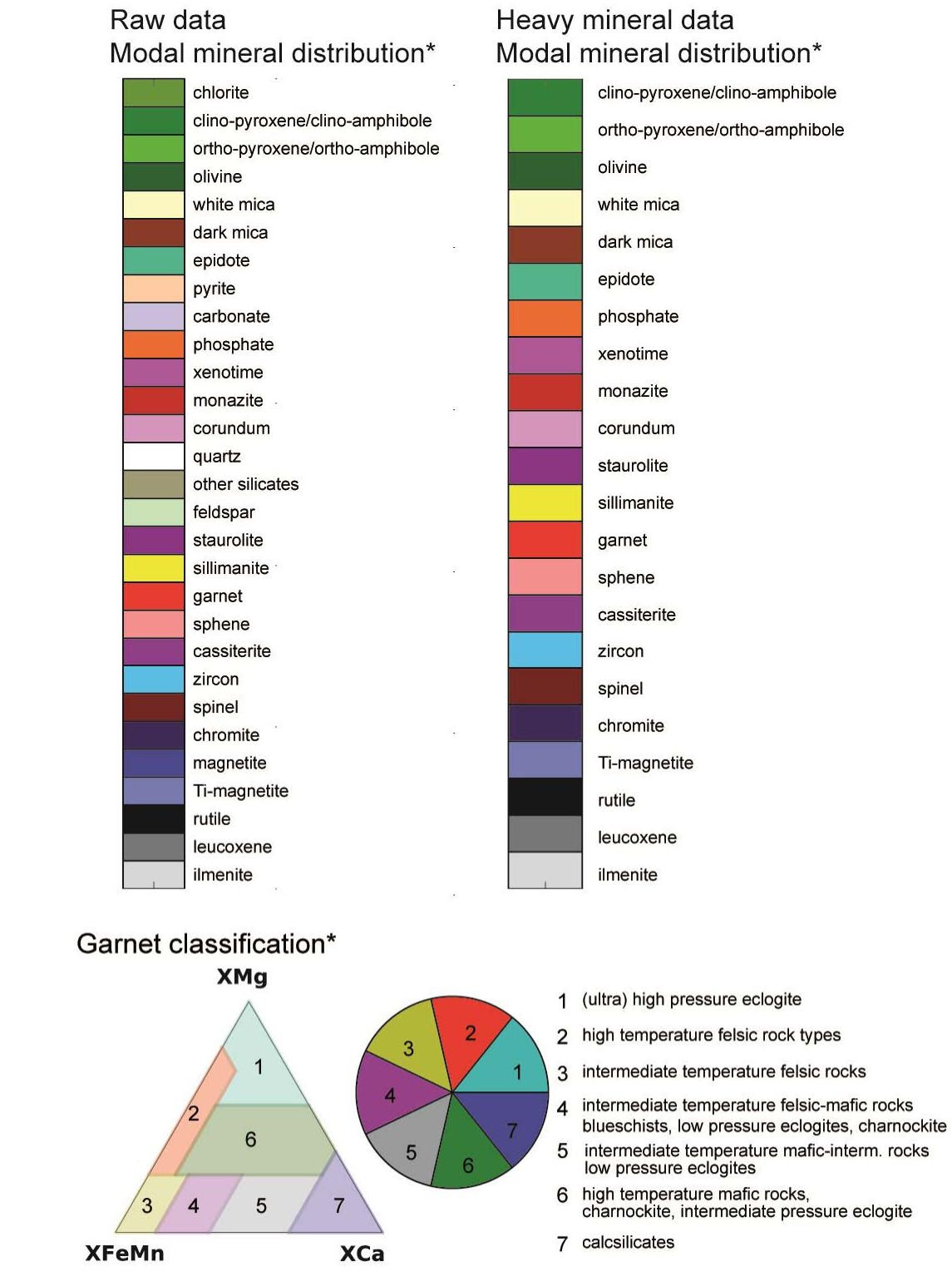

Figure A1: Legend for Appendix A.

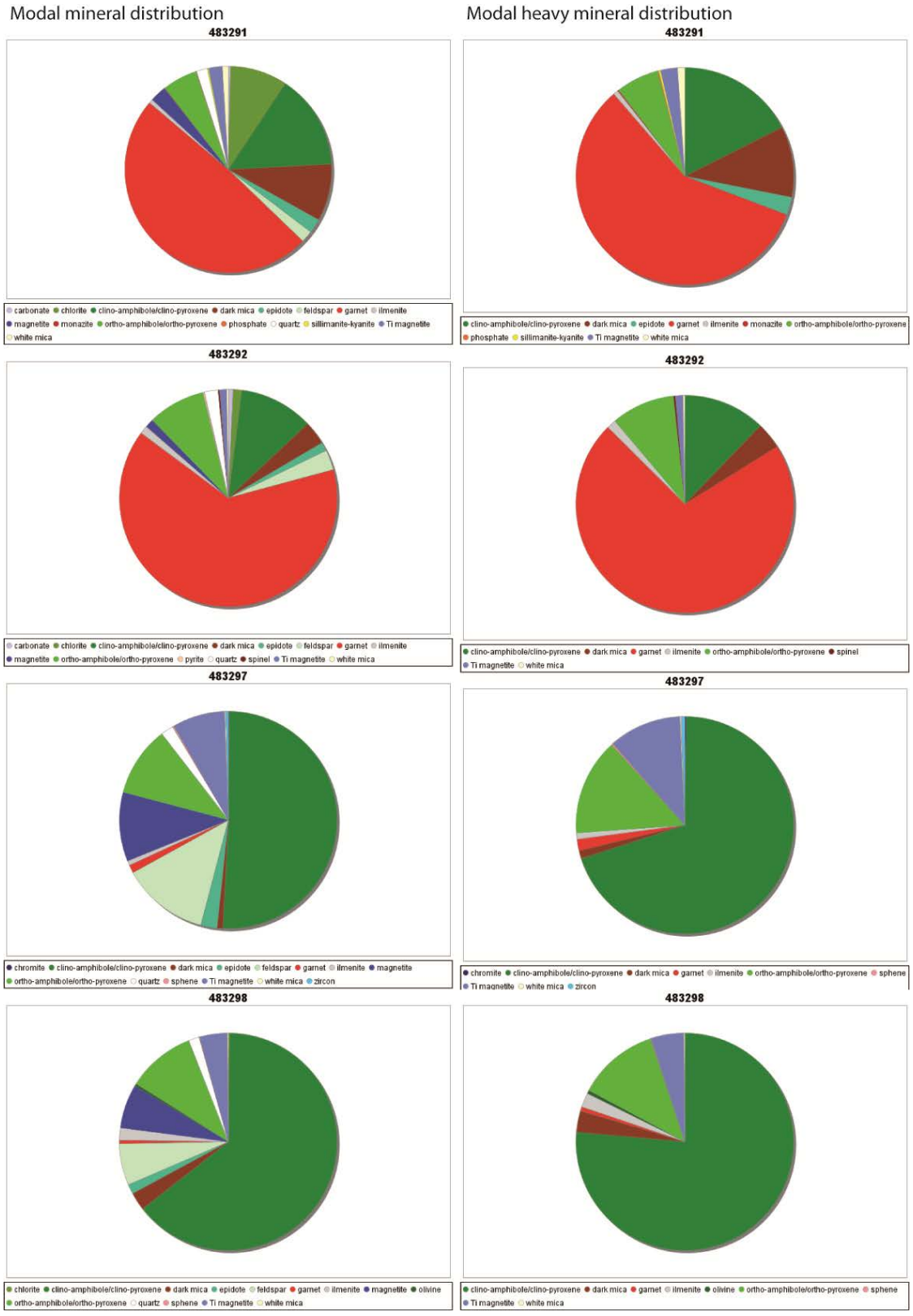

Figure A2: Modal mineral composition for the stream sediment samples 483291, 489292, 489397, and 483298. Raw CCSEM modal mineral distribution in the left half of the Figure, corresponding modal heavy mineral composition for the same samples in the right half of the Figure.

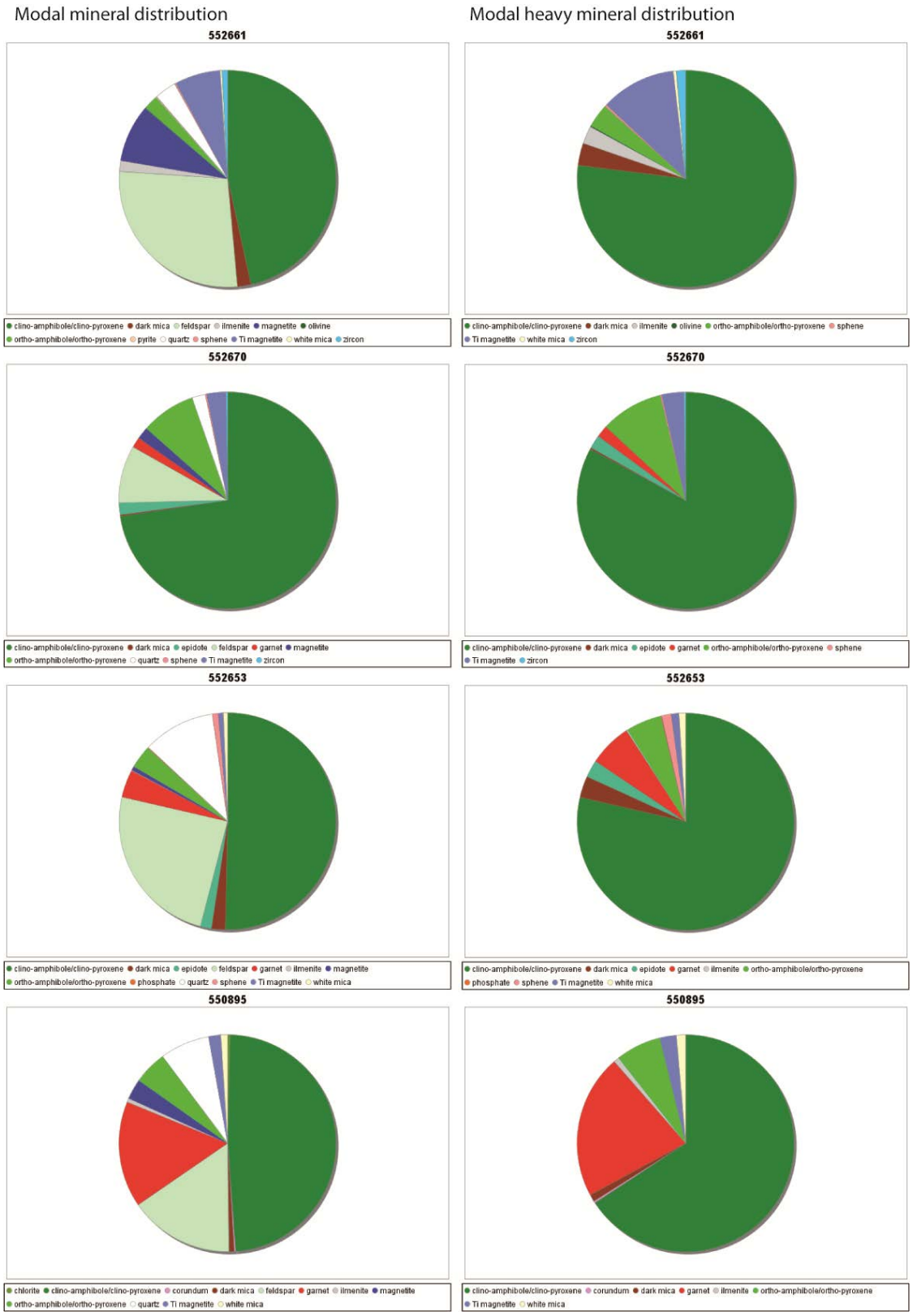

Figure A3: Modal mineral composition for the stream sediment samples 552661, 552670, 552653, and 550895. Raw CCSEM modal mineral distribution in the left half of the Figure, corresponding modal heavy mineral composition for the same samples in the right half of the Figure.

Figure A4: Modal mineral composition for the stream sediment samples 550686, 550903, 550886, and 552708. Raw CCSEM modal mineral distribution in the left half of the Figure, corresponding modal heavy mineral composition for the same samples in the right half of the Figure.

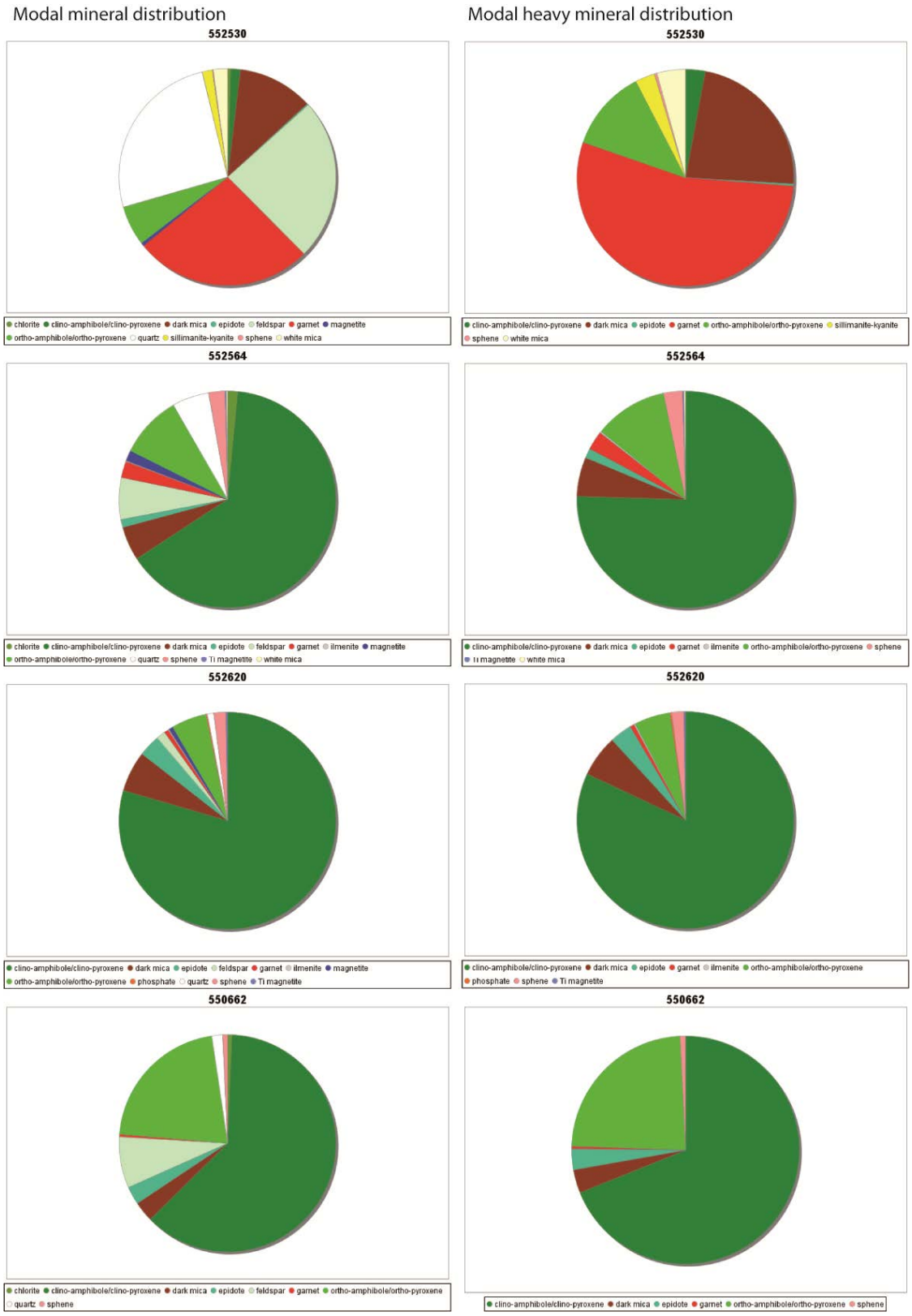

Figure A5: Modal mineral composition for the stream sediment samples 552530, 552564, 552620, and 550662. Raw CCSEM modal mineral distribution in the left half of the Figure, corresponding modal heavy mineral composition for the same samples in the right half of the Figure.

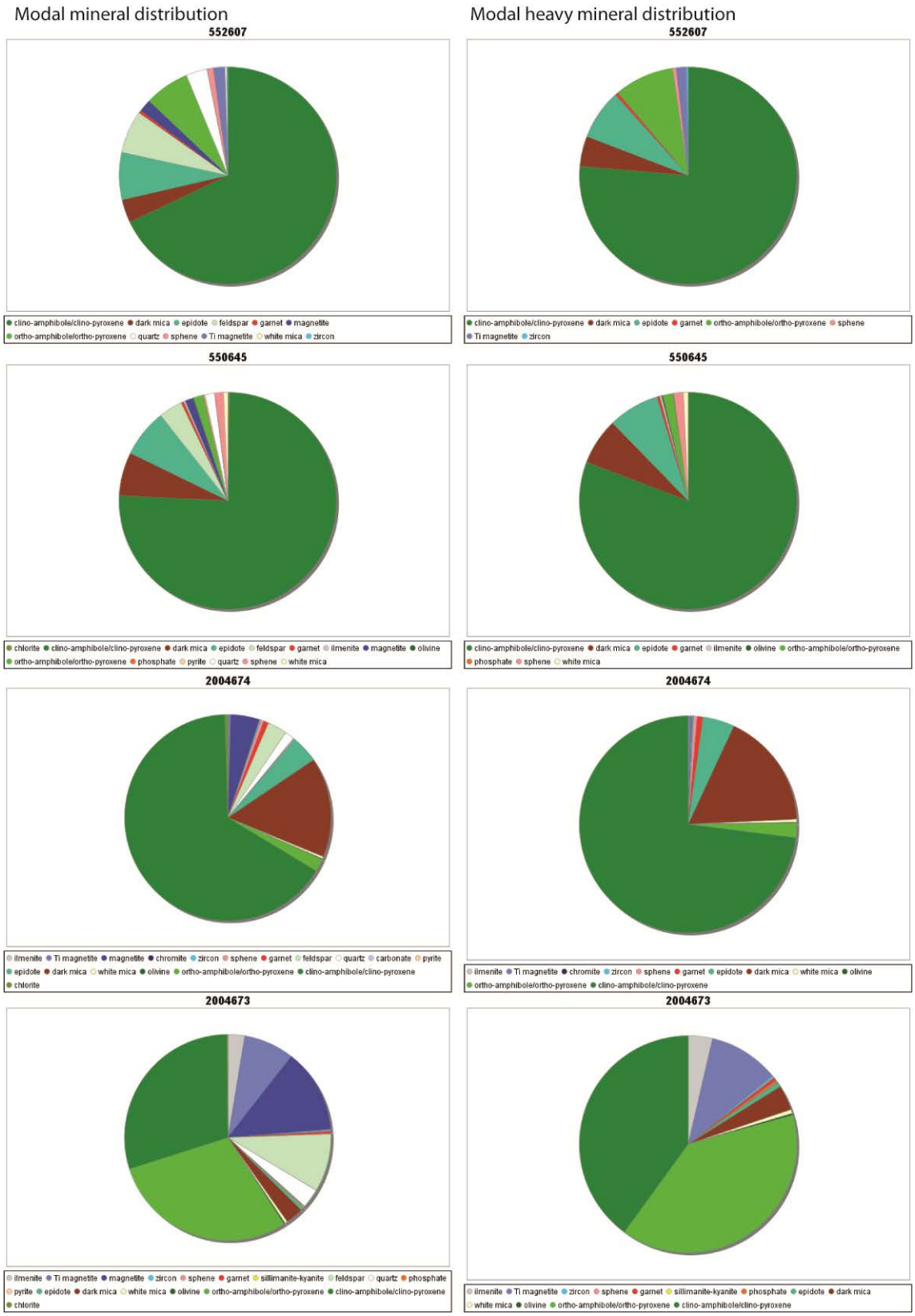

Figure A6: Modal mineral composition for the stream sediment samples 552607, 550645, 550120 (2004674), and 550052(2004673). Raw CCSEM modal mineral distribution in the left half of the Figure, corresponding modal heavy mineral composition for the same samples in the right half of the Figure.

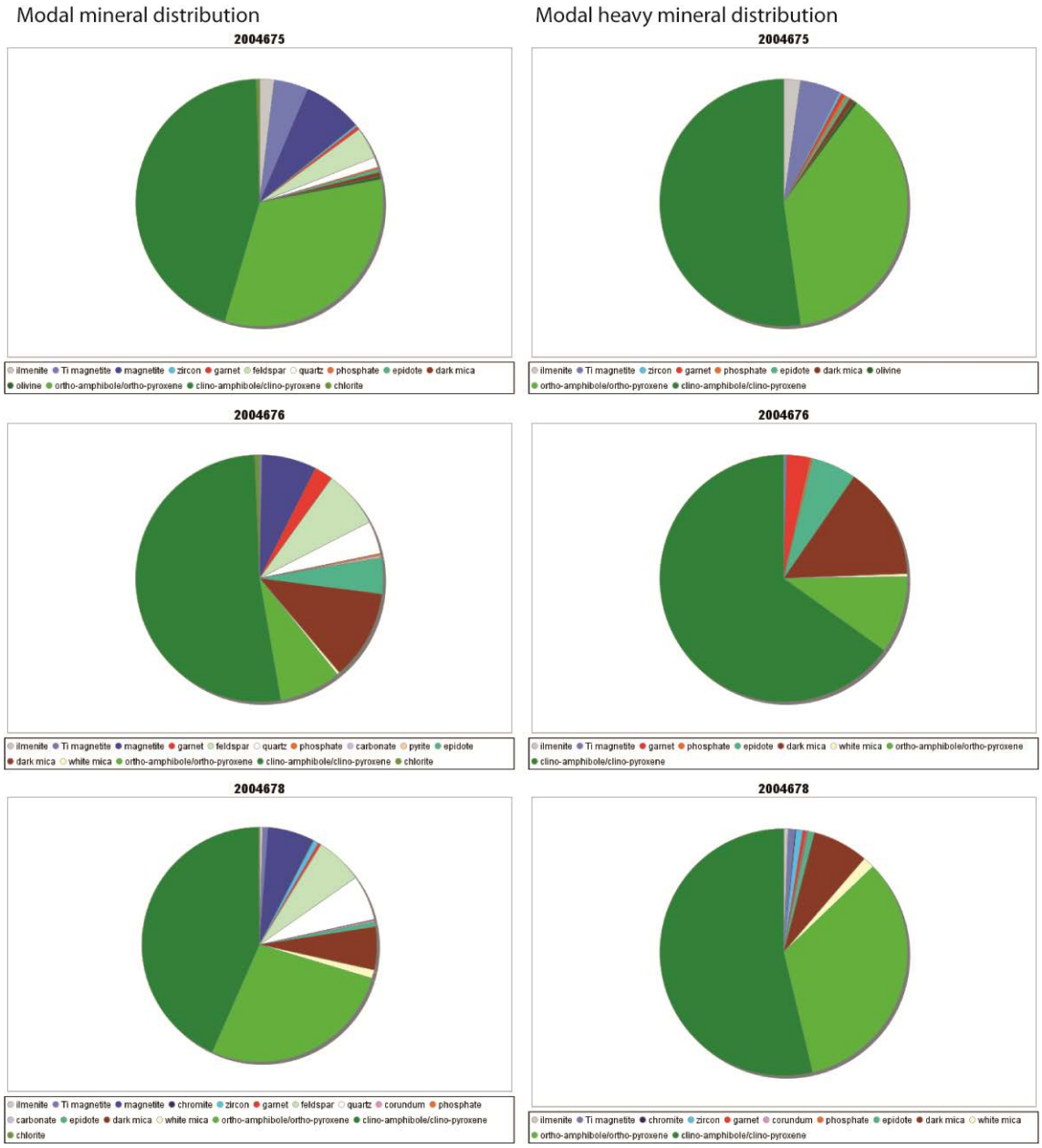

Figure A7: Modal mineral composition for the stream sediment samples 550148(2004676), 550272 (2004676), and 550512 (2004678). Raw CCSEM modal mineral distribution in the left half of the Figure, corresponding modal heavy mineral composition for the same samples in the right half of the Figure.

Garnet composition diagram

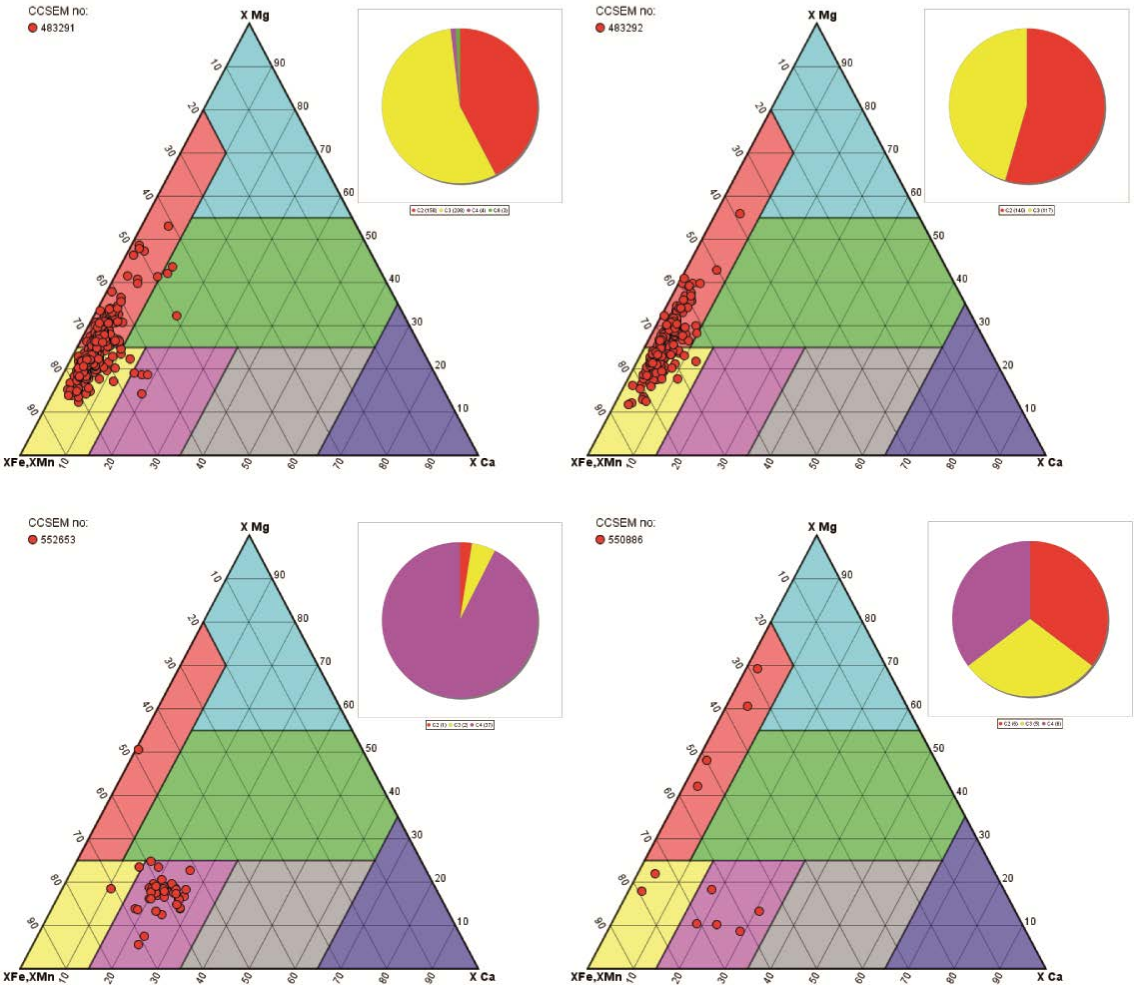

Figure A8: Garnet composition for the stream sediment samples 483291, 483292, 552653, and 550886. Ternary diagram with garnet composition and corresponding circle diagram showing the grouping for the same garnets in the insets.

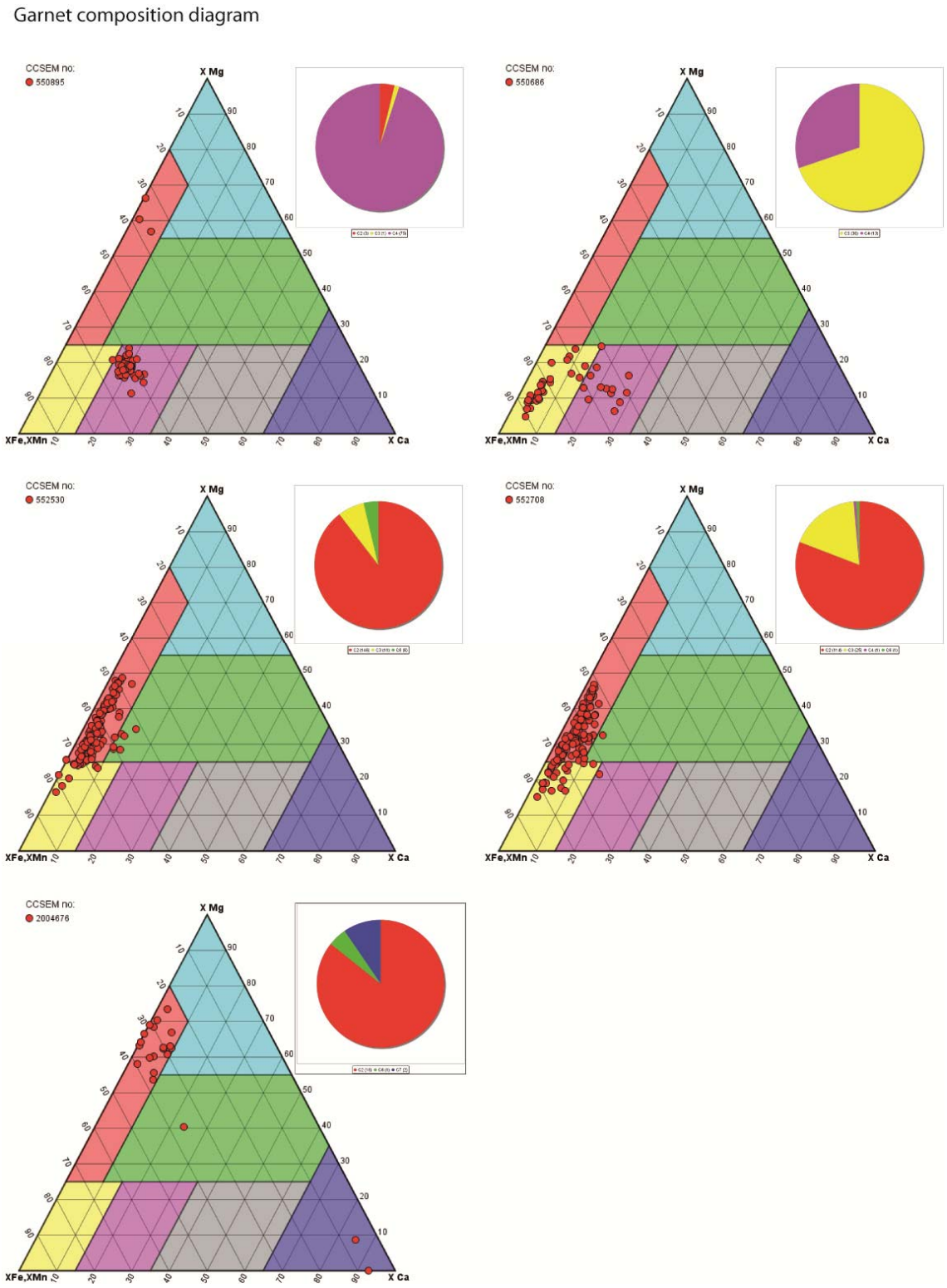

Figure A9: Garnet composition for the stream sediment samples 550895, 550686, 552530, 552708, and 550272. Ternary diagram with garnet composition and corresponding circle diagram showing the grouping for the same garnets in the insets.

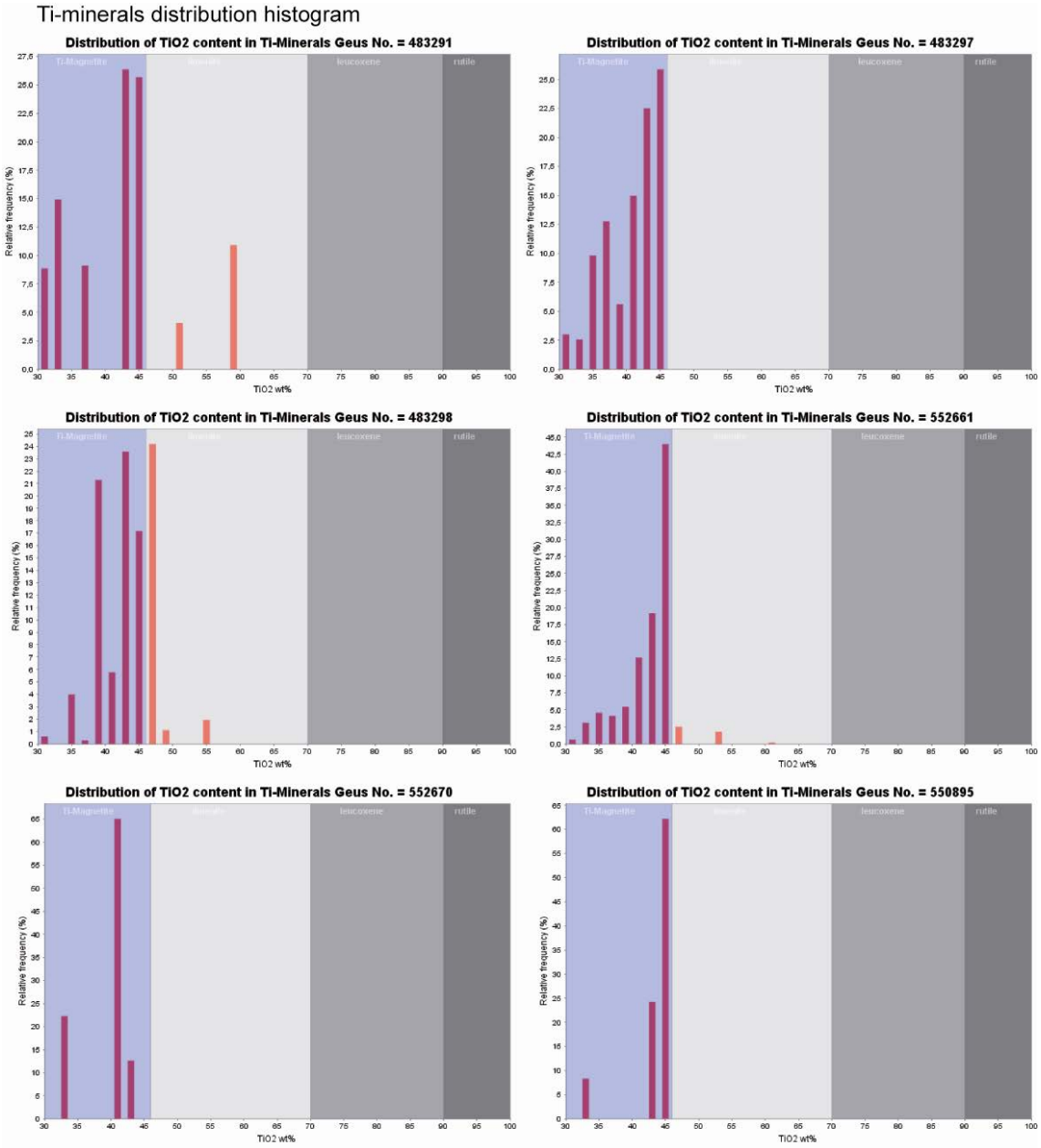

Figure A10: Titanium concentration diagram showing relative frequency of the titanium minerals Ti-magnetite, ilmenite, leucoxene, and rutile for the stream sediment samples 483291, 483297, 483298, 552661, 552670, and 550895.

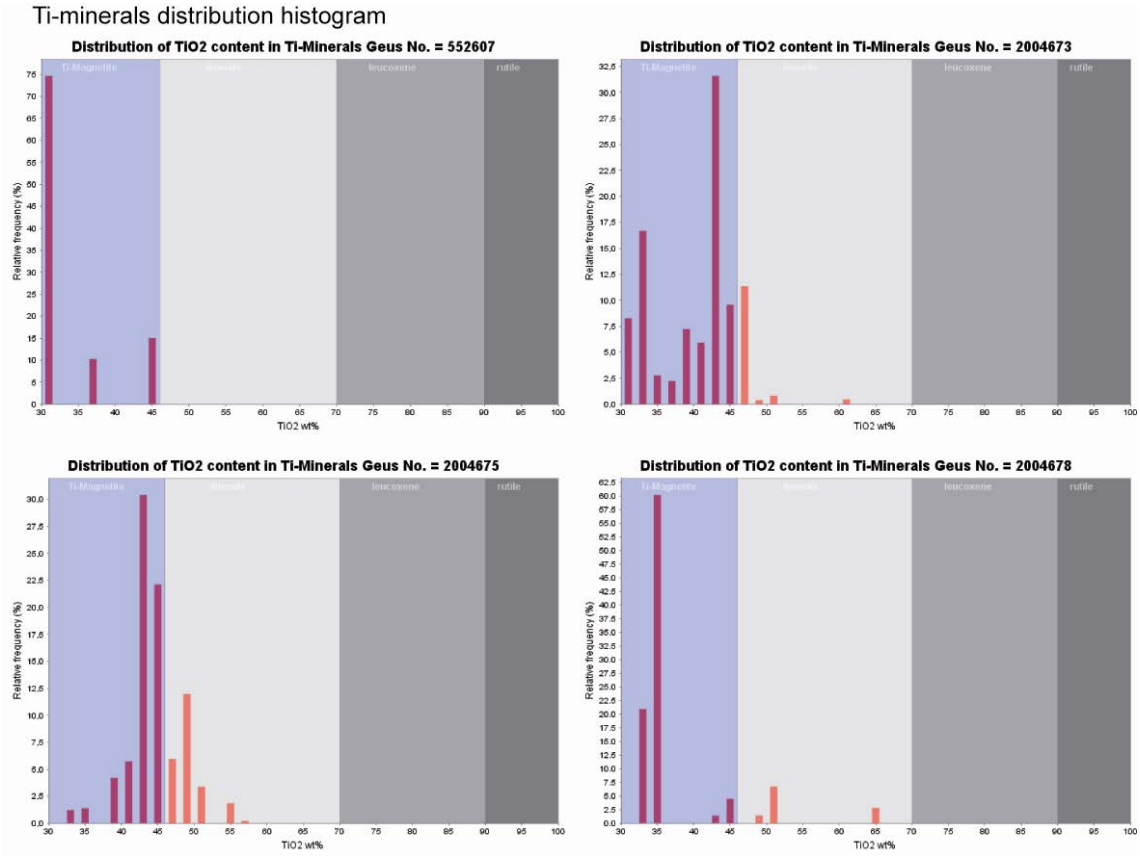

Figure A11: Titanium concentration diagram showing relative frequency of the titanium minerals Ti-magnetite, ilmenite, leucoxene, and rutile for the stream sediment samples 552607, 55052 (2004673), 550148 (2004675), and 550512 (2004678).

Appendix B: Chemistry and mineralogy of pyroxenes and amphiboles

This appendix shows the chemistry and mineralogy of clino-pyroxene/clino-amphibole and ortho-pyroxene/ortho-amphibole resulting from the CCSEM analyses. The Figures show data for these minerals in Al_2O_3 versus SiO_2 and in CaO versus MgO (wt%) plots. The minerals were classified with help of a standard reference work on rock forming minerals (Deer et al.1992), where these four oxides, plus data for FeO/Fe_2O_3, K_2O, Na_2O and TiO_2 (available in the CCSEM database at GEUS) were taken into account. With data on these eight oxides, a rough classification of the pyroxenes and amphiboles was attempted.

Due to the inability of the EDX to measure OH^- in the crystal data and due to normalization of the data, the distinction between pyroxene and amphiboles is still uncertain in some cases. Anthophyllite and pigeonite have a large range of overlap for example, but imply very different metamorphic conditions and a different geological history.

Both pyroxene and amphiboles consist of a solid solution series of many end-members, therefore no sub-classification of the amphiboles has been attempted. In the appendix the most common pyroxene and amphibole in each of the samples have been indicated, or two end-members of a longer series.

In the scatter diagrams in this appendix the data for quartz, feldspar, carbonate, iron oxides (magnetite), pyrite, chlorite and other (i.e., unspecified) silicates have been removed. See the Method description section for a discussion of this procedure.

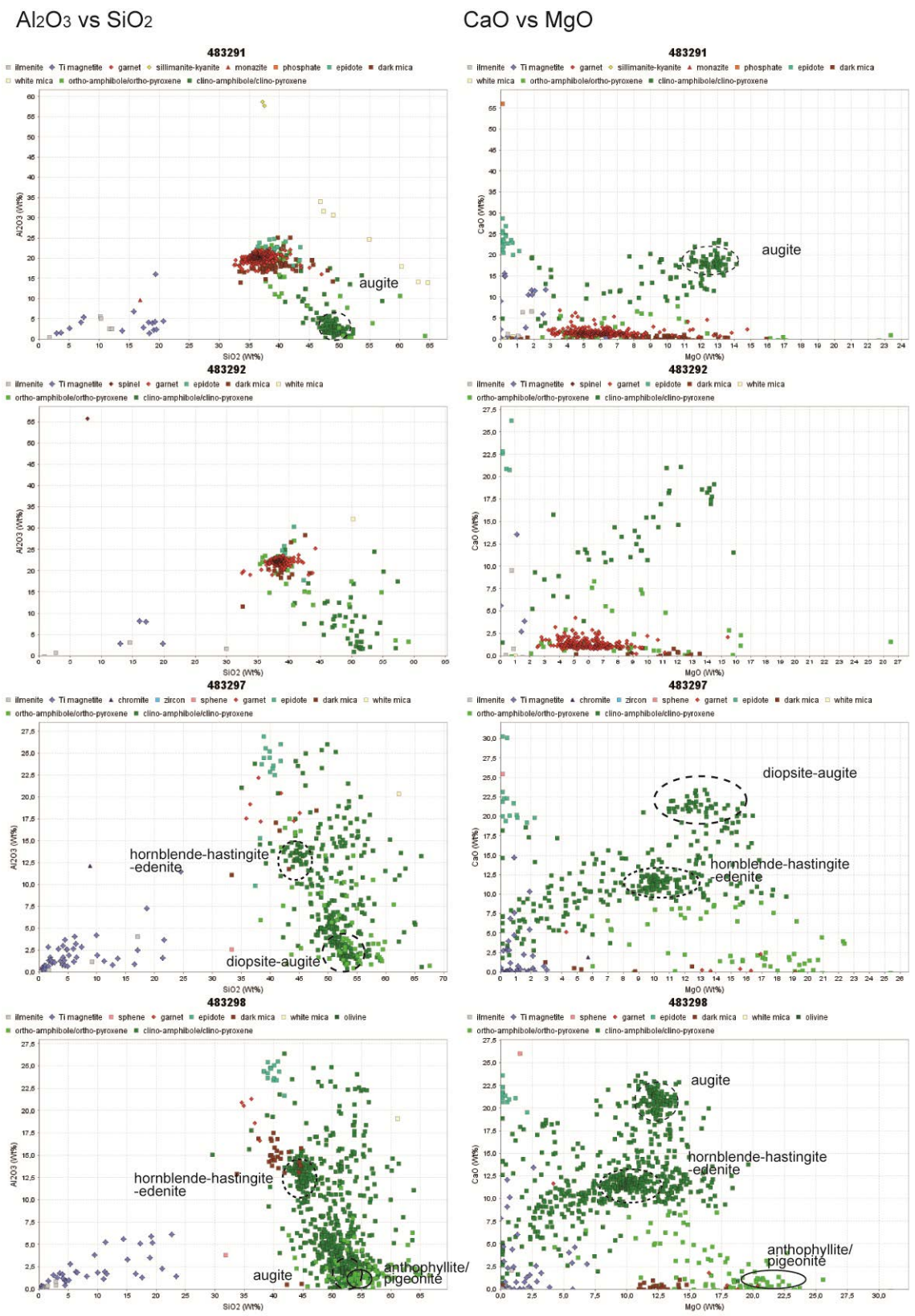

Figure B1: Chemistry for the stream sediment samples 483291, 489292, 489397, and 483298 showing Al_2O_3 vs. SiO_2 and CaO vs. MgO. Possible mineral names for analysed pyroxenes and amphiboles are indicated.

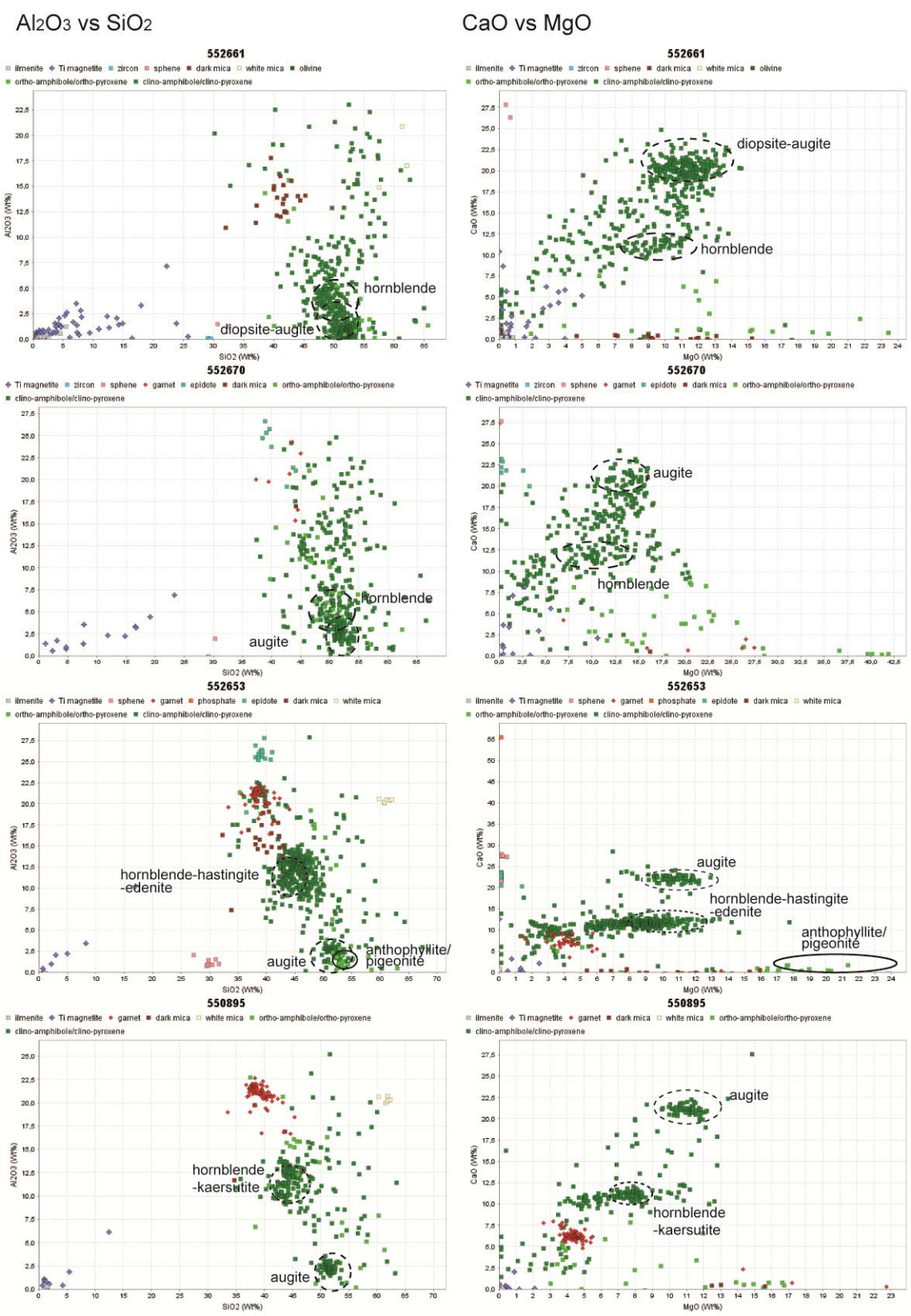

Figure B2: Chemistry for the stream sediment samples 552661, 552670, 552653, and 550895 showing Al_2O_3 vs. SiO_2 and CaO vs. MgO. Possible mineral names for analysed pyroxenes and amphiboles are indicated.

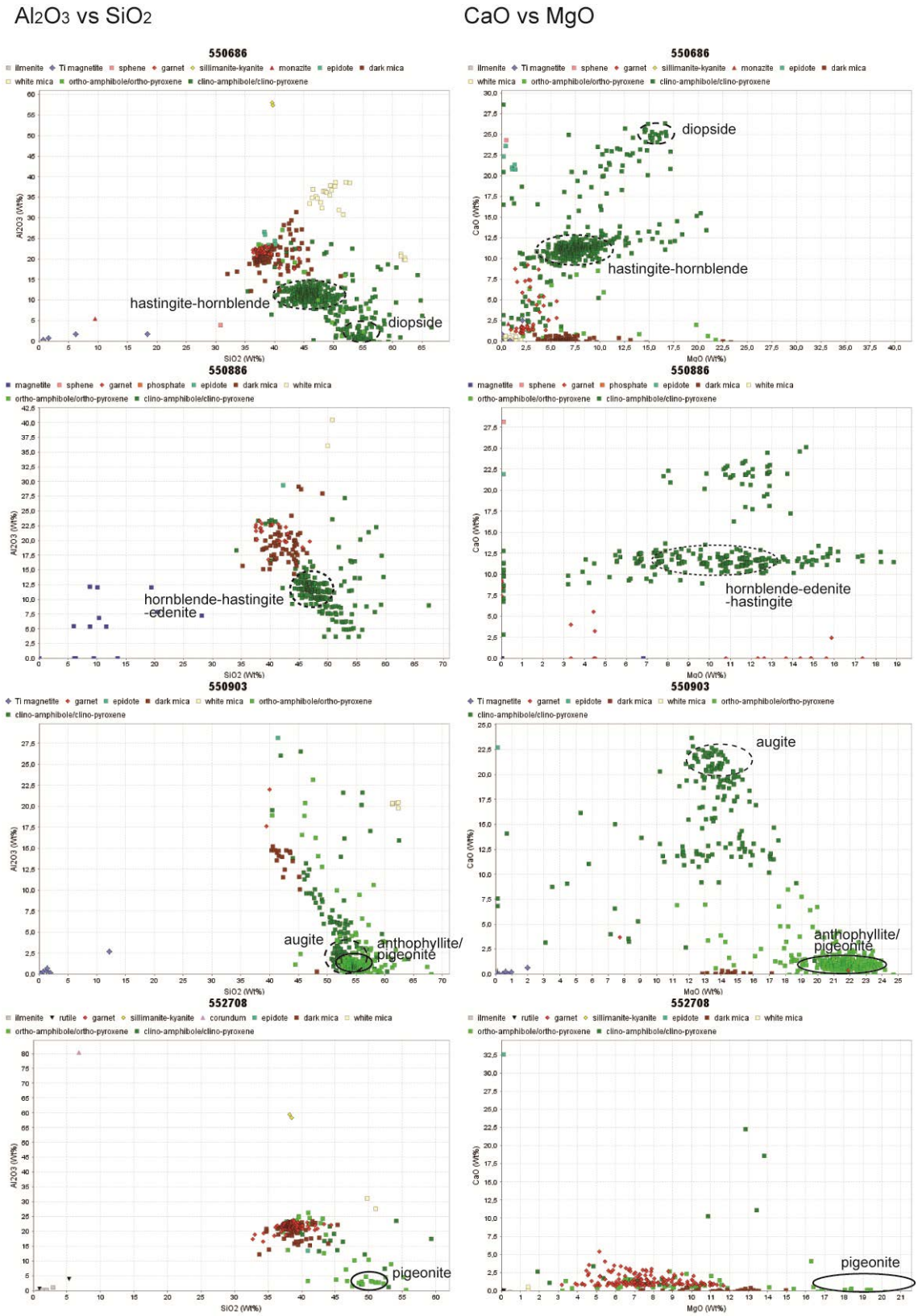

Figure B3: Chemistry for the stream sediment samples 550686, 550886, 550903, and 552708 showing Al_2O_3 vs. SiO_2 and CaO vs. MgO. Possible mineral names for analysed pyroxenes and amphiboles are indicated.

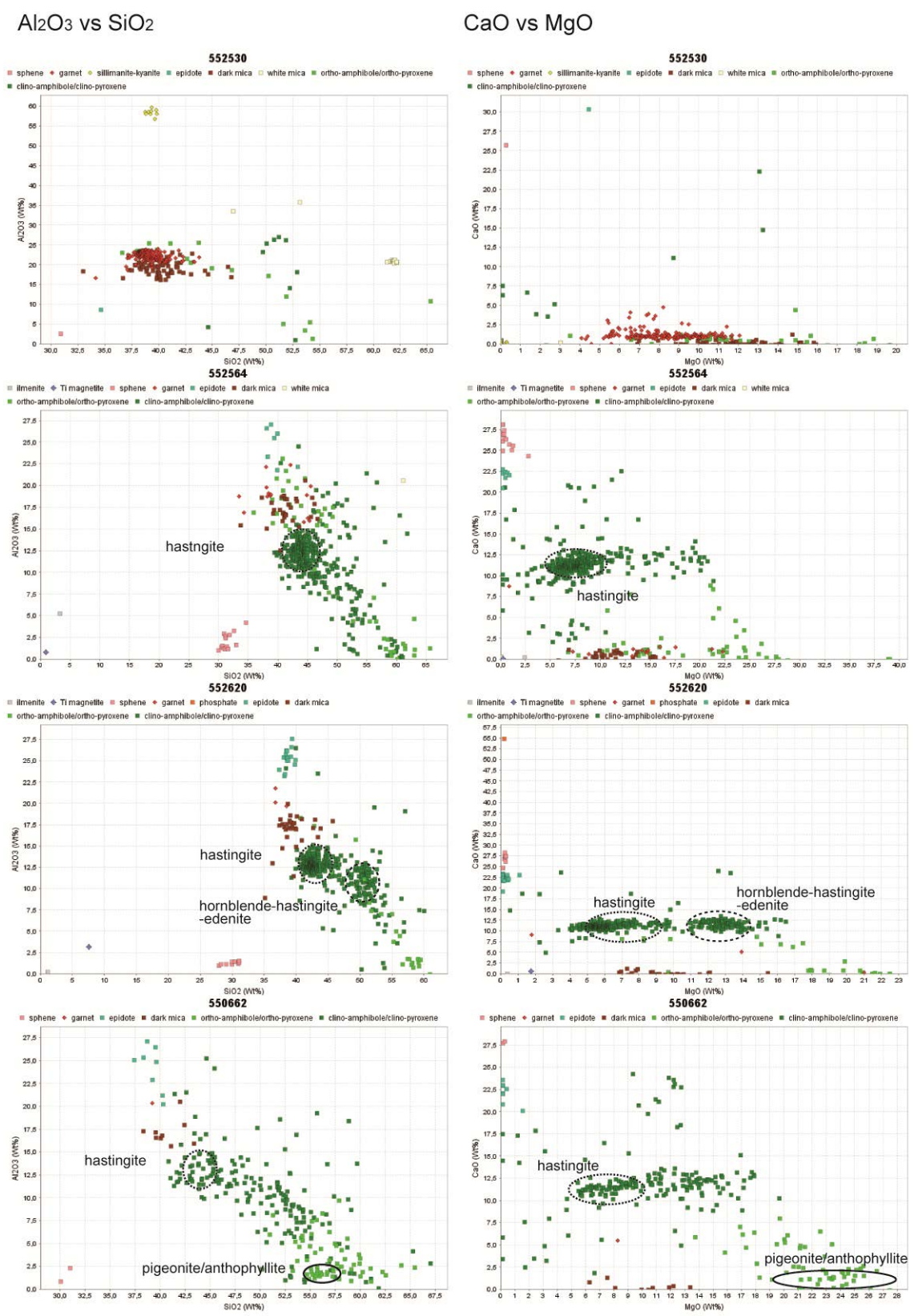

Figure B4: Chemistry for the stream sediment samples 552530, 552564, 552620, and 550662 showing Al_2O_3 vs. SiO_2 and CaO vs. MgO. Possible mineral names for analysed pyroxenes and amphiboles are indicated.

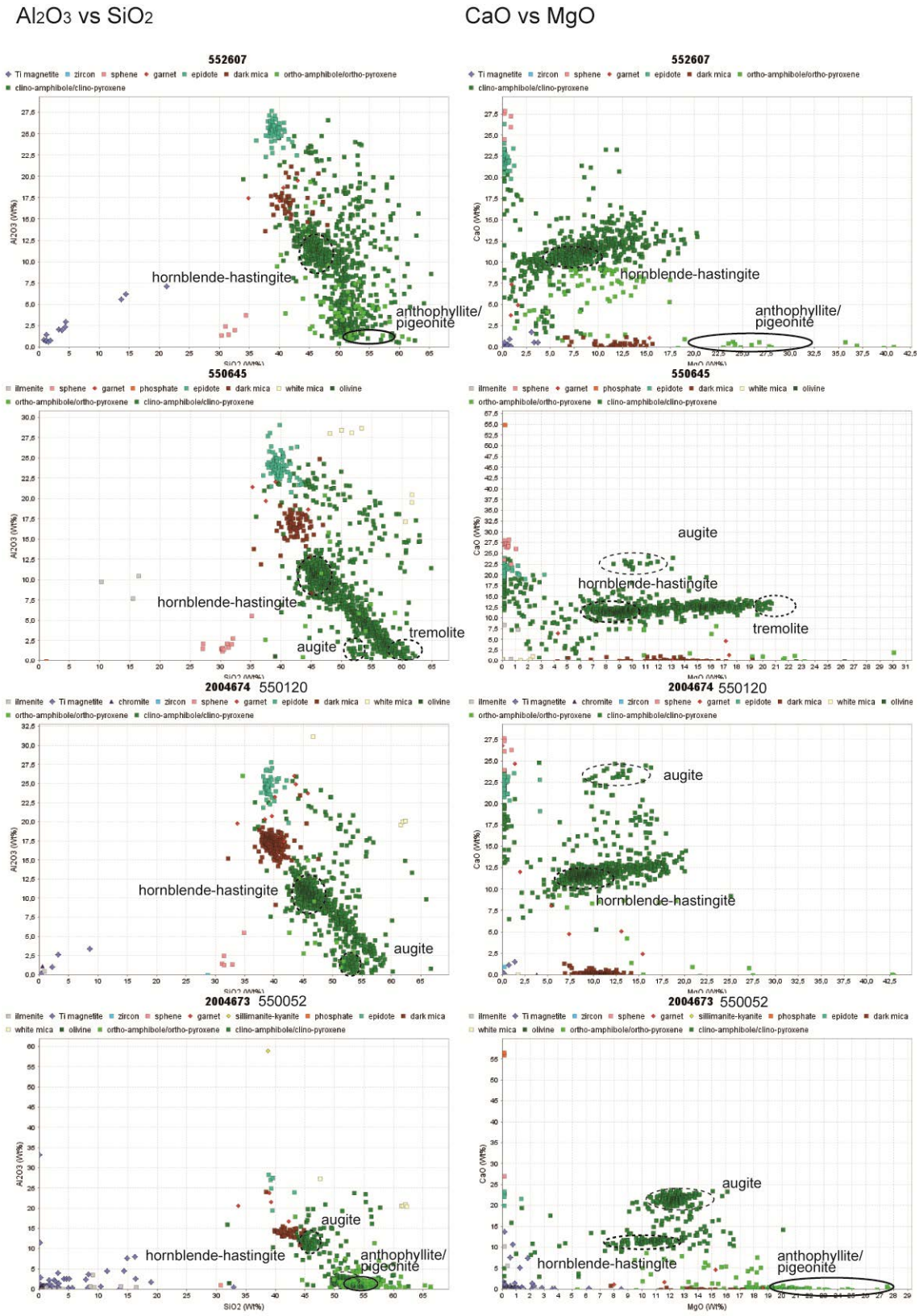

Figure B5: Chemistry for the stream sediment samples 552607, 550645, 550120 (2004674), and 550052(2004673) showing Al_2O_3 vs. SiO_2 and CaO vs. MgO. Possible mineral names for analysed pyroxenes and amphiboles are indicated.

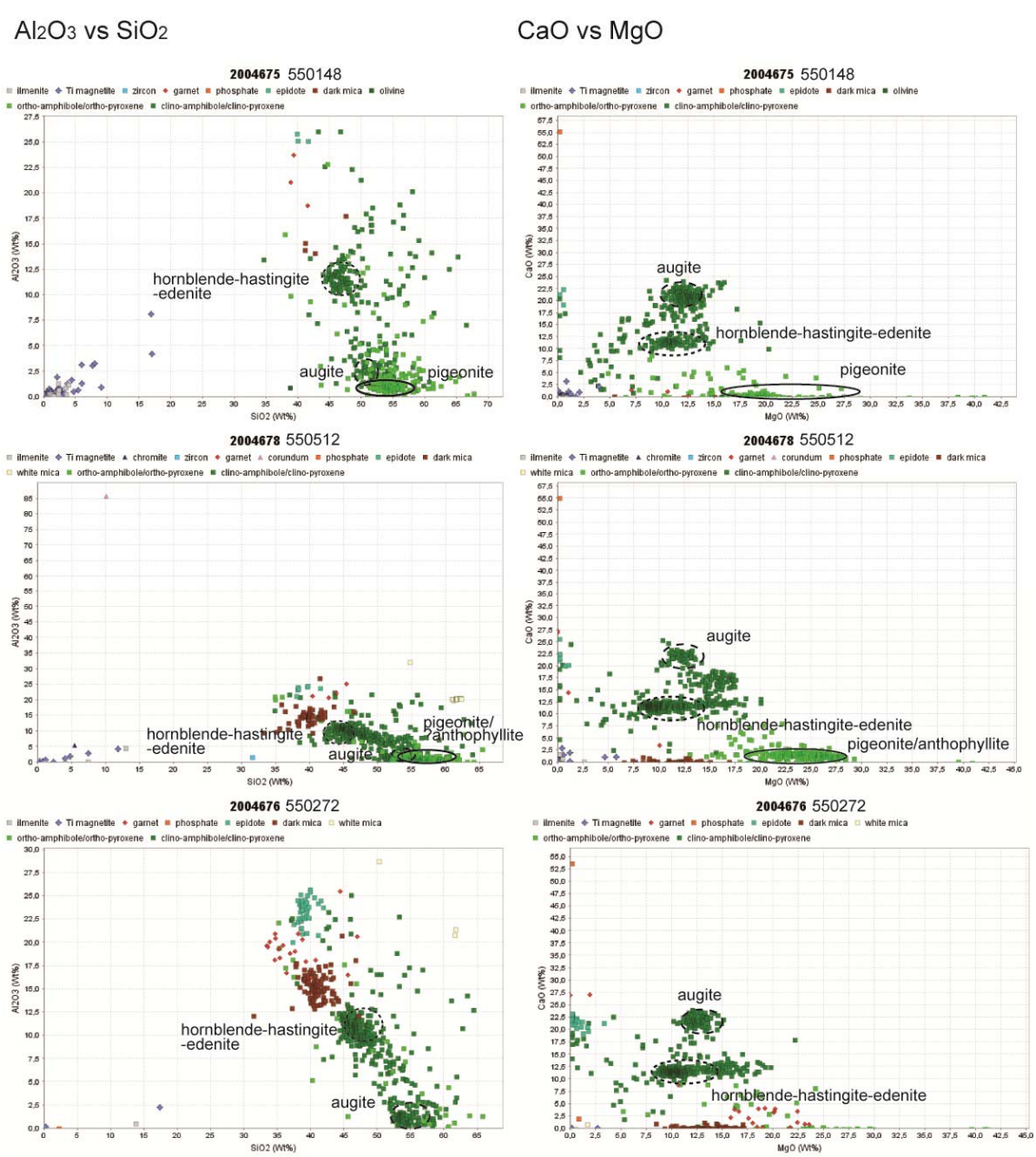

Figure B6: Chemistry for the stream sediment samples 550148 (2004676), 550512 (2004678), and 550272 (2004676) showing Al_2O_3 vs. SiO_2 and CaO vs. MgO. Possible mineral names for analysed pyroxenes and amphiboles are indicated.

Appendix C: Background information on CCSEM and Garnet classification

Computer-Controlled Scanning Electron Microscopy

Range of application for the CCSEM technique

The CCSEM technique was initiated at the beginning of the 1980s for the characterisation of coal minerals (Lee & Kelly 1980; Huggins *et al.* 1980) and the study of synthetic crystals for super-conductors and catalysts (Lin & Barnes 1984). Soon it was developed to a broader range of application in the study of dust particles and fibres in lung tissue of mine workers (Friedrichs 1987); in the analyses of aerosols for air quality control and source emission characterisation (e.g. Heasman & Watt 1989); and the degree of sintering and consolidation of coal ash deposits (e.g. Huffman *et al.* 1994). CCSEM has been used in the earth sciences for the determination of the sediment budget of a lake (Yin & Johnson 1984), for the characterisation of soil and dust (Pirrie *et al.* 2004), for provenance analysis of ilmenite-bearing beach sands (Knudsen *et al.* 2005; Bernstein *et al.* 2008), and provenance studies on sandstones in oil-bearing basins (Frei *et al.* 2005b). Other areas where CCSEM has been applied include the characterisation of small inclusions, e.g. impurities in metal alloys or steel (Schwoeble *et al.* 1988), analyses of gun-shot residues (e.g. Steffen *et al.* 2007), and analyses of bladder stones obtained from a skeleton found in a Mesolithic cave-tomb (D'Alessio *et al.* 2005).

Grain morphology analysis

Apart from the geochemical grain by grain investigations, the grain morphology is measured simultaneously.

With the BSE detector a grey-scale image of the grains in the epoxy is made, as is described in the text. Grey-level intensity thresholding by the image analysis function integrated in the software creates a binary image of the BSE micrograph and allowed for the separation and selection of individual grains (Fig. 3B).A 'hole-fill' function enabled more precise measurement of the grain size and shape from the binary image. Since the grains are mounted in epoxy resin in such a fashion that they do not touch each other, no grain separation techniques, as commonly applied in automatic particle analysis software, had to be used. Thus, the original 2D grain shape and grain size were completely available for analyses, without the introduction of artefacts by grain erosion and dilation or median filtering. All standard grain shape factors can be measured. The smallest grains in the sample can be excluded from the analysis to avoid the measurement of particles that are only a few pixels in size, especially if a good grain morphology resolution is required.

For each of the grains the following grain shape parameters are selected for measurement: length (the derived length of particle or fibre, after it is straightened into a rectangle of equal area and perimeter); width, aspect ratio (maximum projection/width), circularity ($\text{perimeter}^2/(4\ \pi\ \text{Area})$).

Cost and efficiency compared to complementing methods

CCSEM provides a rapid and cost efficient way of measuring samples. With CCSEM, analyses on large amounts of single grains can be performed in a short amount of time and without intensive labour by an operator. CCSEM is as well able to provide additional data on the grain size and grain shape of each of the particles. However, CCSEM analyses are based on EDX measurements; these are standard-less semi-quantitative measurements and are therefore not comparable in accuracy to XRF or microprobe data. The electron microscope EDX system was not developed for the measurements of trace elements in samples.

method	**XRF**	**microprobe**	**CCSEM**
Multi grain analysis	no	no	yes
Single grain analysis	no	yes	yes
Bulk analysis	yes	no	yes
Grain size and shape	no	limited	yes
error	very low	low	medium
cost	low	high	low-medium

Table C1: Overview of the costs, advantages and errors of XRF, microprobe and CCSEM analyses.

Validity of the CCSEM measurements

Accuracy of the CCSEM in comparison to the electron microprobe

To test the accuracy of the CCSEM, indicator minerals from the 'Garnet Lake' kimberlite body in West Greenland were used. A series of hand-picked pyrope (garnet) grains were mounted in epoxy resin. The sample was analysed using CCSEM, with extended counting times (5000 counts in the highest peak) to ensure good statistics: the relative error in the reproducibility of the measurements is *ca.* 1–2% for major elements (>20 wt %) and *ca.* 4–8% for minor elements (>2 wt %). The accuracy of CCSEM was tested by comparing the results with compositional data obtained from electron microprobe analyses for the same minerals, as reported in Hutchison (2005). A good reproduction of the EMP measurements was achieved by CCSEM (Fig. C1); the statistical correlation between the two methods for these elements is 70%. The three outliers reflect those garnet grains that show a compositional gradient from core to rim. The EMP point analyses were carried out on the cores of the grains, whereas the CCSEM analyses average the whole surface of the grains, therefore providing slightly different results that are closer to the bulk composition of the grains.

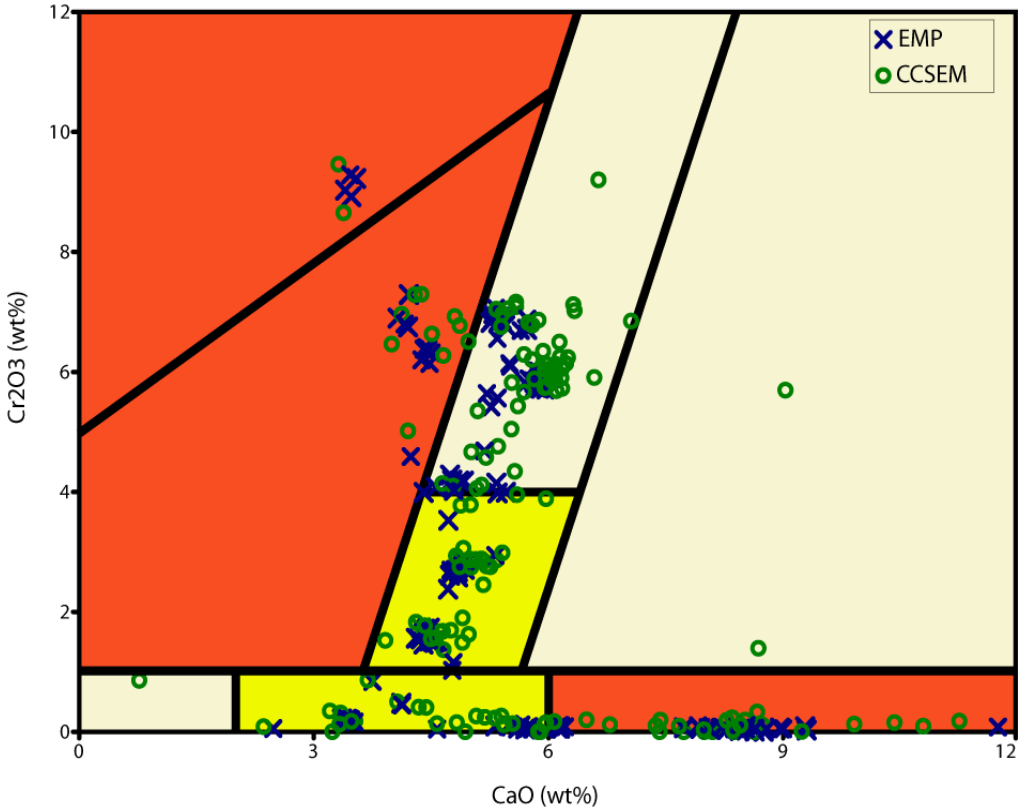

Fig. C1: Comparison of electron microprobe (EMP) and CCSEM measurements for chromium oxide and calcium oxide in Mg-rich garnets from diamond bearing rocks. Note the good correlation between the results obtained with CCSEM and the EMP data. Figure from: Keulen et al. 2008 after Grütter et al. 2004.

Precision of the CCSEM analyses

Figure C2 shows the precision of the CCSEM method for a major element (TiO_2; 93.71 wt %), a minor element (Fe_2O_3; 2.19 wt %) and a trace element (SO_2; 0.21 wt %), measured repeatedly from the same grain. Five sets of measurements at nine different maximum peak count settings (equivalent to nine different time periods) were undertaken to evaluate the reproducibility of the data. For standard (i.e. approximately 60 seconds measuring time) single spot or single grain analyses the relatively errors are high compared to other analytical methods: 2–3% for major elements (>20 wt %), 5–10% for minor elements (>2 wt %) and 50–100% for elements present in smaller quantities. However, these figures can easily be improved by increasing the counting time slightly, as is shown in Figure C2. This shows that the analysis time can be usefully tailored to the sample set depending on the required precision of the measurements and the amount of available time or money.

Empirical measurements of bulk CCSEM precision shows that these error values are much lower than expected from extrapolation from single grain measurement (Fig. C2).

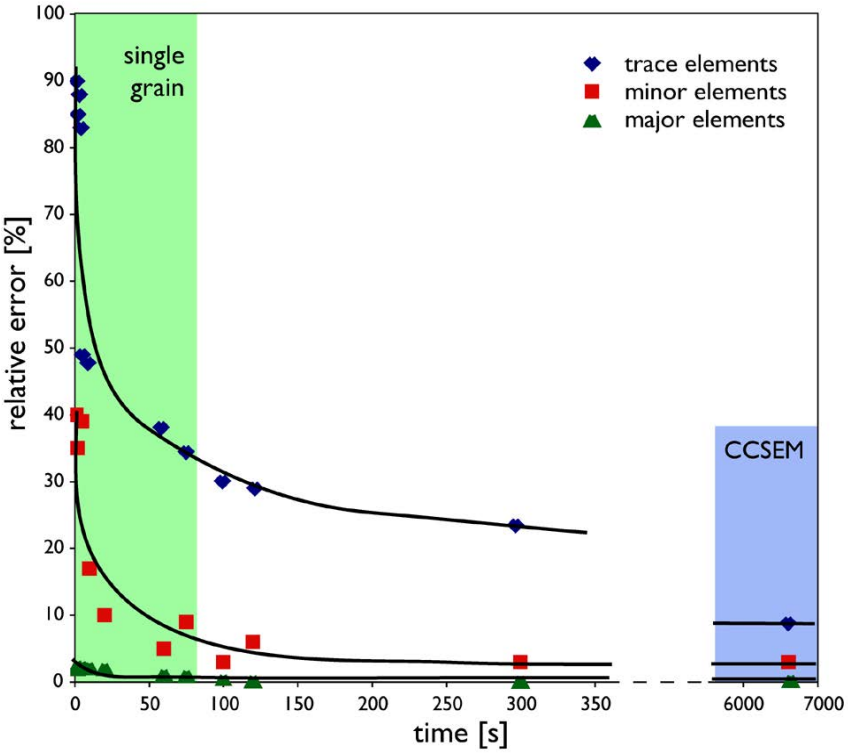

Fig. C2: Precision of single grain (green background) and bulk sample CCSEM (blue background) analyses as a function of measurement times. Note that two detectors were used for the analyses. The precision increases with longer counting time, thus bulk sample (average of all grains) values have a much lower analytical error than single grain analyses.

Repetitive analysis test

Circa 2 kg of beach sand was collected from Bellevue Strand near Copenhagen. The sand was thoroughly mixed and split into a set of samples of ca. 100g each. Nine of these were treated with the same heavy liquid and sieving treatment as the samples in this study. Epoxy mounts with the heavy mineral separate were created and measured in the electron microscope following the CCSEM procedure.

The results are shown in Figure C3: small variations in the ratios between different minerals occur. These variations are most likely due to insufficient mixing of the original sample material (K. Esbensen, pers. comm.) and can therefore be treated as a maximum estimate for the error induced by the preparation and measurement techniques.

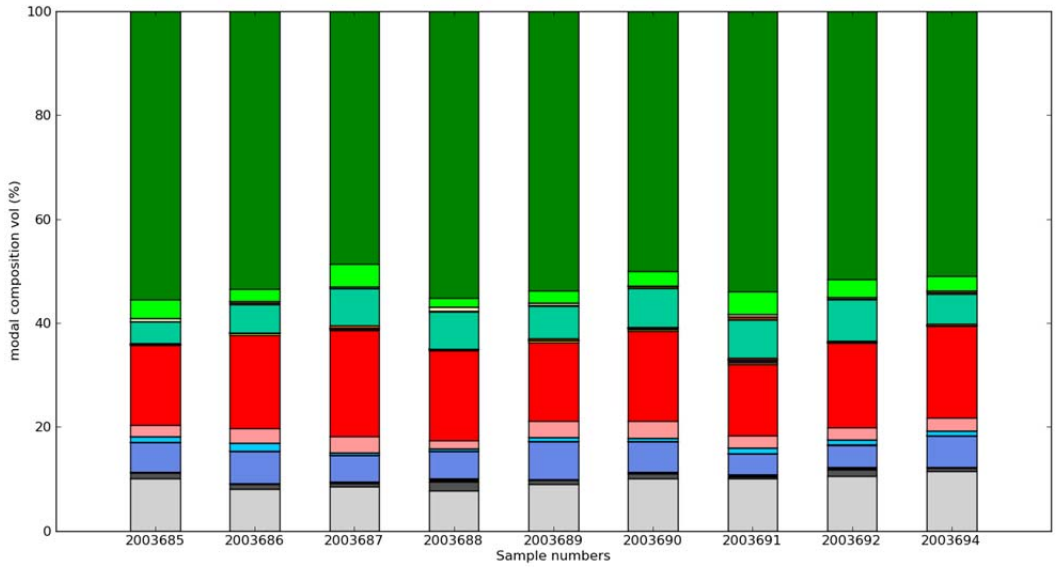

Fig. C3: Nine analyses on separate samples made from the same bulk volume of beach sediment. Variations in ratios between heavy minerals reflect the maximum error induced by the preparation method and measuring technique.

Garnet classification

Background

Garnet is a mineral that is observed in many metamorphic and igneous rock types (e.g. Deer, Howie & Zussman 1992). The composition of garnet varies widely between garnets from felsic rock types, like metapelite, metasediments, meta-granitic and meta-granodioritic rocks, mafic rock types (like metagabbros, kimberlites, metaperidotites and eclogites) and calc-silicate rocks (like siliceous marbles). The mineral adjusts it composition according to the pressure (*p*) and temperature (*T*) conditions that it was formed or recrystallised in. This property, the possibility to exchange cat-ions with nearby other minerals to adjust for the environmental conditions of the mineral, has been known in long time (e.g. Ramberg 1952; Kretz 1958) and forms the basis for geothermometers and geobarometers that have been developed, e.g. for garnet-biotite (Ferry & Spear 1978), for garnet-clinopyroxene (Krogh Ravna 2000), garnet-orthopyroxene (Sen & Bhattacharaya 1984), garnet-olivine (O'Neill & Wood 1979) and for garnet-cordierite (Hensen & Green 1972).

These and other geothermometers and geobarometers have been used to estimate the temperature and pressure of garnets in metamorphic rocks. For eclogitic garnets, minor elements like Ti, Na, and Cr play a major role (Grütter et al. 2004). For aluminium-rich garnets especially Mg, Fe and Ca are indicative of composition, and *pT* of the host rocks. For these geothermometers and geobarometers it is important, that the minerals are regarded in the right settings; the chemistry and mineralogy of the sample and the contact to the exchanging grain are of the highest importance.

In heavy mineral provenance analyses, the individual minerals are usually derived from either sandstones or from river or beach sediments. The original setting of the individual minerals in their host-rock (chemistry and mineralogy) is lost in most cases and none of the retrieved garnet grains is still in contact with its exchange partner (e.g. biotite, olivine, cordierite, zoisite, plagioclase, clinopyroxene or orthopyroxene). Nevertheless, it is often desired to get information on the source rock of the garnets. Here, we show that even where detailed pT investigations are no longer possible, garnets can still be used to get a crude estimate of the chemistry (felsic, mafic or calc-silicate) and metamorphic facies (amphibolite or granulite facies) of the source rock.

With CCSEM only aluminous garnets (with the endmembers pyrope (Mg), spessartine (Mn), grossular (Ca) and almandine(Fe)) are classified. This group covers the large majority of garnets in igneous and metamorphic rocks. Andradite and uvarovite garnets are excluded.

Method

The garnet composition of metamorphic rocks was taken from 46 publications on areas covering many countries on all continents and many different geological settings. The literature study is limited to aluminous garnets (pyrope, spessartine, grossular and almandine). Maximum fifteen measurements of each publication were used, to avoid a bias to a certain area. The metamorphic facies or *pT* conditions, which were calculated using geothermometers and geobarometers, and the rock type, were copied from the publication. All garnet compositions were plotted in a triangular diagram, using pyrope (XMg), almandine+spessartine (XFe+Mn), and grossular (XCa) as end-member compositions. The diagrams were divided into different areas by their metamorphic facies and by their chemistry and their prevalence in Greenland (see the coloured fields in Figure C4). While the temperature has a larger influence on the definition of the garnet group than pressure has, eclogites could not be separated out from the amphibolites and granulites, thus eclogites do not occur as separate groups.

Garnets in group 1 include kimberlitic garnets and other garnets that suffered from ultra-high pressure metamorphism. They are mainly derived from rock types with a mafic to ultramafic composition. Garnets in group 2 are mainly felsic granulites. “Felsic” includes all source rock with a pelitic, semipelitic, metasedimentary, granitic and granodioritic composition. Group 3 comprises mainly felsic amphibolite facies rocks; these are the lower temperature equivalents of group 2. The transition between these two groups is artificially put to XMg = 25, which corresponds to a temperature of ca. 700-750 ºC. Group 4 consists of 1) garnet amphibolites, generally formed at lower pressure conditions, or 2) felsic amphibolite facies rocks that either have a more Ca-rich or more intermediate composition, like Ca-rich semipelites, or 3) felsic rocks that underwent eclogite facies metamorphism, or 4) charnockitic rocks. Group 5 includes intermediate and mafic amphibolites, and intermediate and mafic eclogites that were formed under relatively low temperature. Group 6 comprises most garnet amphibolites, mafic granulites and higher temperature mafic eclogites. Garnets derived from calc-silicates and anorthositic rocks plot in group 7.

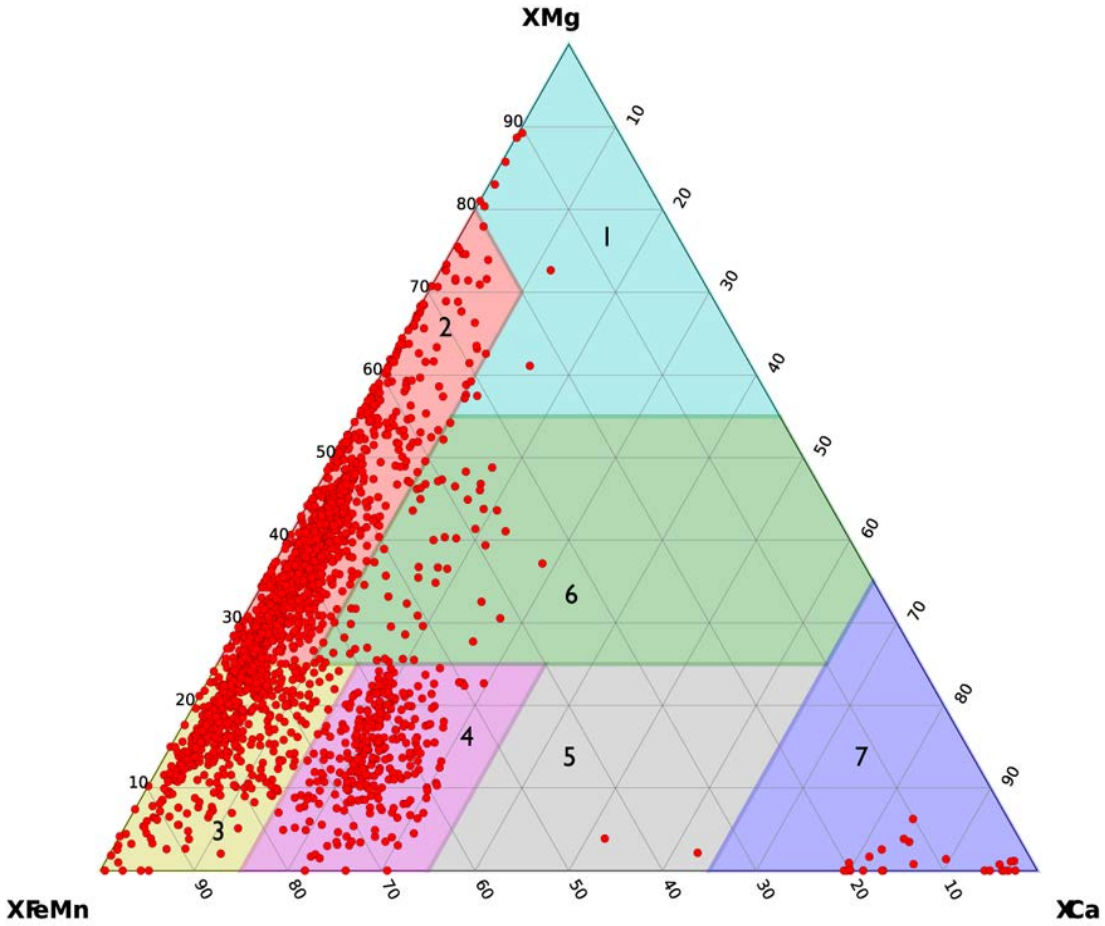

Figure C4: Ternary diagram showing garnet grains from the Greenlandic western coast. Garnets are plotted by their end-member compositions pyrope (XMg), almandine+spessartine (XFeMn) and grossular (XCa). The garnets were divided into seven groups after Keulen & Heijboer 2011, see text for discussion.

Visualisation of the results

All mineral phases in the sample are measured and classified in the CCSEM database. Figure C5 shows the result after classification. Part of the minerals is quartz (white) and feldspar (pale green), and carbonates which fall through the heavy liquid if they are coated, have large inclusions, or are carried down by other grains. Since these minerals are not heavy minerals and the total amount of quartz in the original sample is unknown, they are removed from the heavy mineral suite. One of the categories in the classification scheme is “other silicates” (beige). These are often small lithic fragments, consisting of two or three minerals. Since they do not give any provenance information, these minerals are also removed. Chlorite (olive green), pyrite (orange), and iron oxide (magnetite, hematite or goethite or siderite: marine blue) are also removed from the heavy mineral spectrum, as they usually are diagenetic minerals and therefore do not give any provenance information.

The resulting spectrum (of the same sample set) is shown in Figure C6. Since im-

portant, none provenance related, information can be gained from the overview over all minerals, these are shown in Appendix A.

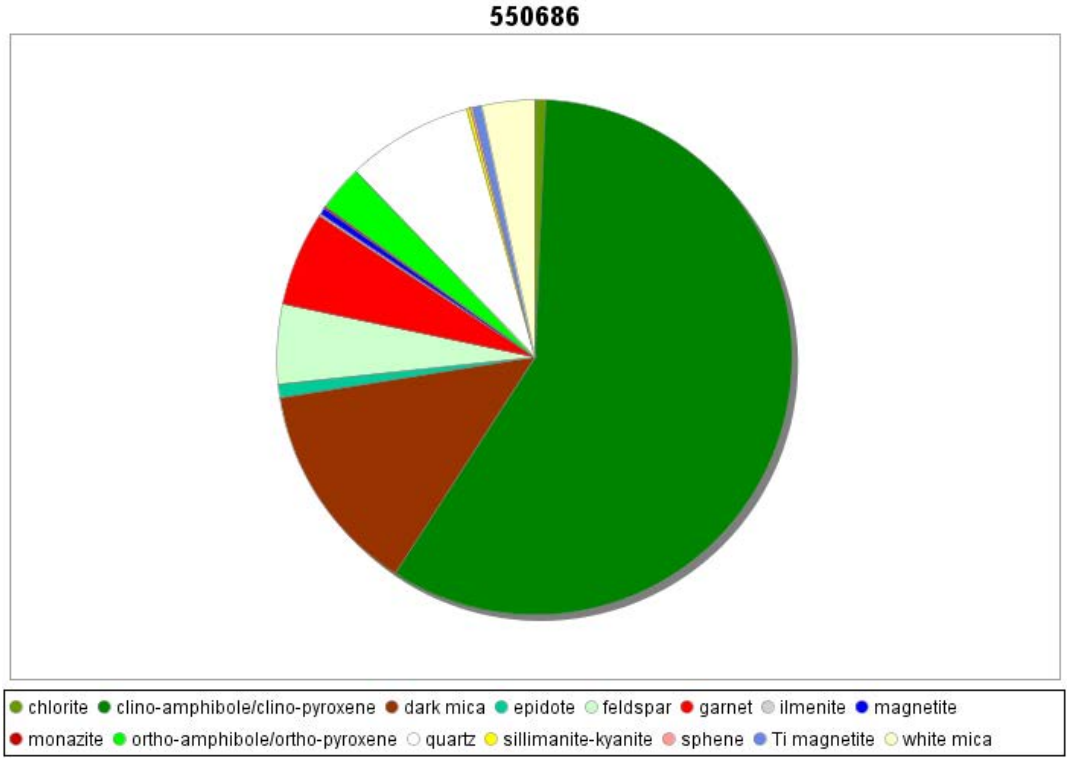

Figure C5: Pie diagram showing the modal composition for all classified minerals.

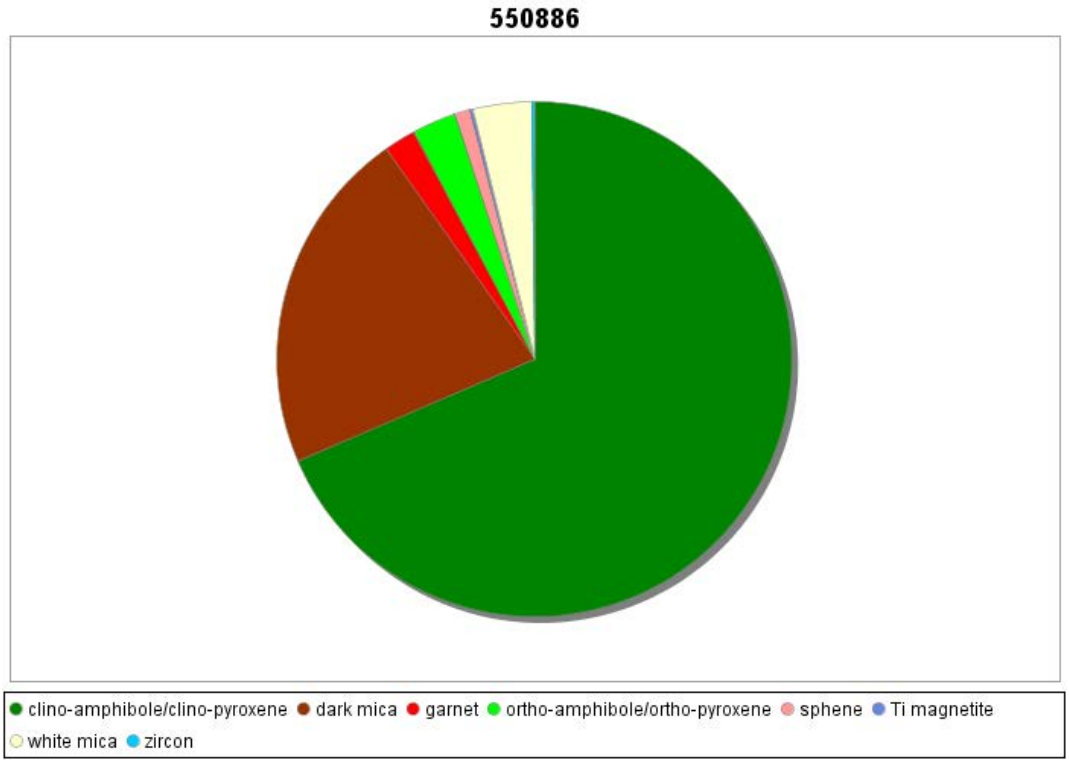

Figure C6: Pie diagram showing the modal composition for the heavy mineral suite.

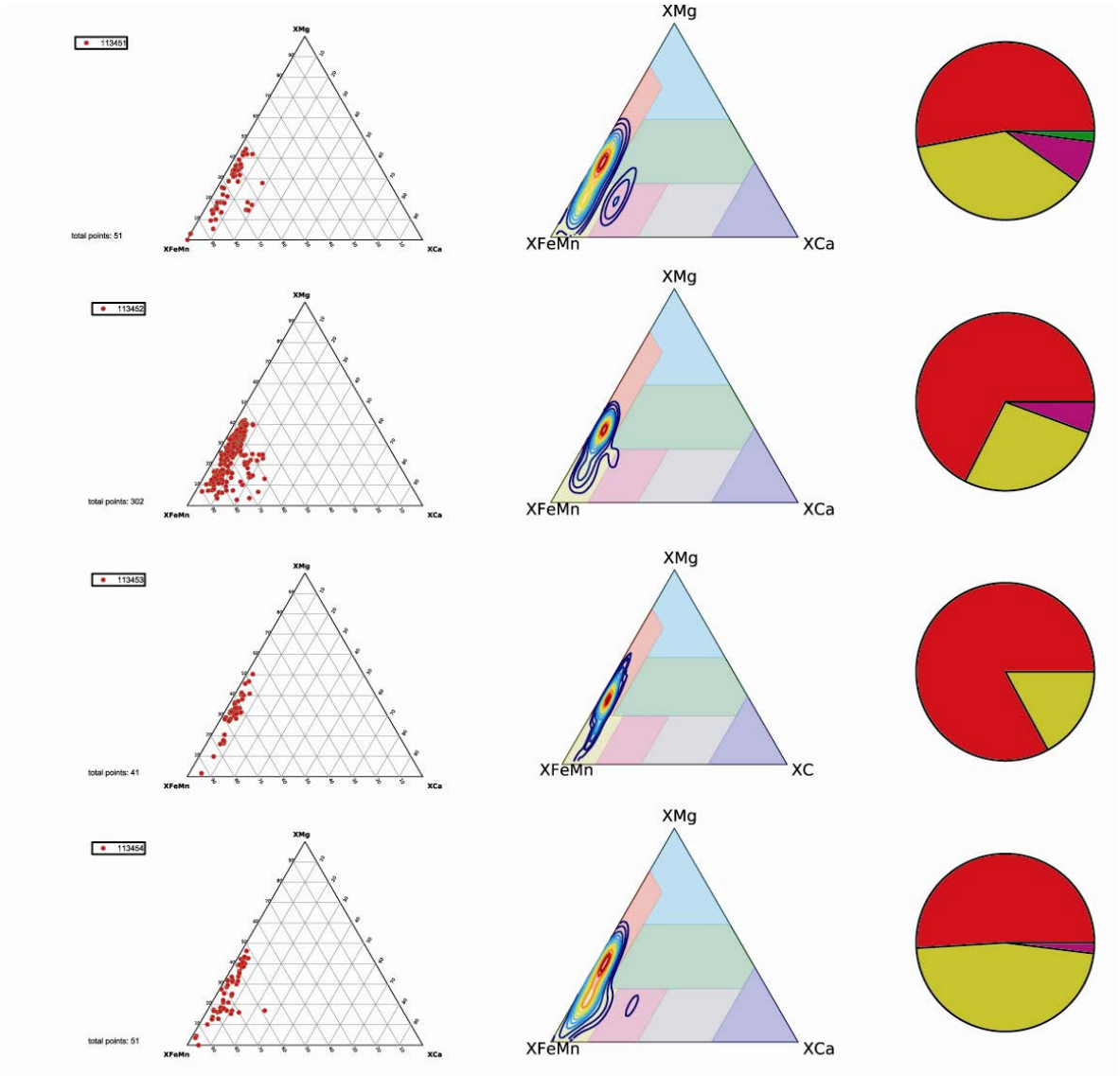

Figure C7: Three types of garnet plots, showing the same sample in three different ways. Ternary diagram (left) showing the composition of individual garnet grains (red dots). Garnet is plotted by the three endmember compositions pyrope (XMg), almandine+spessartine (XFeMn) and grossular (XCa). The garnet classification in seven groups is given in coloured fields (see Chapter on Garnet classification in this Appendix), showing the garnet composition for the individual samples as contour diagrams (middle). Pie plots, showing the garnet distribution for the same samples, where each colour represents the amount of garnets in one of the colour fields in the ternary diagrams.

Apart from the modal mineral distribution, the garnet composition of every garnet grain was measured and these results are displayed for samples with more than 10 garnet grains. The garnet data is plotted in three different ways, as is shown in Figure C7. In the left column, the raw data is shown, the column in the centre gives the interpretation in the seven different groups, as discussed above in the Chapter “Garnet Classification”.

The garnet classification is superimposed on either ternary diagrams with compositions of individual garnet grains (Fig. C8), or in contour plots of the garnet distribution (Fig. C7). The results of this classification are then plotted in a circle diagram, visualising the relative abundance for the individual garnet groups (Fig. C7). Diagrams as shown in Figures C8 and C7 are used in Appendix A and in the main text.

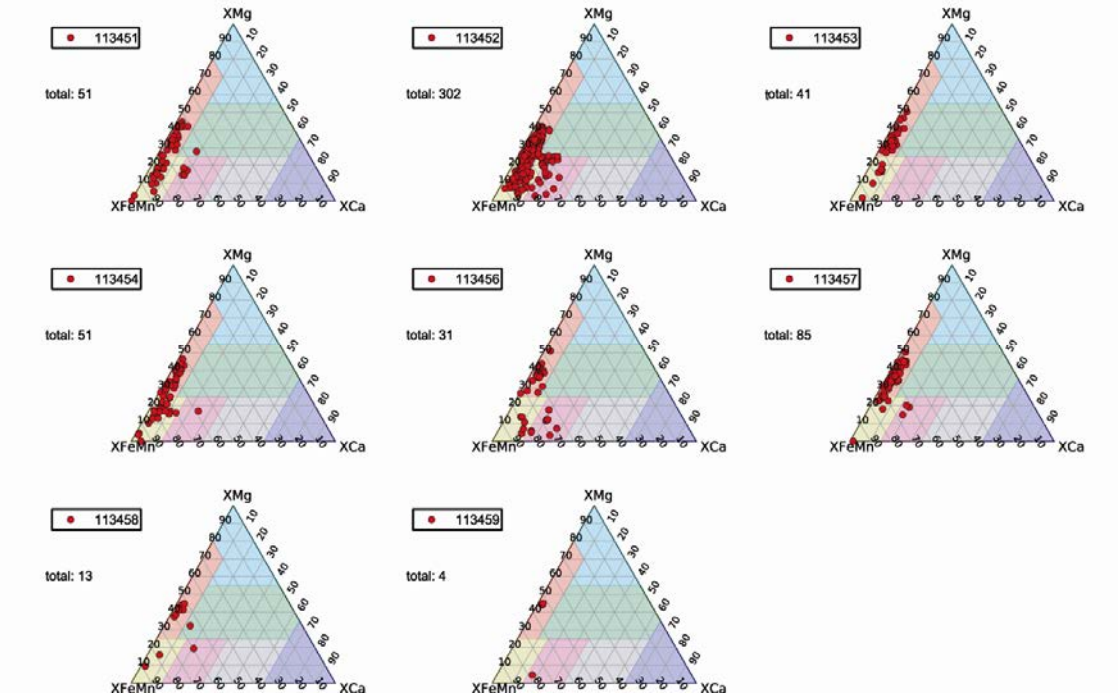

Figure C8: Ternary diagram showing the composition of individual garnet grains (red dots). Garnet is plotted by the three endmember compositions pyrope (XMg), almandine+spessartine (XFeMn) and grossular (XCa). The garnet classification in seven groups is given in coloured fields (see Chapter on Garnet classification).